A FINITE ELEMENT ANALYSIS OF ADHESIVELY BONDED COMPOSITE JOINTS INCLUDING GEOMETRIC NONLINEARITY, NONLINEAR VISCOELASTICITY, MOISTURE DIFFUSION AND DELAYED FAILURE

by

Samit Roy

Dissertation submitted to the Faculty of the
Virginia Polytechnic Institute and State University
in partial fulfillment of the requirements
for the degree of

Doctor of Philosophy

in

Engineering Mechanics

APPROVED:

J. N. Reddy, Chairman

C. W. Smith

E. G. Henneke

E. R. Johnson

H. F. Brinson

November 1987

Blacksburg, Virginia

A FINITE ELEMENT ANALYSIS OF ADHESIVELY BONDED JOINTS INCLUDING GEOMETRIC NONLINEARITY, NONLINEAR VISCOELASTICITY, MOISTURE DIFFUSION AND DELAYED FAILURE

by

Samit Roy

Engineering Mechanics

(ABSTRACT)

A two-dimensional finite-element computational procedure is developed for the accurate analysis of the strains and stresses in adhesively bonded joints. The large displacements and rotations experienced by the adherends and the adhesive are taken into account by invoking the updated Lagrangian description of motion. The adhesive layer is modeled using Schapery's nonlinear single integral constitutive law for uniaxial and multiaxial states of stress. Effect of temperature and stress level on the viscoelastic response is taken into account by a nonlinear shift factor definition. Penetrant sorption is accounted for by a nonlinear Fickean diffusion model in which the diffusion coefficient is dependent on the penetrant concentration and the dilatational strain. A delayed failure criterion based on the Reiner-Weisenberg failure theory has also been implemented in the finite element code. The applicability of the proposed models is demonstrated by several numerical examples.

ACKNOWLEDGEMENTS

I am deeply indebted to my advisor, Dr. J. N. Reddy, for the support, guidance and encouragement he provided throughout this research effort. Special thanks are extended to the other members of the dissertation committee, Professor C. W. Smith, Dr. E. R. Johnson, Dr. E. G. Henneke and Dr. H. F. Brinson, for their suggestions and comments. The support of this research by the Materials Division of the Office of Naval Research through Contract N00014-82-K-0185 is gratefully acknowledged. I express my gratitude to Dr. Didier Lefebvre for his valuable ideas and suggestions.

I would like to thank my parents and my fiancee, Mabel Sequeira, for their love and support. I would also like to thank Ms. Vanessa McCoy for her time and effort in typing this dissertation.

TABLE OF CONTENTS

TABLE OF CONTENTS

LIST OF TABLES

LIST OF ILLUSTRATIONS

CHAPTER 1

INTRODUCTION

1.1 General Comments

Adhesive bonding is increasingly used to fasten (metallic to metallic or metallic to composite) structural components together. This is because in many present day applications, conventional fasteners such as bolts, rivets, welds etc., are unsuitable, especially if the components are made of polymeric or composite materials. Penetration methods (i.e., drilling holes, etc.) cause high stress concentrations and, in the case of composites, sever the fiber reinforcement which in turn reduces the strength of the joint. On the other hand, bonded joints tend to be damage-tolerant due to the high damping behavior of the adhesive layer and less expensive due to lower fabrication cost. The use of adhesives increases the joint strength, distributes the loads more evenly, and enables alternative jointing methods to be reduced or eliminated. Dissimilar materials (e.g., steel, aluminum, plastics, glass, etc.) can be joined together by bonding even where it is impossible to gain access to either side of the joint, thereby increasing the design flexibility.

Adhesives are not free of disadvantages, however. Adhesives are polymers and as such have time dependent (viscoelastic) moduli and strength properties which are susceptible to environmental effects, especially temperature and moisture. Most polymeric adhesives are

rate sensitive materials and hence exhibit viscoelasticity. Furthermore, certain types of epoxy resins have been found to be nonlinearly viscoelastic in character. The nonlinear viscoelastic behavior is typified by a stress-enhanced creep. Basically, at elevated stresses the material moduli seem to soften and the creep progresses at accelerated rates. Time dependent properties of adhesives raise serious questions regarding their long term reliability or durability under creep or other more complicated loading conditions. A delayed failure (creep rupture) long after the initial design and fabrication process is possible. Thus, methods are needed by which long term failures on the order of a structure design life time (perhaps as long as 5-20 years) can be anticipated and thereby avoided. Such a process is especially important in applications where failures may be life threatening as is the case for automobiles, airplanes, missiles, etc.

Failure in an adhesive joint can occur in one of two ways: (i) adhesive failures that occur at the interfaces between the adhesive and adherends, and (ii) cohesive failures, which occur either in the adhesive or in the adherends. The determination of the strength, failure and reliability of an adhesive joint requires both an understanding of the mechanisms of adhesion and a knowledge of deformation and stresses in the joint. The mechanisms of adhesion is closely related to the chemical and physical properties of the adhesive polymers. The deformation and stress states can be

determined once the geometry, loading, boundary conditions and mechanical properties of the constituent materials of the joint are known. The mechanical properties of the adhesive and adherend materials enter the stress analysis via constitutive models, which relate strains, temperature and moisture gradients and density to stresses and fluxes in the joint. The chemical, physical and mechanics aspects of the constituent materials enable the formulation of appropriate constitutive models for adhesive joints. The determination of stresses allow the prediction of the strength, failure and reliability, in macromechanics sense, of adhesive joints.

The stresses in an adhesive joint depend on the geometry, boundary conditions, the mechanical properties of the regions involved, and the type and distribution of loads acting on the joint. In practice, most adhesives exhibit, depending on the stress levels, nonlinear-viscoelastic behavior, and the adherends exhibit elasto-plastic behavior. Most theoretical studies conducted to date on the stress analysis of adhesively bonded joints have made simplifying assumptions of linear and elastic and/or viscoelastic behavior in the interest of obtaining closed form solutions.

A good understanding of the process of adhesion from the mechanics view point and the predictive capability for structural failures associated with adhesive bonding require realistic theoretical analysis methods to determine stress distributions in the joint. The finite element method is the most powerful analysis tool

that can be used to determine stress and displacement fields in complicated structures.

At present there are numerous computer programs available for analyzing bonded joints. However, most of these computer codes incorporate linearly elastic material behavior, and some allow for nonlinearly elastic and plastic behavior. Computer programs which incorporate viscoelastic material behavior are quite often limited to the simple spring-dashpot type of model for linear materials. Such inaccurate modelling of the constitutive behavior of the structure can seriously compromise the accuracy of the analytical predictions.

1.2 Objectives of Present Research

The primary objective of the present research is to present a finite-element computational procedure for the accurate analysis of adhesively bonded joints. With this aim in mind, a nonlinear viscoelastic analysis code (NOVA for short) has been developed. The finite element program NOVA uses linearly elastic elements to model the adherends. The adherends may be represented as isotropic, orthotropic or laminated composite materials. The large displacements and rotations experienced by the adherends in many types of loading are accounted for by the updated Lagrangian description of motion presented in Section 2.1. It should be noted that this description is valid only for small strains.

The adhesive layer is modeled using a special element that employs a multi-axial extension of Schapery's nonlinear single

integral stress-strain law as the constitutive equation. The finite element formulation for the viscoelastic material representation has been described in detail in Chapter 3. The element library contains an eight noded isoparametric element which employs quadratic interpolation functions to represent the displacement field as well as element geometry. The program can be used to conduct plane stress, plane strain, or axisymmetric analysis of an adhesively bonded structure subject to a time varying thermal and mechanical loading. A nonlinear Fickean moisture diffusion model and a energy-based delayed failure criterion are also provided in NOVA.

1.3. A Review of the Literature

Adhesive bonding has been in use for many years. Most of the early bonds used animal and vegetable glues, and the structural use of these glues has been confined mostly to timber. The use of synthetic resins in the structural bonding of timber began in early 1930's. Synthetic resins are less susceptible to moisture, fungi and bacteria. In recent years, synthetic polymers, because of their strength and other bonding properties have been widely used to bond metals and composite materials. As noted in the introduction, adhesive joints have several advantages over the conventional mechanical fasteners (e.g. bolts, rivets and welding). These include: lighter weight, savings in production cost, avoid stress concentrations and thermal distortions due to the hole drilling or welding, and bonding of dissimilar and/or brittle materials.

An analysis of adhesive stresses in bonded joints which included the effects of load eccentricity was first performed by Goland and Reissner [3] in 1944 under the following assumptions:

1. Adhesive flexibility is negligible, and joint is homogeneous (i.e., ignore the presence of the adhesive),
2. No axial stress exists, and other stresses do not vary through the thickness of the adhesive layer.

Under these simplifying assumptions, Goland and Reissner [3] developed one-dimensional elasticity solutions for two limiting cases: (i) the case in which the adhesive layer is homogeneous, thin and stiff so that its deformation can be neglected, the axial stress is zero and stresses do not vary through the adhesive layer; and (ii) the case in which the adhesive layer is soft and flexible and the joint flexibility is mainly due to the deformation of the adhesive layer (i.e., adherends are rigid), the axial stress is zero and stresses do not vary through the adhesive layer. In the first case, the peel stress is found to be very high at the edge of the joint, while the shear stress is zero. In the second case, the maximum values of the peel and shear stresses occur at the edges of the joint. The Goland-Reissner analysis gives resonable solutions for shear and peel stresses in the interior of the adhesive layers; the joint-edge loads are not in equilibrium.

Erdogan and Ratwani [4] presented analytical solution based on a one-dmensional model for calculating stresses in a stepped lap

joint. One adherend was treated as isotropic and the second as orthotropic, and linear elastic behavior was assumed. The thickness variation of the stresses in both the adherends and in the adhesive was neglected.

Wooley and Carver [5] determined stress distributions in a simple lap joint using the finite element method. The constant strain quadrilateral obtained by combining four constant strain triangular elements was used. One end of the adherend was assumed to be hinged and other end was allowed to move freely in the direction parallel to the original bond line. They investigated the influence of the ratio of the Young's moduli of adherend to adhesive materials and geometries on the peel and shear stress distributions. The results compared favorably with the results of Goland and Reissner.

Hart-Smith [6] improved upon the approach of Goland and Reissner by considering a third free-body-diagram for the adherend outside the joint in addition to the two free-body-diagrams from each of the upper and lower halves of the joint. With three separate sections to consider, three relations between displacements and bending moments were obtained. Additional boundary conditions involving displacements and their first derivatives, not considered by Goland and Reissner, were imposed in order to solve for the additional unknowns. In addition to the improvement on the analysis of Goland and Reissner, Hart-Smith [6] also established a quantitative influence of adhesive plasticity in shear. The elastic-plastic

theory used by Hart-Smith predicts an increase in joint strength, and was shown to be capable of explaining premature failure predictions found when using linear elastic analyses. The quantitative effects of stiffness imbalance were also accounted for.

A finite-element stress analysis for adhesive lap joints using linear elasticity and elasto-plasticity theories was reported by Liu [7]. Stress distributions in the adhesive layer for different joint parameters (geometry, material properties, and loading conditions) were studied and compared. The existence of stress gradients through the thickness of the adhesive layer, close to the joint edges, was observed by Adams and Peppiatt [8]. They subsequently performed a linear elastic finite element analysis on adhesively bonded lap joints employing more than one element through the thickness of the adhesive layer, close to the joint edges. Adams and Peppiatt [9] also studied the adhesive yielding in double bevel and scarf joints. The adhesive was assumed to be elastic-perfectly plastic. A nonlinear finite-element analysis of single and double lap joints was presented by Humphreys and Herakovich [10]. The nonlinear stress-strain response was represented by the Ramberg-Osgood approximation. Mechanical and thermal loadings were considered but only one element through the thickness of the adhesive layer was used.

Allman [11] presented an elastic stress analysis based on the strain energy density of a particular joint. The effects of bending,

stretching and shearing of the adherends were included, and the shearing and tearing action in the adhesive was accounted for. All conditions of stress equilibrium in the joint and stress-free surface conditions were satisfied. It was assumed, however, that the axial stress varies linearly through the adherend thicknesses and that the shear stress is constant through the adhesive thickness. Allman obtained solutions for the single lap joint, although the method also appears to be applicable to other joint configurations. He found that the average shear stress concentration is 11% higher than that of Goland and Reissner's first analysis, while the average peel stress at the joint edge is 67% lower. Compared with the second analysis of Goland and Reissner, Allman's method yielded a shear stress concentration of 15% and 31% less for metal and composite adherends, respectively, while the average peel stress at the joint edge was 27% higher and 36% lower for the same types of adherends, respectively.

Phenomenological considerations were discussed by Hart-Smith [12] which greatly improve our understanding of the sources of non-uniform load transfer, viz., adherend extensivity, stiffness imbalance and thermal mismatch. He also explained how the lightly loaded central area of the joint, away from the joint edges, restricts cumulative creep damage, and suggests that this region is vital for long term durability. The amount of lightly loaded central area is a function of the overlap length.

Yuceoglu and Updike [13] presented a numerical method for solving peel and shear stresses in the adhesive of double lap, double strap and stiffner plate joints. Bending and transverse shear were included in the analytical model. Shear stresses were not required to drop to zero at the joint edges after reaching peak values close to the edges. Yuceoglu and Updike maintained that an analytical model which would allow the shear stresses to drop to zero at the joint edges would give approximately the same or slightly lower peak values of shear and peel stresses. Their method also reveals that adherend bending has a significant effect on both adhesive shear and peel stresses, especially the latter.

Delale and Erdogan [14,15] performed a plate analysis similar to that of Goland and Reissner on the single lap joint assuming linear elastic adherends and a linear viscoelastic adhesive. Separate stress distributions were calculated for membrane loading, bending, and transverse shear loading. They further extended their viscoelastic analysis of the single lap joint to include time-dependent temperature variations approximated by a piecewise constant function.

Gali and Ishai [16] performed a finite element analysis on a symmetric doubler model with linear elastic adherends and the adhesive obeying a nonlinear effective-stress-strain relationship. The effective-stress-strain relationship was derived from stress-strain curves obtained by tensile and shear test data, and based on

the Von Mises deviatoric energy yield criterion. An iteration procedure was applied to the linearly elastic finite element problem using a specific secant modulus for each element separately. The secant modulus was found from the corresponding effective strain of the previous solution and the corresponding effective stress was found from the experimental stress-strain curves. Gali and Ishai analyzed their symmetric doubler model using both plane stress and plane strain and found that the plane strain solutions converged faster and yielded less conservative results, i.e., lower stresses, than the plane stress solutions. Nonlinear solutions were also found to be considerably lower than the linear solutions, the difference being more pronounced in the plane stress case. The problem was also solved with the adhesive following an elastic-perfectly-plastic effective-stress-strain law. The difference between these results and those of the continuous nonlinear effective-stress-strain case was found to be very small.

Nagaraja and Alwar [17] analyzed a tubular lap joint with the finite element method assuming linear elastic adherends and a nonlinear biaxial stress-strain law in the adhesive. The constants appearing in the nonlinear law were obtained from uniaxial tension test data. The stress-strain relationship, however, was assumed to be time-independent. Nagaraja and Alwar demonstrated that for low stress levels, of the order of 12% of the fracture stress, the nonlinear stresses were as much as 15% lower in shear and 8% lower in

peel than the linear stresses. Nagaraja and Alwar [18] also performed a finite element analysis on a single lap joint, treating the adherends as linear elastic materials but the adhesive as a linear viscoelastic material. The relaxation modulus was assumed to be equal to the inverse of the creep compliance, the latter being obtained experimentally.

Only recently, work involving the time dependent fracture characteristics of adhesively bonded joints has been under way. Francis et al. [19] discussed the effects of a viscoelastic adhesive layer, geometry, mixed mode fracture response, mechanical load history, environmental history and processing variations on the fracture processes of adhesively bonded joints. However, their finite element analysis includes only linear elastic fracture mechanics.

Dattaguru, et al. [20] have performed cyclic de-bond research on the crack lap specimen and performed analyses with a finite element program GAMNAS, developed in-house at NASA-Langley. Their program includes geometric and material nonlinearities but does not include viscoelastic capability. Also, fracture is modeled using linear elastic fracture mechanics but no failure law is included.

Botha, Jones and Brinson [21], Henriksen [22], Becker, et al. [23], and Yadagiri and Papi Reddy [24] reported results of viscoelastic finite-element analysis of adhesive joints. Henriksen used Schapery's [25] nonlinear viscoelastic model to verify the

experimental results of Peretz and Weitsman [26] for an adhesive layer. The work of Becker et al. [23] is largely concerned with the development of a finite-element stress analysis program, called VISTA, for adhesively bonded joints. The 'intrinsic nonlinear model' based on free-volume concept of Knauss and Emri [27] was used in VISTA. The work of Yadagiri and Papi Reddy [24] is limited to linear viscoelastic analysis. Botha et al. [21] considered linear and bilinear viscoelastic models in their study.

Pickett and Hollaway [28] presented both classical and finite element solutions for elastic-plastic adhesive stress distributions in bonded lap joints. Single, double and tubular lap configurations having both similar and dissimilar adherends were considered. The results show how the development of adhesive yielding will occur as the joints are loaded to a failure condition. The detrimental effect of adherend-stiffness-imbalance on the adhesive stress distribution was also shown.

An approximate method to analyze viscoelastic problems has been outlined by Schapery [29]. In this method, the solution to a viscoelastic problem is approximated by a corresonding elasticity solution wherein the elastic constants have been replaced by time dependent creep or relaxation functions. The method may be applied to linear as well as nonlinear problems. Weitsman [30] used Schapery's quasi-elastic approximation to investigate the effects of nonlinear viscoelasticity on load transfer in a symmetric double lap

joint. Introducing a stress-dependent shift factor, he observed that the enhanced creep causes shear stress relief near the edges of the adhesive joint.

Aivazzadeh and Verchery [31] developed several special interface finite elements based on Reissner's principle which take into account all the continuity conditions at the adhesive-adherend interface. These elements were then used to perform a two-dimensional analysis of an adhesively bonded butt joint. It was observed that the interface stress distribution could be evaluated more accurately using the interface finite elements compared to classical ones.

The analytical procedures reviewed in the preceding pages are primarily applicable for bonded joints with homogeneous isotropic adherends. These procedures have been modified for composite adherends to account for their anisotropic and heterogeneous nature. A comprehensive review of publications relating to all aspects of adhesively bonded joints in composite materials is presented in [32].

Reddy and Sinha [33] extended the work of Erdogan and Ratwani [4] to obtain analytically, the stress distribution in adhesively bonded joints between two orthotropic materials. Similarly, Renton and Vinson [34] extended the work of Goland and Reissner [3] to obtain the linear elastic response of two generally orthotropic adherends adhesively bonded together. Barker and Hatt [35] used linear elastic finite-element analysis to evaluate the behavior of an

adhesive joint bonding an advanced composite to a metallic substrate. A special element was used to model the adhesive layer as a separate elastic medium of finite thickness in order to remove the stress singularity that exists when dissimilar materials are joined. Adams and Peppiatt [36] performed two dimensional finite element stress analysis on lap, bevel and scarf joints. The adherends were treated as homogeneous anisotropic materials with linear elastic properties, while the adhesive was treated as an elastic-perfectly plastic material. The effect of adhesive spew fillets on the stress distribution was also taken into account in this analysis. It was observed that the predicted joint efficiency was almost doubled when non-linear adhesive behavior was accounted for.

Renton and Vinson [37] used laminated plate theory coupled with a structural mechanics approach to obtain analytical solutions for stresses and deformations within a bonded single lap joint. The closed form solutions were then used to conduct a parametric study which revealed that changes in adhesive moduli, adherend longitudinal modulus, and bond overlap length have a significant effect on the magnitude of the peak stresses within the adhesive. However, changes in adherend ply orientation appeared to have only a modest influence on adhesive peak stresses. These predictions were verified by the authors from experimental observations.

Schaffer and Adams [38] carried out a nonlinear viscoelastic analysis of a unidirectional composite laminate using the finite element method. The nonlinear viscoelastic constitutive law proposed by Schapery [25] was used in conjunction with elastoplastic constitutive relations to model the composite response beyond the elastic limit.

Ghoneim and Chen [39] developed a viscoelastic-viscoplastic law based on the assumption that the total strain rate tensor can be decomposed into a viscoelastic and a viscoplastic component. A linear viscoelasticity model is used in conjunction with a modified plasticity model in which hardening is assumed to be a function of viscoplastic strains as well as the total strain rate. The resulting finite element algorithm is then used to analyze the strain rate and pressure effects on the mechanical behavior of a viscoelastic-viscoplastic material.

Analysis of crack growth in viscoelastic media are mainly limited to linear isotropic, homogeneous materials. Schapery [40] proposed the use of parameters similar to the J integral for quasi-static crack growth in a class of nonlinear viscoelastic materials subject to finite strains.

Czarnocki and Piekarski [41] used a nonlinear elastic stress-strain law for three-dimensional failure analysis of a symmetric lap joint. Taking into account the variation of Poisson's ratio with strain within the adhesive, the authors concluded that the failure of

the adhesive layer originates in the central plane of a joint (at the front edge). It was also observed that the joint width does not have any effect on the stress peaks in the central plane and that the application of a weaker but more flexible adhesive results in higher load carrying capacity and lower stress concentrations in the adherends.

Over the years several time-dependent failure criteria have been proposed for predicting yield and fracture of polymeric materials. Nagdhi and Murch [42] and Crochet [43] have used a modified von Mises criteria for viscoelastic materials by assuming that the radius of the yield surface depends upon the strain history. An energy based delayed failure criterion for polymeric materials subjected to isothermal creep was developed by Reiner and Weissenberg [44]. According to this theory, failure occurs when the stored deviatoric strain energy in a viscoelastic material reaches a certain maximum value called the resilience, which is a material constant. Brüller [45] and Hiel et al. [46] applied the Reiner-Weisenberg failure criterion to various viscoelastic materials, including composite laminates, and obtained good agreement with experimental observations.

It is now well known that moisture diffusion can have a significant effect on the stress field within an adhesive layer in a bond. Weitsman [47] used a variational method coupled with Fickean diffusion law to study the interfacial stresses in viscoelastic

adhesive-layers due to moisture sorption. From the results of this uncoupled linear thermoelastic analysis, he concluded that the location of the maximum interfacial tensile stress depends on the geometry of the joint as well as the progress of the diffusion process within the joint. Weitsman [48] used the correspondence principle to generate a linear viscoelastic solution from the linear elastic analysis of moisture sorption within an adhesive layer. He observes that the viscoelastic analysis predicts detrimental effects due to stress reversals caused by fluctuations in relative humidity, that are not predicted in an elastic analysis. However, he acknowledged the omission of the effect of moisture content on the viscoelastic response of the resins in his analysis.

Tobing, et al. [49] used the finite element method to study the micro-mechanical effect of moisture sorption in graphite-epoxy composites. Using a constitutive equation based on the Flory-Huggins lattice model for polymer solvent interactions, they concluded that the stresses at the graphite-epoxy interface have a strong dependence on moisture content, fiber spacing, and applied load.

Yaniv and Ishai [50] developed a linear viscoelastic closed form solution as well as a nonlinear finite element solution algorithm to study the hygrothermal effects in a bonded fiber-reinforced plastic/aluminum system. The linear solution was used for short-term predictions at low strain levels, whereas the finite element solution was used for long term predictions in which geometric and material

nonlinearities were taken into account. The authors observed that the presence of moisture tends to considerably reduce the stress level in the adhesive layer and may lead to significant variation in the time-dependent deformation of the test specimen as compared to the dry state.

In the references cited above, various authors have underscored the effect of moisture content on the viscoelastic response of the test specimen. However, the effect of the viscoelastic stress field on the diffusion coefficient was not considered. Lefebvre et al. [51] extended the free volume concept to define a diffusion coefficient that is a function of temperature, dilatational strain and solvent concentration. The proposed nonlinear diffusion model showed good predictive capability for different values of temperature and moisture conentrations. They concluded that in order to obtain an accurate solution for the hygrothermal effects within an adhesive bond, the nonlinear diffusion problem needs to be solved in conjunction with the nonlinear viscoelastic boundary-value problem until convergence is achieved.

A review of the literature reveals that previous finite-element analyses of adhesive joints were either based on simplified theoretical models or the analyses themselves did not exploit the full potential of the finite element method. Also, several investigations involving finite element analyses of the same adhesive joint have reported apparent contradicting conclusions about the

variations of stresses in the joint [24,52]. Thus, there is a need for a closer examination of the theories, underlying assumptions on material behavior and boundary conditions, and the finite element formulations used in the analyses of adhesive joints.

CHAPTER 2

NONLINEAR DESCRIPTION OF SOLIDS

2.1 Introduction

In the linear description of the motion of solid bodies it is assumed that the displacements and their gradients are infinitely small and that the material is linearly elastic. In addition, it is also assumed that the nature of the boundary conditions remains unchanged during the entire deformation process. These assumptions imply that the displacement vector $\underset{\sim}{u}$ is a linear function of the applied load vector $\underset{\sim}{F}$, i.e., if the applied load vector is a scalar multiple $\alpha\underset{\sim}{F}$ then the corresponding displacements are $\alpha\underset{\sim}{u}$.

The nonlinearity in solid mechanics arises from two distinct sources. One due to the kinematics of deformation of the body and the other from constitutive behavior (e.g., stress-strain relations). The analyses in which the first type of nonlinearity is considered are called *geometrically nonlinear* analyses, and those in which the second type are considered are called *materially nonlinear* analyses. The geometrically nonlinear analysis can be subclassified according to type of nonlinearities considered. Two such cases are: (i) large displacements, large rotations, but small strains, and (ii) large displacements, large rotations and large strains. In the first case it is assumed that rotations of line elements are large, but their extensions and changes of angles between two line elements are small. In the second case the

extension of a line element and angle changes between two line elements are large, and displacements and rotations of a line element are also large.

2.2 Incremental Equations of Motion

In the Lagrangian description of motion all variables are referred to a reference configuration, which can be the initial configuration or any other convenient configuration. The description in which all variables are referred to the initial configuration is called the *total Lagrangian description,* and the one in which all variables are referred to current configuration is called the *updated Lagrangian description.*

The equations of the Lagrangian incremental description of motion can be derived from the principles of virtual work (i.e., virtual displacements, virtual forces or mixed virtual displacements and forces). Since our ultimate objective is to develop the finite element model of the equations governing a body, we will not actually derive the differential equations of motion but utilize the virtual work statements to develop the finite element models.

The *displacement finite element model* is based on the principle of virtual displacements. The principle requires that the sum of the external virtual work done on a body and the internal virtual work stored in the body should be equal to zero (see [53]):

$$\int_{V_2} {}^{2}\tau_{ij}\, \delta({}_{2}e_{ij})\, dV - \delta({}^{2}F) = 0 \qquad (2.1)$$

where

$$\delta({}^{2}F) = \int_{V_2} {}^{2}f_i\, \delta u_i\, dV + \int_{S_2} {}^{2}t_i\, \delta u_i\, dS$$

${}^{2}\tau_{ij}$ = the Cartesian components of the Cauchy stress tensor in configuration C_2 at time $(t + \Delta t)$ occupying the volume V_2

${}_{2}e_{ij}$ = the Cartesian components of the infinitesimal strain tensor associated with the displacements u_i in going from configuration C_1 at time t to C_2 at time $(t + \Delta t)$:

$${}_{2}e_{ij} = \frac{1}{2}\left(\frac{\partial u_i}{\partial x_j} + \frac{\partial u_j}{\partial x_i}\right) \qquad (2.2)$$

x_i = Cartesian components of a point in configuration C_2

${}^{2}f_i$ = Cartesian components of the body force vector measured in C_2

${}^{2}t_i$ = Cartesian components of the surface stress vector measured in C_2.

Here δ denotes the variational symbol (i.e., δu_i denotes the virtual displacement in u_i) and dV and dS denote the volume and surface elements in configuration over which the integrals are defined.

Equation (2.1) is not so useful in its present form because the integrals are defined over the volume V_2 and surface S_2 of the configuration C_2, which is yet unknown. In the linear analysis, it is assumed that the configuration of the body remains unchanged and therefore Eq. (2.1) applies to the initial (undeformed) configuration. The fact that the configuration of the body changes continuously in a nonlinear analysis requires us to use appropriate measures of stress and strain and their interrelationship (i.e., constitutive equations) so that Eq. (2.1) can be used to calculate the configuration C_2. In order to compute the current configuration C_2 (often, the displacements, strains and stresses) from the knowledge of applied forces and displacements, and known previous configuration C_1, we must make some assumptions. A description of the procedure based on the updated Lagrangian approach is given below.

The coordinates of a general point in C_0 and C_1 and C_2 are denoted by (X_1^o, X_2^o, X_3^o); (X_1, X_2, X_3), and (x_1, x_2, x_3), respectively. The displacements of a general point in C_1 are denoted $({}^1u_1, {}^1u_2, {}^1u_3)$. In C_2 they are given by

$$ {}^2u_i = {}^1u_i + u_i , \quad i = 1,2,3 \tag{2.3} $$

where u_i are the components of the displacement vector from C_1 to C_2.

During the motion of the body, its volume, surface area, density, stresses and strains change continuously. The stress

measure that we shall use is the 2nd Piola-Kirchhoff stress tensor. The components of the 2nd Piola-Kirchhoff stress tensor in C_1 will be denoted by S_{ij}. To see the meaning of the 2nd Piola-Kirchhoff stress tensor, consider the force $d\underset{\sim}{F}$ on surface dS in C_2. The Cauchy stress tensor $\underset{\sim}{\tau}$ is defined by

$$(\hat{\underset{\sim}{n}} \cdot \underset{\sim}{\tau})\, dS = d\underset{\sim}{F} \tag{2.4a}$$

where $\hat{\underset{\sim}{n}}$ is the unit normal to dS in C_2. Note that the Cauchy stress is the force per deformed area (i.e. measured in C_2) and referred to C_2. The 2nd Piola-Kirchhoff stress tensor at time $t + \Delta t$ referred to C_1 is defined by

$$(\hat{\underset{\sim}{n}}_o \cdot {}^2_1\underset{\sim}{S})\, dS_o = d\underset{\sim}{F}_o \tag{2.4b}$$

where $\hat{\underset{\sim}{n}}_o$ denotes the unit normal to the surface element dS_o in C_1. The force $d\underset{\sim}{F}_o$ is related to $d\underset{\sim}{F}$ by

$$d\underset{\sim}{F}_o = \underset{\sim}{J}^{-1} \cdot d\underset{\sim}{F} \tag{2.4c}$$

where

$$\underset{\sim}{J}^{-1} = \left(\frac{\partial \underset{\sim}{X}}{\partial \underset{\sim}{x}}\right)^T .$$

From the definition it is clear that the 2nd Piola-Kirchhoff stress is measured in C_2 but referred to C_1. It can be shown that that the components ${}^2S_{ij}$ and ${}^2\tau_{ij}$ are related according to

$${}^2_1S_{ij} = \frac{\rho_o}{\rho} \left(\frac{\partial X_i}{\partial x_m}\right)^2 \tau_{mn} \left(\frac{\partial X_j}{\partial x_n}\right) \tag{2.5a}$$

$$ {}^{2}\tau_{ij} = \frac{\rho}{\rho_o} \left(\frac{\partial X_i}{\partial X_m}\right)^{2}_{1} S_{mn} \left(\frac{\partial X_j}{\partial X_n}\right) \qquad (2.5b) $$

where ρ_o denotes the density in C_1 and ρ is the density in C_2. The 2nd Piola-Kirchhoff stress tensor is symmetric whenever the Cauchy stress tensor is symmetric. Note that ${}^{2}_{2}S_{ij} = {}^{2}\tau_{ij} \equiv {}^{2}_{2}\tau_{ij}$.

Similarly, the Green-Lagrange strain tensor E_{ij} and the infinitesimal strain tensor e_{ij} are related by

$$ {}^{2}_{1}E_{ij} = \frac{\partial X_m}{\partial X_i} \frac{\partial X_n}{\partial X_j} \; {}^{2}e_{mn}. \qquad (2.6) $$

It is also important to note that the 2nd Piola-Kirchhoff stress tensor is <u>energetically conjugate</u> to the Green-Lagrange strain tensor and the Cauchy stress is energetically conjugate to the infinitesimal strain tensor. In other words, we have

$$ \int_{V_1} {}^{2}_{1}S_{ij} \, \delta({}^{2}_{1}E_{ij}) dV = \int_{V_2} {}^{2}\tau_{ij} \, \delta({}_{2}e_{ij}) dV. \qquad (2.7) $$

Substituting Eq. (2.7) into Eq. (2.1), we obtain

$$ 0 = \int_{V_1} {}^{2}_{1}S_{ij} \, \delta({}^{2}_{1}E_{ij}) \, dV - \delta({}^{2}F). \qquad (2.8) $$

Next we use the incremental decompositions of the stress and strains:

$$ \begin{aligned} {}^{2}_{1}S_{ij} &= {}^{1}\tau_{ij} + {}^{1}S_{ij} \\ {}^{2}_{1}E_{ij} &= {}^{1}e_{ij} + {}^{1}\eta_{ij} \end{aligned} \qquad (2.9) $$

where

$$
\begin{aligned}
{}_1S_{ij} &= \text{incremental components of 2nd Piola-Kirchhoff stress tensor} \\
{}_1e_{ij} &= \text{(incremental) components of the infinitesimal strain tensor} \\
&= \frac{1}{2}\left(\frac{\partial u_i}{\partial X_j} + \frac{\partial u_j}{\partial X_i}\right), \\
{}_1\eta_{ij} &= \frac{1}{2}\frac{\partial u_m}{\partial X_i}\frac{\partial u_m}{\partial X_j}.
\end{aligned}
\tag{2.10}
$$

Recall that u_i is the i-th displacement component of a generic point in C_1 (in going from C_1 to C_2). Substituting Eq. (2.9) into Eq. (2.8), we have

$$
0 = \int_{V_1} ({}^1\tau_{ij} + {}_1S_{ij})\ \delta({}_1e_{ij} + {}_1\eta_{ij})\ dV - \delta({}^2F)
$$

or

$$
\int_{V_1} {}_1S_{ij}\ \delta({}_1e_{ij} + {}_1\eta_{ij})\ dV + \int_{V_1} {}^1\tau_{ij}\delta({}_1\eta_{ij})dV =
$$

$$
- \int_{V_1} {}^1\tau_{ij}\ \delta({}_1e_{ij})dV + \delta({}^2F). \tag{2.11}
$$

Linearize the equations by assuming that

$$
{}_1S_{ij} = {}_1C_{ijrs}\ e_{rs},\ \delta\ {}^2_1E_{ij} = \delta_1e_{ij} \tag{2.12}
$$

where ${}_1C_{ijrs}$ are the components of the linear elasticity tensor. Constitutive equations of linear and nonlinear viscoelasticity will be presented later. We obtain the <u>approximate</u> equation of equilibrium,

$$\int_{V_1} {}_1C_{ijrs}\ {}_1e_{rs}\ \delta({}_1e_{ij})\ dV + \int_{V_1} {}_1\tau_{ij}\ \delta({}_1\eta_{ij})dV =$$

$$- \int_{V_1} {}_1\tau_{ij}\ \delta({}_1e_{ij})dV + \delta({}^2F). \qquad (2.13)$$

This linearization can be interpreted as a representation of the nonlinear curve between two consecutive load steps by linear line segments.

2.3 Finite Element Model

Here we construct the finite element model of Eq. (2.13) for the two-dimensional case (see Reddy [54]). Let each displacement increment be approximated as

$$\Delta u_i = \sum_{j=1}^{n} \Delta u_i^j\ \psi_j(x_1,x_2). \qquad (2.14)$$

Substituting Eq. (2.14) into Eq. (2.13) we obtain

$$([K^L] + [K^\sigma])\ \{\Delta u\} = \{F^L\} - \{F^\sigma\} \qquad (2.15)$$

where

$$[K^L] = h \int_{A_1} [B^L]^T\ [C]\ [B^L]\ dA\ ,\ h = \text{thickness}$$

$$[C] = \begin{bmatrix} C_{11} & C_{12} & 0 \\ C_{12} & C_{22} & 0 \\ 0 & 0 & C_{66} \end{bmatrix}\ ,$$

$$\underset{(3\ \times\ 2n)}{[B^L]} = \begin{bmatrix} \psi_{1,1} & 0 & \psi_{2,1} & 0 & \cdots & \psi_{n,1} & 0 \\ 0 & \psi_{1,2} & 0 & \psi_{2,2} & \cdots & 0 & \psi_{n,2} \\ \psi_{1,2} & \psi_{1,1} & \psi_{2,2} & \psi_{2,1} & \cdots & \psi_{n,2} & \psi_{n,1} \end{bmatrix}$$

$$[K^{\sigma}] = h \int_{A_1} [B^{\sigma}]^T [\tau] [B^{\sigma}] \, dA$$

$$[\tau] = \begin{bmatrix} \tau_{11} & \tau_{12} & 0 & 0 \\ \tau_{12} & \tau_{22} & 0 & 0 \\ 0 & 0 & \tau_{11} & \tau_{12} \\ 0 & 0 & \tau_{12} & \tau_{22} \end{bmatrix}$$

$$\underset{(4 \times 2n)}{[B^{\sigma}]} = \begin{bmatrix} \psi_{1,1} & 0 & \psi_{2,1} & 0 & \cdots & \psi_{n,1} & 0 \\ \psi_{1,2} & 0 & \psi_{2,2} & 0 & \cdots & \psi_{n,2} & 0 \\ 0 & \psi_{1,1} & 0 & \psi_{2,1} & \cdots & 0 & \psi_{n,1} \\ 0 & \psi_{1,2} & 0 & \psi_{2,2} & \cdots & 0 & \psi_{n,2} \end{bmatrix}$$

$$\{F^L\} = h \int_{A_1} [\Psi]^T \{f\} dA, \quad \{F^{\sigma}\} = h \int_{A_1} [B^L]^T \{\tau\} dA$$

$$\underset{(2 \times 2n)}{[\psi]} = \begin{bmatrix} \psi_1 & 0 & \psi_2 & 0 & \cdots & \psi_n & 0 \\ 0 & \psi_1 & 0 & \psi_2 & \cdots & 0 & \psi_n \end{bmatrix},$$

$$\{\tau\} = \begin{bmatrix} \tau_{11} \\ \tau_{22} \\ \tau_{12} \end{bmatrix}, \quad \{f\} = \begin{bmatrix} f_1 \\ f_2 \end{bmatrix} \tag{2.16}$$

It should be noted that ${}^1\tau_{ij}$ should be computed using the Almansi strain tensor,

$$ {}^{1}\tau_{ij} = {}^{1}C_{ijkm}\ {}^{1}\epsilon_{km} \tag{2.17} $$

where,

$$ {}^{1}\epsilon_{km} = \frac{1}{2}\left(\frac{\partial u_k}{\partial X_m} + \frac{\partial u_m}{\partial X_k} - \frac{\partial u_n}{\partial X_k}\frac{\partial u_n}{\partial X_m}\right) $$

Also, since Eq. (2.13) is a linearized version of Eq. (2.11), the error introduced into the calculation of the displacements u_i between configurations can drift the solution away from the true solution (especially, if the load steps are large). Therefore, a correction should be made to the displacements at each load step. This can be done as follows: The solution $\{\Delta u\}$ of Eq. (2.15) allows us [with the aid of Eq. (2.3)] to compute the total displacements at time $(t + \Delta t)$,

$$ {}^{2}u_i = {}^{1}u_i + \Delta u_i $$

which can be used to compute the strains and stresses (with appropriate constitutive equation) at time $t + \Delta t$. By the principle of virtual displacements, the true displacements, strains and stresses at any time, say at time $t + \Delta t$, are such that the internal virtual work is equal to the external virtual work done. Since Δu_i (hence the strains and stresses computed from them) are approximations, there will be imbalance between the internal and external virtual works performed on the body. This imbalance can be minimized by updating the internal virtual work through an iteration (for a fixed system of loads and time); the iteration is continued until the imbalance is reduced to a preassigned value (i.e., a convergence limit). For example, displacement increment

at the (r + 1)st iteration is calculated from the equations

$$([K^L] + [K^\sigma]_r)\ \{\Delta u\}_{r+1} = \{F^L\} - \{F^\sigma\}_r \qquad (2.18)$$

wherein $[\tau]$ and $\{\tau\}$ are calculated using the displacements,

$$({}^2u_i)_r = ({}^2u_i)_{r-1} + (\Delta u_i)_r \qquad (2.19)$$

Equations (2.18) and (2.19) correspond to the Newton-Raphson iteration. If the left hand side (i.e. $[K^\sigma]$) is not updated during the iteration, the iterative scheme is known as the modified Newton-Raphson iteration.

CHAPTER 3

NONLINEAR VISCOELASTIC FORMULATION

3.1 Introduction

A thermodynamically consistent theory for a single integral representation of nonlinear viscoelasticity was first proposed by Schapery [25]. The law can be derived from fundamental principles using the concepts of irreversible thermodynamics. A comprehensive review of the thermodynamics basis of Schapery's theory has been presented by Hiel et al. [55].

The following two sections deal with the review and application of Schapery's single integral constitutive law to problems with uniaxial and multiaxial states of stress respectively. The constitutive equations thus obtained are suitable for non-linear viscoelastic finite element analysis.

3.2 Uniaxial Stress State

The uniaxial nonlinear viscoelastic constitutive equation of Schapery [25] can be written for an isotropic material as,

$$\varepsilon^t = g_0^t \sigma^t D_0 + g_1^t \int_0^t \Delta D(\psi^t - \psi^s) \frac{d}{ds} [g_2^s \sigma^s] ds \qquad (3.1)$$

In Eq. (3.1), ε^t represents uniaxial kinematic strain at current time t, σ^t is the Cauchy stress at time t, D_0 is the instantaneous elastic compliance and $\Delta D(\psi)$ is a transient creep compliance function. Superscript, t, denotes current time. The factor g_0^t defines stress and temperature effects on the instantaneous elastic compliance and is a

measure of state dependent reduction (or increase) in stiffness, $g_o^t = g_o(\sigma,T)$. Transient (or creep) compliance factor g_1^t has similar meaning, operating on the creep compliance component. The factor g_2^t accounts for the influence of load rate on creep, and depends on stress and temperature. The function ψ^t represents a reduced time scale parameter defined by,

$$\psi^t = \int_0^t (a_{\sigma_T}^s)^{-1} ds \tag{3.2}$$

where, $a_{\sigma T}^s$ is a time scale 'shift factor'. For thermorheologically simple materials, $a = a(T)$ is a function of temperature T only. This function modifies, in general, viscoelastic response as a function of temperature and stress. Mathematically, $a_{\sigma T}^s$ shifts the creep data parallel to the time axis relative to a master curve for creep strain versus time. In this model, four material parameters (g_o^t, g_1^t, g_2^t and a^t) are available to characterize nonlinear behavior instead of only one with the time scale shifting procedure of Knauss and Emri [27].

The transient creep compliance, $\Delta D(\psi)$, can be expressed in the following exponential form,

$$\Delta D(\psi) = \sum_r D_r [1 - e^{-\lambda_r \psi^t}]. \tag{3.3}$$

where D_r and λ_r are constants. Substituting (3.3) in (3.1), gives,

$$\varepsilon^t = g_o^t D_o \sigma^t + g_1^t \int_0^t \sum_r D_r [1 - e^{-\lambda_r(\psi^t - \psi^s)}] \frac{d}{ds} [g_2^s \sigma^s] ds. \tag{3.4}$$

Letting the product $g_2^s \sigma^s$ be expressed as G^s and simplifying the integrand on the right hand side of Eq. (3.4) yields,

$$\varepsilon^t = g_o^t D_o \sigma^t + g_1^t \sum_r D_r \int_0^t \frac{d}{ds} G^s ds - g_1^t \sum_r D_r \int_0^t e^{-\lambda_r(\psi^t - \psi^s)} \frac{dG^s}{ds} ds. \tag{3.5}$$

The third integration term on the right hand side of Eq. (3.5) is now separated into two parts, the first part having limits from zero to $(t - \Delta t)$ and the second integral spanning only the current load step, i.e., from $(t - \Delta t)$ to t. Hence,

$$\int_0^t e^{-\lambda_r(\psi^t - \psi^s)} \frac{dG^s}{ds} ds = \int_0^{t-\Delta t} e^{-\lambda_r(\psi^t - \psi^s)} \frac{dG^s}{ds} ds + \int_{t-\Delta t}^t e^{-\lambda_r(\psi^t - \psi^s)} \frac{dG^s}{ds} ds. \tag{3.6}$$

The first term on the right hand side of Eq. (3.6) can be rewritten as,

$$\int_0^{t-\Delta t} e^{-\lambda_r(\psi^t - \psi^s)} \frac{dG^s}{ds} ds$$

$$= \int_0^{t-\Delta t} e^{-\lambda_r(\psi^t - \psi^{t-\Delta t})} e^{-\lambda_r(\psi^{t-\Delta t} - \psi^s)} \frac{dG^s}{ds} ds$$

$$= e^{-\lambda_r(\psi^t - \psi^{t-\Delta t})} \int_0^{t-\Delta t} e^{-\lambda_r(\psi^{t-\Delta t} - \psi^s)} \frac{dG^s}{ds} ds$$

$$= e^{-\lambda_r \Delta \psi^t} q_r^{t-\Delta t} \tag{3.7}$$

where,

$$\Delta\psi^t = \psi^t - \psi^{t-\Delta t} \tag{3.8}$$

$$q_r^{t-\Delta t} = \int_0^{t-\Delta t} e^{-\lambda_r(\psi^{t-\Delta t}-\psi^s)} \frac{dG^s}{ds}\, ds. \tag{3.9}$$

The second integral on the right hand side of Eq. (3.6) is now integrated by parts. To carry out the integration, it is assumed that G^t varies linearly over the current time step Δt. Hence,

$$\int_{t-\Delta t}^{t} e^{-\lambda_r(\psi^t-\psi^s)} \frac{dG^s}{ds}\, ds$$

$$= \frac{dG^s}{ds} \frac{e^{-\lambda_r(\psi^t-\psi^s)}}{\lambda_r}\Bigg|_{t-\Delta t}^{t} - \int_{t-\Delta t}^{t} \frac{d^2G^s}{ds^2} \frac{e^{-\lambda_r(\psi^t-\psi^s)}}{\lambda_r}\, ds$$

$$= \frac{dG^t}{dt} \frac{1}{\lambda_r} - \frac{dG^{t-\Delta t}}{dt} \frac{e^{-\lambda_r(\psi^t-\psi^{t-\Delta t})}}{\lambda_r}$$

$$= \frac{dG^t}{dt} \left[\frac{1 - e^{-\lambda_r \Delta\psi^t}}{\lambda_r}\right]. \tag{3.10}$$

In arriving at the second step, the fact that G^s is assumed to be linear, hence its second derivative is zero, is used. Since G^t has been assumed to be a linear function of time over the current load step Δt, we can write,

$$\frac{dG^t}{dt} = \frac{G^t - G^{t-\Delta t}}{\psi^t - \psi^{t-\Delta t}}$$

or,
$$\frac{dG^t}{dt} = \frac{G^t - G^{t-\Delta t}}{\Delta\psi^t} \tag{3.11}$$

Substituting (3.11) into (3.10), gives

$$\int_{t-\Delta t}^{t} e^{-\lambda_r(\psi^t-\psi^s)} \frac{dG^s}{ds}\, ds = [G^t - G^{t-\Delta t}][\frac{1 - e^{-\lambda_r\Delta\psi^t}}{\lambda_r\Delta\psi^t}]$$

or,
$$\int_{t-\Delta t}^{t} e^{-\lambda_r(\psi^t-\psi^s)} \frac{dG^s}{ds}\, ds = [G^t - G^{t-\Delta t}]\beta_r^t \tag{3.12}$$

where,
$$\beta_r^t = \frac{1 - e^{-\lambda_r\Delta\psi^t}}{\lambda_r\Delta\psi^t}. \tag{3.13}$$

Substituting (3.9) and (3.12) back into (3.5) and writing $G^t = g_2^t\sigma^t$

$$\varepsilon^t = g_o^t D_o\sigma^t + g_1^t \sum_r D_r g_2^t\sigma^t - g_1^t \sum_r D_r\{e^{-\lambda_r\Delta\psi^t} q_r^{t-\Delta t} + [g_2^t\sigma^t - g_2^{t-\Delta t}\sigma^{t-\Delta t}]\beta_r^t\}. \tag{3.14}$$

Collecting those terms in Eq. (3.14) that are multiplied by current stress σ^t yields,

$$\varepsilon^t = [g_o^t D_o + g_1^t g_2^t \sum_r D_r - g_1^t g_2^t \sum_r D_r\beta_r^t]\sigma^t + g_1^t\{\sum_r D_r[g_2^{t-\Delta t}\beta_r^t\sigma^{t-\Delta t} - e^{-\lambda_r\Delta\psi^t} q_r^{t-\Delta t}]\}. \tag{3.15}$$

Defining instantaneous compliance D_I^t as the compliance term multiplying the instantaneous stress σ^t, and the remaining terms in Eq.

(3.15) as hereditary strains E^t, yields,

$$\varepsilon^t = D_I^t \sigma^t + E^t \equiv F(\sigma) \tag{3.16}$$

where,

$$D_I^t = g_o^t D_o^t + g_1^t g_2^t \sum_r D_r - g_1^t g_2^t \sum_r D_r \beta_r^t \tag{3.17}$$

$$E^t = g_1^t \{ \sum_r D_r [g_2^{t-\Delta t} \beta_r^t \sigma^{t-\Delta t} - e^{-\lambda_r \Delta \psi^t} q_r^{t-\Delta t}] \}. \tag{3.18}$$

Hence, Eq. (3.16) expresses Schapery's single integral constitutive law in terms of a stress operator that includes instantaneous compliance and hereditary strains.

It is to be noted that the term $q_r^{t-\Delta t}$ in Eq. (3.18) is the r^{th} component of the hereditary integral series at the end of the previous load step (i.e. at time equals $t - \Delta t$). The expression for the hereditary integral at the end of the current load step (i.e. at time t) can be derived in the form of a recurrence formula as shown below.

By definition [see. Eq. (3.9)],

$$q_r^t = \int_0^t e^{-\lambda_r (\psi^t - \psi^s)} \frac{dG^s}{ds} ds$$

$$= \int_0^{t-\Delta t} e^{-\lambda_r (\psi^t - \psi^s)} \frac{dG^s}{ds} ds + \int_{t-\Delta t}^t e^{-\lambda_r (\psi^t - \psi^s)} \frac{dG^s}{ds} ds. \tag{3.19}$$

Using the results from Eqs. (3.9) and (3.12), the above equation reduces to,

$$q_r^t = e^{-\lambda_r \Delta\psi^t} q_r^{t-\Delta t} + [g_2^{t}\sigma^{t} - g_2^{t-\Delta t}\sigma^{t-\Delta t}]\beta_r^t \tag{3.20}$$

where β_r^t is defined by Eq. (3.13).

3.3 Multiaxial Stress State

For a thermorheologically simple anisotropic viscoelastic material under a multiaxial state of stress, the constitutive law proposed by Schapery [25] is,

$$e_{ij} = -\frac{\partial G_R}{\partial \sigma_{ij}} + \frac{\partial \hat{\sigma}_{mn}}{\partial \sigma_{ij}} \Delta\hat{e}_{mn} \tag{3.21}$$

$$\Delta\hat{e}_{mn} = \int_{-\infty}^{t} \Delta S_{mn}^{ij}(\psi^t - \psi^\tau) \frac{\partial}{\partial \tau} (\hat{\sigma}_{ij}/a_G) d\tau \tag{3.22}$$

where, e_{ij} and σ_{ij} are the strain and stress tensors respectively, G_R is the Gibbs free energy, $\hat{\sigma}_{ij}$ and ΔS_{mn}^{ij} are second and fourth order material property tensors respectively and a_G is a material kernel function defined in [25]. The quantities G_R, a_G and $\hat{\sigma}_{mn}$ are, in general, functions of ten variables, σ_{ij} and temperature T. Note that all repeated indices in Eqs. (3.21) and (3.22) are to be summed out over their range (1,2,3).

Due to the complex nature of Eq. (3.21) it is not possible to determine the material properties in this equation from the uniaxial tests outlined in [25]. However, it is possible to construct a set of small strain, three dimensional constitutive equations from (3.21), which is consistent with the thermodynamic theory in [25], and which yet enables all properties to be evaluated from uniaxial tests. The

assumptions which need to be made for this purpose are as follows:

(a) The Gibb's free energy G_R is a quadratic function of stress.

(b) $\hat{\sigma}_{ij} = \sigma_{ij}$ (3.23)

When the free energy G_R is a quadratic function of stress,

$$-\frac{\partial G_R}{\partial \sigma_{ij}} = S_{ij}^{mn}(0)\sigma_{mn} \tag{3.24}$$

where $S_{ij}^{mn}(0)$ are the instantaneous components of the linear viscoelastic creep compliance tensor. Equation (3.24) implies that the initial response of the material is linearly elastic under suddenly applied stresses, which is often the case for metals and plastics.

The second assumption, on the other hand, leads to the linearization of the coefficient of the transient term in Eq. (3.21). Mathematically, this is given by,

$$\frac{\partial \hat{\sigma}_{mn}}{\partial \sigma_{ij}} = \begin{cases} 1, & \text{if } i = m \text{ and } j = n \\ 0, & \text{if } i \neq m \text{ and } j \neq n \end{cases} \tag{3.25}$$

Equation (3.25) implies that the jump in strain due to load application equals the jump when the load is removed. This behavior is exhibited by some types of plastics [56].

Substituting Eqs. (3.24) and (3.25) in (3.21) and (3.22),

$$e_{ij}^t = S_{ij}^{mn}(0)\sigma_{mn} + \Delta\hat{e}_{ij}^t \tag{3.26}$$

$$\Delta\hat{e}_{ij}^t = \int_{-\infty}^{t} \Delta S_{ij}^{mn}(\psi^t - \psi^\tau)\frac{\partial}{\partial \tau}(g_2^\tau \sigma_{mn}^\tau)d\tau \tag{3.27}$$

where, $g_2^\tau = 1/a_G^\tau$. Superscript, t, denotes current time. Equation (3.26) is a set of three dimensional constitutive equations for

anisostropic viscoelastic materials which includes the nonlinear functions g_2^t and $a_{\sigma T}^t$ appearing in the uniaxial relations (3.1) and (3.2). Note that the functions g_2^t and $a_{\sigma T}^t$ are expressed as a function of the octrahedral shear stress, which is a stress invariant.

For a homogeneous isotropic nonlinear viscoelastic material, Eq. (3.25) reduces to the form presented by Schapery ([25] and [56]),

$$e_{ij}^t = \{J\}\{g_2^t \sigma_{ij}^t\} + \{D - J\}\{g_2^t \sigma_{mm}^t\}\delta_{ij} \tag{3.28}$$

where,

$$\{J\}\{g_2^t \sigma_{ij}^t\} = J(0)\sigma_{ij} + \int_0^t \Delta J(\psi^t - \psi^\tau) \frac{\partial}{\partial \tau} (g_2^\tau \sigma_{ij}^\tau) d\tau \tag{3.29}$$

$$\{D - J\}\{g_2^t \sigma_{mm}^t\} = [D(0) - J(0)]\sigma_{mm}^t + \int_0^t [\Delta D(\psi^t - \psi^\tau) - \Delta J(\psi^t - \psi^\tau)] \frac{\partial}{\partial \tau} (g_2^\tau \sigma_{mm}^\tau) d\tau \tag{3.30}$$

in which,

$$\psi^t - \psi^\tau = \int_\tau^t (a_{\sigma T})^{-1} ds \tag{3.31}$$

Expanding Eq. (3.28) term by term for the strains,

$$e_{11}^t = \{J\}\{g_2^t \sigma_{11}^t\} + \{D - J\}\{g_2^t \sigma_{11}^t + g_2^t \sigma_{22}^t + g_2^t \sigma_{33}^t\}$$

Arranging terms,

$$e_{11}^t = \{D\}\{g_2^t \sigma_{11}^t\} + \{D - J\}\{g_2^t \sigma_{22}^t\} + \{D - J\}\{g_2^t \sigma_{33}^t\} \tag{3.32}$$

Similarly,

$$e_{22}^t = \{D - J\}\{g_2^t\sigma_{11}^t\} + \{D\}\{g_2^t\sigma_{22}^t\} + \{D - J\}\{g_2^t\sigma_{33}^t\} \tag{3.33}$$

$$\gamma_{12}^t = 2\{J\}\{g_2^t\sigma_{12}^t\} \tag{3.34}$$

$$e_{33}^t = \{D - J\}\{g_2^t\sigma_{11}^t\} + \{D - J\}\{g_2^t\sigma_{22}^t\} + \{D\}\{g_2^t\sigma_{33}^t\} \tag{3.35}$$

The transient components of the creep and shear compliances can be written in the form of Prony series as,

$$\Delta D(\psi) = \sum_r D_r[1 - e^{-\lambda_r\psi}] \tag{3.36}$$

$$\Delta J(\psi) = \sum_r J_r[1 - e^{-\eta_r\psi}] \tag{3.37}$$

where λ_r and η_r are the reciprocal of the retardation times in creep and shear respectively. Also, let,

$$D(0) = D_o \tag{3.38}$$

$$J(0) = J_o \tag{3.39}$$

Considering a term of the form $\{D\}\{g_2^t\sigma_{ij}^t\}$ in Eq. (3.32) and substituting Eqs. (3.36) to (3.39) gives,

$$\{D\}\{g_2^t\sigma_{ij}^t\} = D_o\sigma_{ij}^t + \int_0^t \sum_r D_r[1 - e^{-\lambda_r(\psi^t - \psi^\tau)}] \frac{d}{d\tau}[g_2^\tau\sigma_{ij}^\tau]d\tau \tag{3.40}$$

Recognizing that Eq. (3.40) is similar in appearance to Eq. (3.6) and making use of the results derived in Section 3.2,

$$\{D\}\{g_2^t\sigma_{ij}^t\} = D_I^t\sigma_{ij}^t + Q_{ij}^t \tag{3.41}$$

where D_I^t is the instantaneous creep compliance function at time t, given

by,

$$D_I^t = D_o + g_2^t \sum_r D_r(1 - \beta_r^t), \tag{3.42}$$

Q_{ij}^t are the hereditary strain components due to tensile creep at time t,

$$Q_{ij}^t = \sum_r [g_2^{t-\Delta t}\beta_r^t\sigma_{ij}^{t-\Delta t} - e^{-\lambda_r\Delta\psi^t} q_{r,ij}^{t-\Delta t}] \tag{3.43}$$

$$\beta_r^t = \frac{1 - e^{-\lambda_r\Delta\psi^t}}{\lambda_r\Delta\psi^t} \tag{3.44}$$

and, $q_{r,ij}^t$ are components of the hereditary integral given by the recurrence formula,

$$q_{r,ij}^t = e^{-\lambda_r\Delta\psi^t} q_{r,ij}^{t-\Delta t} + [g_2^t\sigma_{ij}^t - g_2^{t-\Delta t}\sigma_{ij}^{t-\Delta t}]\beta_r^t \tag{3.45}$$

Similarly, a term of the form $\{J\}\{g_2^t\sigma_{ij}^t\}$ in Eq. (3.32) can be expressed as,

$$\{J\}\{g_2^t\sigma_{ij}^t\} = J_I^t\sigma_{ij}^t + P_{ij}^t \tag{3.46}$$

where, J_I^t is the instantaneous shear compliance function at time t, and is given by,

$$J_I^t = J_o + g_2^t \sum_r J_r(1 - \Gamma_r^t), \tag{3.47}$$

P_{ij}^t are the hereditary strain components due to shear at time t,

$$P_{ij}^t = \sum_r [g_2^{t-\Delta t}\Gamma_r^t\sigma_{ij}^{t-\Delta t} - e^{-\eta_r\Delta\psi^t} p_{r,ij}^{t-\Delta t}] \tag{3.48}$$

$$\Gamma_r^t = \frac{1 - e^{-\eta_r \Delta\psi^t}}{\eta_r \Delta\psi^t} \tag{3.49}$$

and, $p_{r,ij}^t$ are components of the hereditary integral given by the recurrence formula;

$$p_{r,ij}^t = e^{-\eta_r \Delta\psi^t} p_{r,ij}^{t-\Delta t} + [g_2^t \sigma_{ij}^t - g_2^{t-\Delta t} \sigma_{ij}^{t-\Delta t}] \Gamma_r^t \tag{3.50}$$

Substituting Eq. (3.41) and (3.46) in Eqs. (3.32) to (3.35), and dropping superscripts, gives,

$$e_{11} = D_1 \sigma_{11} + (D_I - J_I)\sigma_{22} + (D_I - J_I)\sigma_{33} + H_{11} \tag{3.51}$$

$$e_{22} = (D_I - J_I)\sigma_{11} + D_I \sigma_{22} + (D_I - J_I)\sigma_{33} + H_{22} \tag{3.52}$$

$$\gamma_{12} = 2J_I \sigma_{12} + H_{12} \tag{3.53}$$

$$e_{33} = (D_I - J_I)\sigma_{11} + (D_I - J_I)\sigma_{22} + D_I \sigma_{33} + H_{33} \tag{3.54}$$

where,

$$H_{11} = Q_{11} + Q_{22} + Q_{33} - P_{22} - P_{33} \tag{3.55}$$

$$H_{22} = Q_{11} + Q_{22} + Q_{33} - P_{11} - P_{33} \tag{3.56}$$

$$H_{12} = 2P_{12} \tag{3.57}$$

$$H_{33} = Q_{11} + Q_{22} + Q_{33} - P_{11} - P_{22}. \tag{3.58}$$

Written in form of a matrix equation, this becomes,

$$\{e\} = [N]\{\sigma\} + \{H\}. \tag{3.59}$$

Note that the left hand side of Eq. (3.59) is a vector containing the algebraic difference of kinematic strains $\{\varepsilon\}$ and dilatational strains $\{\delta_{ij}\theta\}$,

$$\{e\}^T = \{(\varepsilon_{11} - \theta),(\varepsilon_{22} - \theta),\gamma_{12},(\varepsilon_{33} - \theta)\} \tag{3.60}$$

while, $\{\sigma\}$ contains four components of Cauchy stress,

$$\{\sigma\}^T = \{\sigma_{11},\sigma_{22},\sigma_{12},\sigma_{33}\} \tag{3.61}$$

and $\{H\}$ is a vector of hereditary strains given by,

$$\{H\}^T = \{H_{11},H_{22},H_{12},H_{33}\}. \tag{3.62}$$

The matrix [N] is a 4 x 4 coefficient matrix given by,

$$[N] = \begin{bmatrix} D_I & (D_I-J_I) & 0 & (D_I-J_I) \\ (D_I-J_I) & D_I & 0 & (D_I-J_I) \\ 0 & 0 & 2J_1 & 0 \\ (D_I-J_I) & (D_I-J_I) & 0 & D_I \end{bmatrix} \tag{3.63}$$

Pre-multiplying Eq. (3.59) by $[N]^{-1}$, an explicit expression for stresses in terms of strains is obtained,

$$\{\sigma\} = [M](\{e\} - \{H\}) \tag{3.64}$$

where,

$$[M] = [N]^{-1} \tag{3.65}$$

Equations (3.64) and (3.65) provide a general viscoelastic constitutive relation that can be applied to either plane stress, plane strain or axisymmetric problems. For plane strain, the out-of-plane strain component e_{33} is identically zero. The corresponding stress component, σ_{33}, may be obtained from Eq. (3.64) by setting $e_{33} = 0$. Since for the plane stress case, σ_{33} is identically zero, the corresponding strain component e_{33} can be evaluated from Eqs. (3.59) and (3.63) as,

$$e_{33} = (D_I - J_I)(\sigma_{11} + \sigma_{22}) + H_{33} \tag{3.66}$$

Note that the use of creep and shear compliances as material property input allows the Poisson's ratio to be time-dependent. Hence, the present formulation is applicable to any thermorheologically simple isotropic viscoelastic material over any length of time.

For the special case where the Poisson's ratio is a constant with time, then,

$$J(\psi) = (1 + \nu)D(\psi). \tag{3.67}$$

The matrix [N] in Eq. (3.59) takes the form,

$$[N] = D_I \begin{bmatrix} 1 & -\nu & 0 & -\nu \\ -\nu & 1 & 0 & -\nu \\ 0 & 0 & 2(1+\nu) & 0 \\ -\nu & -\nu & 0 & 1 \end{bmatrix} \tag{3.68}$$

and, the corresponding hereditary strains are,

$$H_{11} = Q_{11} - \nu(Q_{22} + Q_{33}) \tag{3.69}$$

$$H_{22} = Q_{22} - \nu(Q_{11} + Q_{33}) \tag{3.70}$$

$$H_{12} = 2(1 + \nu)Q_{12} \tag{3.71}$$

$$H_{33} = Q_{33} - \nu(Q_{11} + Q_{22}) \tag{3.72}$$

If the viscoelastic properties of a material are defined by its bulk and shear compliances instead of the creep and shear compliances, then the creep compliance $D(\psi)$ in Eq. (3.28) is replaced by the bulk and shear properties. Using the viscoelastic relationship betwen creep, bulk and shear compliances given by,

$$D(\psi) = \frac{1}{9} M(\psi) + \frac{2}{3} J(\psi) \tag{3.73}$$

and substituting in Eq. (3.28), the matrix relation given by (3.59) is obtained. However, for this case the matrix [N] has the form,

$$[N] = \begin{bmatrix} (\frac{1}{9} M_I + \frac{2}{3} J_I) & (\frac{1}{9} M_I - \frac{1}{3} J_I) & 0 & (\frac{1}{9} M_I - \frac{1}{3} J_I) \\ (\frac{1}{9} M_I - \frac{1}{3} J_I) & (\frac{1}{9} M_I + \frac{2}{3} J_I) & 0 & (\frac{1}{9} M_I - \frac{1}{3} J_I) \\ 0 & 0 & 2J_I & 0 \\ (\frac{1}{9} M_I - \frac{1}{3} J_I) & (\frac{1}{9} M_I - \frac{1}{3} J_I) & 0 & (\frac{1}{9} M_I + \frac{2}{3} J_I) \end{bmatrix} \tag{3.74}$$

and the corresponding hereditary strains are,

$$H_{11} = \frac{1}{9}(Q_{11} + Q_{22} + Q_{33}) + \frac{2}{3}P_{11} - \frac{1}{3}(P_{22} + P_{33}) \quad (3.75)$$

$$H_{22} = \frac{1}{9}(Q_{11} + Q_{22} + Q_{33}) + \frac{2}{3}P_{22} - \frac{1}{3}(P_{11} + P_{33}) \quad (3.76)$$

$$H_{12} = 2P_{12} \quad (3.77)$$

$$H_{33} = \frac{1}{9}(Q_{11} + Q_{22} + Q_{33}) + \frac{2}{3}P_{33} - \frac{1}{3}(P_{11} + P_{22}) \quad (3.78)$$

3.4 Finite Element Model

This section describes the finite element implementation of the nonlinear viscoelastic constitutive law presented in Sections 3.2 and 3.3. Since viscoelastic materials often undergo large displacements especially when subjected to creep type of loading, the geometrically nonlinear analysis described in Chapter 2 has been incorporated into the viscoelastic formulation.

Invoking the principle of virtual work and following the procedure outlined in Section 2.2 gives,

$$\int_{v_1} {}^1M_{ijrs}\, {}^1e_{rs}\delta({}^1e_{ij})dV + \int_{v_1} {}^1\tau_{ij}\delta({}^1\eta_{ij})dV$$

$$= -\int_{v_1} {}^1\tau_{ij}\delta({}^1e_{ij})dV + \int_{v_1} {}^1f_i\delta u_i dV + \int_{s_1} {}^1t_i\delta u_i dS \quad (3.79)$$

where, ${}^1M_{ijrs}$ are the components of the viscoelasticity constitutive tensor. The rest of the quantities and the superscripts in Eq. (3.79) have the same definitions as in Section 2.2. Let each displacement increment at any time t, be approximated as,

$$\Delta u_i = \sum_{j=1}^{n} \Delta u_i^j \psi_j(x_1, x_2). \tag{3.80}$$

Substituting Eq. (3.80) into Eq. (3.79) gives,

$$([K^L] + [K^\sigma])\{\Delta u\} = \{F^L\} - \{F^\sigma\} \tag{3.81}$$

where,

$$[K^L] = h\int_{A_1} [B^L]^T[M][B^L]dA, \quad h = \text{thickness} \tag{3.82}$$

and [M] is the 4x4 viscoelastic constitutive matrix defined in Eq. (3.65). Note that for the nonlinear viscoelastic case, the 'linear' stiffness matrix $[K^L]$ is not really linear, but has nonlinearities imbedded in it due to the presence of the material kernel functions (g_0, g_1, g_2) in the matrix [M]. The nonlinear stiffness matrix $[K^\sigma]$ is the direct result of the geometrically nonlinear formulation and is given by,

$$[K^\sigma] = h\int_{A_1} [B^\sigma]^T[\tau][B^\sigma]dA \tag{3.83}$$

The definitions of matrices $[B^L]$, $[B^\sigma]$, $\{F^L\}$, $\{F^\sigma\}$ and $[\tau]$ are the same as in Eq. (2.16). The Cauchy stress components, are computed by using the viscoelastic relation,

$$\{\sigma\} = [M](\{e\} - \{H\}) \tag{3.84}$$

which has been derived in Section 3.3. For a geometrically nonlinear analysis, the vector $\{e\}$ contains components of the Almansi strain tensor given by,

$$e_{km} = \frac{1}{2}\left(\frac{\partial u_k}{\partial x_m} + \frac{\partial u_m}{\partial x_k} - \frac{\partial u_n}{\partial x_k}\frac{\partial u_n}{\partial x_m}\right) - \delta_{km}\theta \tag{3.85}$$

It is evident that Eq. (3.81) contains two possible sources of nonlinearities: material nonlinearity due to Schapery's law and, geometric nonlinearity arising from the large displacement formulation. In order to obtain a solution to this nonlinear equation at any time step, the Newton-Raphson iterative technique is used. The incremental displacement $\{\Delta u\}_r$ obtained at the end of the r^{th} iteration is used to update the total displacement for the n^{th} time step,

$$^{n}u_r = {}^{n}u_{r-1} + \Delta^{n}u_r \tag{3.86}$$

The iterative procedure continues until a convergence criterion is satisfied. After that, the solution proceeds to the next time step. Note that for the first time-step, $^{n}u_{r-1} = 0$.

The complete solution procedure for each individual time step is presented in a logical step-wise fashion and can be used directly for programming purposes:

1. At the beginning of each time step, the stress vector $\{\sigma\}$ from the previous time step is accessed. Note that for the initial or starting time step, the stress vector $\sigma(t - \Delta t)$ denotes the initial stress state at $t = 0$, given by $\{\sigma^o\}$. Since it is customary to assume a stress free state to exist at the start of the solution, $\{\sigma^o\}$ is usually set to be zero.
2. Temperature T at time t is computed from $T = f(t)$ which is supplied by the user for problems involving thermal loads.

3. The parameters g_0, g_1, g_2, and $a_{\sigma T}^t$, which are known functions of temperature and stress, are evaluated next, using the stress vector obtained from previous load step.

4. Assuming $a_{\sigma T}^t$ to be a linear function of time over the time step Δt, the average value of shift factor is given as $a_{\sigma T_{avg}}^t = (a_{\sigma T}^{t-\Delta t} + a_{\sigma T}^t)/2$ and the change in reduced time $\Delta\psi^t$ is computed as $\Delta\psi^t = \Delta t/a_{\sigma T_{avg}}^t$. In order for this assumption to be valid Δt should be made sufficiently small.

5. Hereditary integral $\{q_r^t\}$ is computed using the recursive formula given by Eq. (3.45).

6. $\{F_{ext}\} = \lambda[F_{app}\}$ where λ is the load factor that corresponds to the time step under consideration.

7. The residual vector $\{R\}$ is computed for each element as,

$$\{R\}^e = \{F_{ext}\}^e - \int_{V_e} [B]^T\{\sigma\}^e dV.$$

8. The tangent stiffness matrix $[K_T]^e = \int_{v_e} [B]^T[M][B]dv.$

9. Incremental displacement $\{\Delta u\} = [K_T]^{-1}\{R\}$.

10. Total displacement $\{u\}_i = \{u\}_{i-1} + \{\Delta u\}_i$ where the subscript i denotes the number of iterations.

11. The strains and stresses are computed using the known displacement.

12. Steps 3 through 12 are repeated till $\dfrac{\|\{\Delta u_i\}\|}{\|\{u_i\}\|} <$ tolerance.

13. Solution proceeds to the next time step for which steps 1 through 12 are repeated.

CHAPTER 4

MOISTURE DIFFUSION AND DELAYED FAILURE

4.1 Governing Equations for Diffusion

The nonlinear Fickean two-dimensional, diffusion model presented in the present study is the one investigated by Lefebvre, et al. [51]. The diffusion model can also be applied for penetrants other than moisture.

Fick's law for the two-dimensional diffusion of a penetrant within an isotropic material is given by,

$$\frac{\partial}{\partial x}\left(D\,\frac{\partial c}{\partial x}\right) + \frac{\partial}{\partial y}\left(D\,\frac{\partial c}{\partial y}\right) = \frac{\partial c}{\partial t} \qquad (4.1)$$

where, c is the penetrant concentration, which is a function of position and time, and D is the diffusion coefficient.

In order to model the transport phenomena in polymeric materials, Lefebvre et al. [51] derived a nonlinear diffusion coefficient based on the concept of free volume.

According to this theory, the diffusion coefficient for a polymeric material above its glass transition temperature is given by,

$$D = \frac{D_o}{T_o}\,T e^{-B\{1/f - 1/f_o\}} \qquad (4.2)$$

where, D is the diffusion coefficient, T is the temperature, f is the free volume fraction, and B is a material constant. The subscript 'o' denotes values at the reference state. It is then postulated that the change in fractional free volume is due to changes in temperature,

penetrant concentration, and the transient component of the mechanically induced dilatational strain. It is further assumed that these changes are additive, which is similar to the assumptions made by Knauss and Emri [27], giving,

$$f = f_o + 3\alpha\Delta T + \Delta e_{kk} + 3\gamma c^N \tag{4.3}$$

In Eq. (4.3), α is the linear coefficient of thermal expansion, γ is the linear coefficient of expansion due to moisture, N is an exponent for the saturated state, and Δe_{kk} is the transient component of the mechanically induced dilatational strain. The dilatational strain due to the ambient stress state can be written as,

$$e_{kk} = e_{kk}(0) + \Delta e_{kk} \tag{4.4}$$

where $e_{kk}(0)$ and Δe_{kk} are the instantaneous and transient components of the mechanically induced dilatational strain e_{kk}. Hence,

$$e_{kk}(0) = \frac{1}{3} M(0)\sigma_{kk} \tag{4.5}$$

and

$$\Delta e_{kk} = \frac{1}{3} \int_0^t M(\psi^t - \psi^\tau) \frac{\partial}{\partial \tau} (g_2 \sigma_{kk}) d\tau \tag{4.6}$$

where $M(\psi)$ is the bulk compliance of the material. Combining Eqs. (4.4) and(4.5),

$$\Delta e_{kk} = e_{kk} - \frac{1}{3} M(0)\sigma_{kk} \tag{4.7}$$

Substituting (4.7) in (4.3),

$$f = f_o + 3\alpha\Delta T + \{e_{kk} - \frac{1}{3} M(0)\sigma_{kk}\} + 3\gamma c^N \tag{4.8}$$

Substituting (4.8) in (4.2) gives,

$$D = \frac{D_o}{T_o} T \exp\left\{\frac{B}{f_o}\left[\frac{3(\alpha\Delta T + \gamma c^N) + (e_{kk} - \frac{1}{3} M_o \sigma_{kk})}{f_o + 3(\alpha\Delta T + \gamma c^N) + (e_{kk} - \frac{1}{3} M_o \sigma_{kk})}\right]\right\} \qquad (4.9)$$

From the viscoelastic formulation presented in Chapter 3, it is evident that the dilatational strain e_{kk} is dependent on the stress history, temperature and penetrant concentration, that is,

$$e_{kk} = e_{kk}(\sigma_{kk}, T, c) \qquad (4.10)$$

Hence, the two sources of nonlinearity in Eq. (4.1) are moisture concentration c, and dilatational strain e_{kk}. Consequently, in order to accurately model the penetrant transport phenomena, the diffusion boundary-value problem needs to be solved in conjunction with the nonlinear viscoelasticity boundary-value problem by using an iterative procedure. The same solution procedure can also be applied for diffusion in polymeric materials where the plasticizing effect of the penetrant may cause the viscoelastic time-scale shift factor to be concentration dependent, that is,

$$a^t_{\sigma Tc} = a(\sigma, T, c) \qquad (4.11)$$

One example of such a shift factor definition can be found in the work of Knauss and Emri [27], where the authors have used the unifying concept of free volume to define a shift factor given by,

$$a(T, c, e_{kk}) = \exp\left\{-\frac{B}{f_o}\left(\frac{\alpha\Delta T + \gamma c + \delta e_{kk}}{f_o + \alpha\Delta T + \gamma c + \delta e_{kk}}\right)\right\} \qquad (4.12)$$

where δ is the coefficient of the dilatation term. Note that the coefficients α and γ in Eqs. (4.9) and (4.12) are, in general, functions

of T, c and e_{kk} but have been assumed to be constant for the sake of simplicity. This assumption is valid for temperatures above the glass transition temperature.

4.2 Finite Element Formulation

Fick's law for two dimensional diffusion in a homogeneous isotropic material is given by,

$$\frac{\partial}{\partial x}\left(D\frac{\partial c}{\partial x}\right) + \frac{\partial}{\partial y}\left(\frac{\partial c}{\partial y}\right) = \frac{\partial c}{\partial t} \quad \text{in } \Omega \tag{4.13}$$

subject to the boundary conditions,

$$D\frac{\partial c}{\partial x}n_x + D\frac{\partial c}{\partial y}n_y + \hat{q} = 0 \text{ on } \Gamma_1 \quad , \quad t \geq 0 \tag{4.14}$$

and

$$c = \hat{c} \text{ on } \Gamma_2 \quad , \quad t \geq 0 \tag{4.15}$$

with the initial condition,

$$c = c_o \text{ in } \Omega \quad , \quad t = 0 \tag{4.16}$$

where, Ω is the two dimensional region in which diffusion occurs, and Γ is the boundary to this region.

The finite element formulation for Eq. (4.13) incorporating the initial and boundary conditions (Eqs. (4.14) to (4.16)) was carried out following the variational procedure used by Reddy [54]. The time dependent moisture concentration is approximated as,

$$c(x,y,t) = \sum_{j=1}^{n} \psi_j(x,y)c_j(t) \tag{4.17}$$

The resulting finite element equations cast in a matrix form are given by,

$$[M^{(e)}]\{\dot{c}\} + [K^{(e)}]\{c\} = \{F^{(e)}\} \tag{4.18}$$

where,

$$M_{ij}^{(e)} = \int_{\Omega^e} \psi_i \psi_j dxdy \tag{4.19}$$

$$K_{ij}^{(e)} = \int_{\Omega^e} D\left(\frac{\partial \psi_i}{\partial x}\frac{\partial \psi_j}{\partial x} + \frac{\partial \psi_i}{\partial y}\frac{\partial \psi_j}{\partial y}\right)dxdy \tag{4.20}$$

$$F_i^{(e)} = -\int_{\Gamma^e} \psi_i \hat{q} ds \tag{4.21}$$

The superscript (e) is used to denote that the equations are valid over each element. The range of the subscripts i and j is equal to the number of nodes per element.

The time derivative $\{\dot{c}\}$ is approximated using a θ family of approximations given by,

$$\theta\{\dot{c}\}_{n+1} + (1 - \theta)\{\dot{c}\}_n = \frac{\{c\}_{n+1} - \{c\}_n}{\Delta t_{n+1}} \quad \text{for } 0 \le \theta \le 1 \tag{4.22}$$

where, n is the time step. Using the approximations (4.22) in (4.18) for time t_n and t_{n+1} gives,

$$[A^{(e)}]\{c\}_{n+1} - [B^{(e)}]\{c\}_n - \{P^{(e)}\}_n = 0 \tag{4.23}$$

where,

$$[A^{(e)}] = [M^{(e)}] + \theta\Delta t_{n+1}[K^{(e)}] \tag{4.24}$$

$$[B^{(e)}] = [M^{(e)}] - (1 - \theta)\Delta t_{n+1}[K^{(e)}] \tag{4.25}$$

$$\{p^{(e)}\} = \Delta t_{n+1}(\theta\{F^{(e)}\}_{n+1} + (1 - \theta)\{F^{(e)}\}_{n}) \tag{4.26}$$

Recognizing that a source of nonlinearity in the form of the diffusion coefficient D is imbedded in the matrix $[K^{(e)}]$, the Newton-Raphson technique is employed to solve for the concentration $\{c\}_{n+1}$ at each time step. Note that for n = 1, the value of $\{c\}$ in Eq. (4.23) is known from initial conditions.

4.3 Delayed Failure: Uniaxial Formulation

When a viscoelastic material undergoes deformation, only a part of the total deformation energy is stored, while the rest of the energy is dissipated. This behavior is unlike elastic material where all the energy of deformation is stored as strain energy. Reiner and Weisenberg [44] postulated that it is this time-dependent energy storage capacity that is responsible for the transition from viscoelastic response to yield in ductile materials or fracture in brittle ones. According to this theory, failure occurs when the stored deviatoric strain energy per unit volume in a body reaches a certain maximum value called the resilience, which is a material property. Note that when there is no dissipation, that is, when the material is elastic, then Reiner-Weisenberg criterion becomes identical to the von Mises criterion.

Consider the single Kelvin element shown in Fig. 1, subject to the uniaxial tensile load $\sigma(t)$. The total strain response $e(t)$ due to the applied stress can be divided into two components: the instantaneous respone e_o, and the transient response $e_1(t)$. Hence,

$$e(t) = e_o + e_1(t) \tag{4.27}$$

For uniaxial creep, the applied stress $\sigma(t)$ is given as,

$$\sigma(t) = \sigma_o H(t) \tag{4.28}$$

where $H(t)$ is the unit step function.

Substituting Eq. (4.28) into Schapery's nonlinear uniaxial single integral law given by Eq.(3.1), and expressing the transient creep compliance $D_c(\psi)$ as,

$$D_c(\psi) = D_o - D_1(1 - e^{-\lambda_1 \psi}) \tag{4.29}$$

results in,

$$e(\psi) = g_o D_o \sigma_o + g_1 g_2 \sigma_o D_1 (1 - e^{-\lambda_1 \psi}) \tag{4.30}$$

where ψ is the reduced time defined in Eq. (3.2).

Comparing Eq. (4.30) with (4.27),

$$e_o = g_o D_o \sigma_o \tag{4.31}$$

$$e_1(\psi) = g_1 D_1 (1 - e^{-\lambda_r \psi}) g_2 \sigma_o \tag{4.32}$$

For a given applied stress σ_o, stress developed in the nonlinear spring with compliance $D_o g_o$ is σ_o^s and the corresponding strain is e_o^s. For the spring with the nonlinear compliance $D_1 g_1$, the stress is given by,

$$\sigma_1^s = \frac{e_1^s}{g_1 D_1} \tag{4.33}$$

where the superscript 's' denotes quantities related to the springs. From Fig. 1 it is evident that e_1^s and e_1 are equivalent. Hence,

$$\sigma_1^s = g_2(1 - e^{-\lambda_1 \psi})\sigma_o \tag{4.34}$$

The total energy, W^s, stored in the two springs over time t is (see Hiel et al. [55]),

$$W^s = \int_0^{e_o} \sigma_o^s de + \int_0^t \sigma_1^s \dot{e}_1^s dt \tag{4.35}$$

Using results from Eqs. (4.31), (4.33), and (4.34), Eq. (4.35) becomes,

$$W^s = \frac{1}{2} g_o D_o \sigma_o^2 + \frac{1}{2} g_1 D_1 [1 - e^{-\lambda_1 \psi}]^2 (g_2 \sigma_o)^2 \tag{4.36}$$

For a viscoelastic material represented by multiple Kelvin elements in series, Eq. (4.36) takes the form,

$$W^s = \frac{1}{2} g_o D_o \sigma_o^2 + \frac{1}{2} g_1 g_2^2 \sigma_o^2 \sum_{r=1}^{n} [D_r(1 - e^{-\lambda_r \psi})^2] \tag{4.37}$$

According to the Reiner-Weisenberg hypothesis, failure occurs when the stored energy W^s reaches the resilience of the material. Denoting the resilience as R, the expression for the time dependent failure stress obtained from Eq. (4.37) for uniaxial stress state is,

$$\sigma_f = \frac{\sqrt{R}}{\{\frac{1}{2} g_o D_o + \frac{1}{2} g_1 g_2^2 \sum_{r=1}^{n} [D_r(1 - e^{-\lambda_r \psi})^2]\}^{1/2}} \tag{4.38}$$

4.4 Delayed Failure: Multiaxial Formulation

If σ_1, σ_2 and σ_3 are the principal stresses at any point in a viscoelastic material, then by definition, the shear stresses are zero on the principal planes. In order to simplify the derivation, let it be assumed that the viscoelastic material is represented by means of a single Kelvin element (see Fig. 1) in each principal direction. The applied multiaxial creep stresses in the material principal directions are given by,

$$\sigma_{11} = \sigma_1 H(t) \tag{4.39}$$

$$\sigma_{22} = \sigma_2 H(t) \tag{4.40}$$

$$\sigma_{33} = \sigma_3 H(t) \tag{4.41}$$

Substituting Eqs. (4.39), (4.40) and (4.41) in Eqs. (3.32), (3.33) and (3.35) result in the following expressions for the corresponding viscoelastic strains,

$$e_{11}(t) = D_o[\sigma_1 + (1 - \frac{J_o}{D_o})\sigma_2 + (1 - \frac{J_o}{D_o})\sigma_3] + D_1[(1 - e^{-\lambda_r \psi})g_2\sigma_1$$

$$+ \{(1 - e^{-\lambda_r \psi}) + \frac{J_1}{D_1}(1 - e^{-\eta_r \psi})\}g_2\sigma_2 + \{(1 - e^{-\lambda_r \psi})$$

$$+ \frac{J_1}{D_1}(1 - e^{-\eta_r \psi})\}g_2\sigma_3] \tag{4.42}$$

From Eq. (4.42) it is evident that the effective stress developed in the spring with compliance D_o acting in principal direction 1 is given by,

$$\sigma^s_{o1} = \sigma_1 + (1 - \frac{J_o}{D_o})\sigma_2 + (1 - \frac{J_o}{D_o})\sigma_3 \tag{4.43}$$

Similarly, the effective stress developed in the spring with compliance D_1 and acting in principal direction 1 is,

$$\sigma^s_{11}(\psi) = (1 - e^{-\lambda_r \psi})g_2\sigma_1 + \{(1 - e^{-\lambda_r \psi}) + \frac{J_1}{D_1}(1 - e^{-\eta_r \psi})\}g_2\sigma_2$$

$$+ \{(1 - e^{-\lambda_r \psi}) + \frac{J_1}{D_1}(1 - e^{-\eta_r \psi})\}g_2\sigma_3 \qquad (4.44)$$

On the left hand side of Eqs. (4.43) and (4.44), the superscript 's' denotes the effective stress within the spring, the first subscript indicates the spring number, and the second subscript determines the principal direction in which the effective stress acts.

The total energy, W^s_1, stored in the two springs in material direction 1 over time t, can now be obtained by using Eq. (4.35). Hence,

$$W^s_1 = \frac{1}{2} D_o(\sigma^s_{o1})^2 + \frac{1}{2} D_1(\sigma^s_{11})^2 \qquad (4.45)$$

Using a procedure similar to the one just described, it can be shown that for an isotropic material the total stored energies W^s_2 and W^s_3 may be expressed in a form similar to Eq. (4.45). Therefore, the total energy, W^s_j, stored in the springs in direction j, over time t is given by,

$$W^s_j = \frac{1}{2} D_o(\sigma^s_{oj})^2 + \frac{1}{2} D_1(\sigma^s_{1j})^2 \qquad (4.46)$$

If the viscoelastic material is represented by n Kelvin units in series in each material principal direction respectively, then,

$$W_j^s = \frac{1}{2} D_o(\sigma_{oj}^s)^2 + \frac{1}{2} \sum_{r=1}^{n} D_r(\sigma_{rj}^s)^2 \qquad (4.46)$$

where,

$$\sigma_{oj}^s = (1 - \frac{J_o}{D_o})(\sigma_1 + \sigma_2 + \sigma_3) + \frac{J_o}{D_o} \sigma_i \delta_{ij} \qquad (4.47)$$

and,

$$\sigma_{rj}^s = g_2[(1 - e^{-\lambda_r \psi}) - \frac{J_r}{D_r} (1 - e^{-\eta_r \psi})][\sigma_1 + \sigma_2 + \sigma_3]$$

$$+ g_2 \frac{J_r}{D_r} (1 - e^{-\eta_r \psi})\sigma_i \delta_{ij} \quad i,j = 1,2,3 \qquad (4.48)$$

Note that in Eqs. (4.47) and (4.48), repeated indices imply summation, and δ_{ij} is the Kronecker delta operator. Also, the Prony series for the creep and shear compliance are required to have the same number of terms.

Equations (4.46), (4.47) and (4.48) define the energy stored in the j^{th} principal direction in an isotropic viscoelastic material. Therefore, according to the Reiner-Weisenberg failure theory, the criterion for creep rupture in the jth principal direction is given as,

$$W_j^s \geq R \qquad (4.49)$$

where R is the resilience of the isotropic material.

For a material with a constant Poisson's ratio,

$$J(\psi) = (1 + \nu)D(\psi) \qquad (4.50)$$

For such cases, Eq. (4.46) is still valid, but Eqs. (4.47) and (4.48) simplify to,

$$\sigma_{oj}^{s} = -\nu(\sigma_1 + \sigma_2 + \sigma_3) + (1 + \nu)\sigma_i\delta_{ij} \qquad (4.51)$$

and,

$$\sigma_{rj}^{s} = -\nu g_2(1 - e^{-\lambda r^{\psi}})(\sigma_1 + \sigma_2 + \sigma_3) + (1 + \nu)g_2(1 - e^{-\lambda r^{\psi}})\sigma_i\delta_{ij} \qquad (4.52)$$

CHAPTER 5

NUMERICAL RESULTS

5.1 Preliminary Comments

In this section results of a number of linear elastic, linear viscoelastic and nonlinear viscoelastic analyses are discussed in light of available experimental or analytical results. All results are obtained using NOVA on an IBM 3090 computer in double precision arithmetic. The first problem deals with linear elastic (both adhesive and adherend) analysis to show the effect of boundary conditions and mesh on the stress distributions. Next, results of geometric nonlinear analysis are presented and compared with those obtained with VISTA. Then linear and nonlinear viscoelastic analysis results are presented, first, to validate the finite element procedure described in the preceeding chapters and, second, to obtain new results for certain adhesive joints.

5.2 Linear Elastic Analysis: Effects of Boundary Conditions and Mesh

To investigate the influence of boundary cobnditions on the elastic stress distribution in a single lap joint, the three different boundary conditions shown in Fig. 2 were used in the linear elastic analysis. During the present study it was also observed that the type of finite-element mesh (i.e. uniform or nonuniform) has also an effect on the stress distribution in the bondline. The material properties used are given in Table 1.

Figures 3 and 4 show plots of the peel stress obtained by uniform and nonuniform meshes, respectively, along the center of the bond line. Boundary conditions of Type 1 and 3 give almost the same distribution of the stress, while Type 2 differs significantly at the edges of the adhesive. Stresses obtained with Type 1 and 3 boundary conditions exhibit stress distributions that are almost symmetric about the vertical centerline of the joint (with Type 3 being the most symmetric). It is also observed that the distribution is not quite smooth when a uniform mesh is used. For an accurate description of the stress gradients near the edges, a more refined mesh than that used at the center (i.e., nonuniform mesh) must be used. This observation is supported by the results shown in Fig. 3.

The effect of boundary conditions (Type 1 to 3) on the distribution of the peel and shear stresses along the upper and lower bondlines (i.e., interface bewteen the adhesive and adherend) are shown in Figs. 5-8. The nonuniform mesh was used in all cases. From these results it is clear that boundary condition of Type 2 gives significantly different results than Type 1 or 3, especially near the edges.

5.3 Geometric Nonlinear Analysis

Next, geometrically nonlinear analysis of a bonded lap joint was considered. The geometry and boundary conditions of Type 2 shown in Fig. 2 are used. The material constants used are given in Table 2. The present nonlinear elastic analysis results are compared with those

obtained using the VISTA program [23] in Figs. 9 and 10. The results are in excellent agreement.

Next, the nonlinear response of a bonded cantilever plate under distributed transverse loads was investigated. The plate geometry and the two finite element meshes used are shown in Fig. 11. The material properties used are given in Table 3. Both the adhesive and the adherends were assumed to be linearly elastic and isotropic.

The load on the plate was increased in steps until a fairly large free-end deflection was obtained. For the present analysis the magnitude of the deflection was over 50% of the beam length. The resulting load-deflection curves obtained by the two meshes are shown in Fig. 12. The results obtained by using linear analysis is also plotted for comparison purposes. Clearly, the nonlinear analysis predicts a stiffer response. This is due to the fact that the large transverse deflection causes a bending-extension coupling which results in an increase in the flexural stiffness of the beam.

Figure 13 shows the compressive bending stress at a specified point (near the fixed end) in the lower adherend plotted against applied load for the two different meshes. The discrepancy in the two curves is due to the fact that the axial stress values for one curve were obtained at an x-location slightly different from the other curve. The flattening out of the stress curve at higher loads is a result of the shortening of the moment arm due to extensive bending of the beam.

Figures 14-16 show the variation of the flexural, peel and shear stresses in the lower half of the adhesive layer plotted along the plate axis for two different meshes. Adjacent to the clamped end, there exists a narrow region where both the flexural and peel stresses are tensile. However, as one moves further along the plate length, the flexural stress turns compressive, which conforms to what is predicted by the elementary plate theory. The shear stress attains its maximum value near the clamped end and decreases rapidly as one moves out towards the free end. All three stresses vanish at the free end of the plate, thus satisfying the stress free boundary condition.

5.4 Linear Viscoelastic Analysis

The nonlinear constitutive law due to Schapery may be linearized by assuming that the nonlinearizing parameters g_0, g_1, and g_2 have a value of unity. In addition, the stress dependent part of the exponent in the definition of the shift factor is set to zero. Consequently, the constitutive law reduces to the superposition integral form commonly used to describe a linear viscoelastic material.

Two test cases are used to validate the linear viscoelastic analysis capability implemented in the present finite element program named NOVA. In the first case, the tensile creep strain in a single eight noded quadrilateral element was computed for both the plane stress and plane strain cases using the program NOVA. The results were then compared to the analytical solution for the plane strain case presented in [57]. A uniform uniaxial tensile load of 13.79 MPa was applied on

the test specimen. A three-parameter solid model was used to represent the tensile compliance of the adhesive. The following time dependent functions were used in [57] to represent the tensile compliance and the Poisson's ratio for FM-73M at 72°C:

$$D(t) = \frac{J_o}{2[1+\nu(t)]} + \{\frac{J_1}{2[1+\nu(t)]}\}(1 - e^{-t/0.85}) \qquad (5.1)$$

Approximating the Poisson's ratio with the elasticity relation gives,

$$\nu(t) = \frac{[\frac{3K(t)}{2G(t)} - 1]}{[\frac{3K(t)}{G(t)} + 1]}, \qquad (5.2)$$

where G(t) and K(t) are the shear and bulk modulus (mm/mm/MPA) respectively, and J_o, J_1 are the shear compliance coefficients. The analytical solution to the creep problem for the plane strain case is given in [57] as:

$$\varepsilon(t) = 2.728 \times 10^{-2} + 1.334 \times 10^{-2}\, e^{-t/0.85} - 2.659 \times 10^{-4}\, e^{-t/0.3921}$$

It is to be noted that for the three-parameter solid characterization of FM-73M the value of the Poisson's ratio actually increases with time. However, in the present analysis the Poisson's ratio is assumed to be independent of time. Hence two discrete values of the Poisson's ratio are used to match the exact solution for few initial time steps and final time steps. The values of the Poisson's ratio chosen for this purpose are $\nu_o = \lim_{t\to 0} \nu(t) = 0.32$ and $\nu_\infty = \lim_{t\to\infty} \nu(t) = 0.417$. Figure 17a shows the creep curve for $\nu = 0.417$ for both plane strain and plane stress finite-element analyses. As expected, the plane strain results exhibit close agreement with the exact solution for large

values of time, followed by progressive deterioration of predicted value as one moves towards smaller values of time. The finite element results for the plane stress case points to the fact that the strains are higher for plane stress than for plane strain.

Figure 17b shows the creep curve corresponding to $\nu = 0.32$ for the plane strain case. In this case the finite element predictions are accurate only for first few time steps and deviates more and more from the analytical solution as time increases. This is not surprising since the choice of Poisson's ratio for this case makes the comparison meaningful only when t is small.

The above results indicate that the program NOVA provides reasonably accurate results in regions where the input parameters are accurate, and that the variation of Poisson's ratio during the period of analysis may cause significant deviations from the actual solution.

Next, the Model Joint analysis problem presented in [57] was used as the second validation example. In this case, a linear viscoelastic finite element analysis was carried out on a model joint under a constant applied load of 4448 N giving an average adhesive shear stress of 13.79 MPa. The specimen geometry, discretization and boundary conditions are shown in Fig. 18. The thickness of the adhesive layer is taken to be 0.254 mm. A nine parameter solid model was used to represent the tensile creep compliance of FM-73 at 72°C and is given by:

$$D(t) = 0.5988 \times 10^{-3} + 1.637 \times 10^{-5} (1 - e^{-t/0.01})$$
$$+ 0.6031 \times 10^{-4} (1 - e^{-t/0.1})$$
$$+ 0.9108 \times 10^{-4} (1 - e^{-t/1.0})$$
$$+ 2.6177 \times 10^{-4} (1 - e^{-t/10.0})$$

The adhesive Poisson's ratio is assumed to have a value of 0.417 and remains constant with time. The material properties for the aluminum adherends are presented in Table 3.

Figures 19 and 20 contain plots of the bond normal and shear stresses, respectively for t = 50 secs. and t = 60 min. of loading. These stresses represent the value at 1/16 the thickness from the upper adhesive adherend interface. The sharp peak at the left hand edge is due to the singularity caused by the presence of a re-entrant corner in the vicinity of the edge. These results are in good agreement with the results presented in [57] which uses the linear viscoelastic finite element code, MARC.

5.5 Axisymmetric Analysis of a Linearly Viscoelastic Rod

The axial displacement of one end of a linearly viscoelastic rod, subjected to a spatially uniform end traction that varies sinusoidally with time, was obtained by using the program NOVA. The shift factor for the material is defined by the WLF equation and the temperature is held at a constant value. The specimen geometry and material properties are

presented in Table 4. The exact solution to this problem has been presented in [23] and was used to validate the finite element predictions. As can be seen from Fig. 21, the finite element results are in excellent agreement with the closed form solution over one cycle of loading and unloading.

5.6 Nonlinear Viscoelastic Analysis of Adhesive Coupons

In order to validate the nonlinear viscoelastic model, three uniaxial test cases are analyzed. The results are compared with the laboratory tests conducted on similar specimens by Peretz and Weitsman [26]. The material properties used in the verification analysis are those reported in [22]. The creep data, together with other relevant material properties, are given in Table 5. A constant value for the Poisson ratio is assumed for the adhesive. The results from a linear viscoelastic analysis are also presented for comparison.

In the first verification test, a uniaxial stress of 10 MPa is applied to the adhesive coupon for 1200 secs., followed by a step increase to 26.6 MPa for a further 1200 secs. The temperature of the specimen is held constant at 50°C and is assumed to be uniform everywhere. The finite element predictions for this test are plotted together with the experimental data in Fig. 22. The predictions are in good agreement with the experimental results of Peretz and Weitsman [26].

The second test involves creep predictions under simultaneously varying stress and temperature, both increasing linearly with time. The

temperature is again assumed to be uniform throughout the test specimen. The finite element predictions (linear and nonlinear) and experimental data are compared in Fig. 23. There is a good agreement between the two sets of results.

The third test involves creep under a constant stress of 10 MPa with a linearly varying temperature as a function of time. Figure 24 shows the strain vs. time curves obtained in the experiments and finite element analysis. Satisfactory agreement between the experimental results and the analysis is observed.

A further set of tests were conducted in order to evaluate the accuracy of the finite element code for the case where creep is followed by creep recovery. A qualitative depiction of the loading and the resulting creep strain is given in Fig. 25. Rochefort and Brinson [61] presented experimental data and analytical predictions on the creep and creep recovery characteristics of FM-73 adhesive at constant temperature. The Schapery parameters necessary to characterize the viscoelastic response of FM-73 at a fixed temperature of 30°C are obtained by applying a least squares curve fit to the data presented in [61]. The resulting analytical expressions for the creep compliance function $D(\psi)$, the shift function a_σ, and the nonlinear parameters g_0, g_1 and g_2 are presented in Table 6. From the point of view of programming convenience it is more suitable to work with an exponential series than a power law. Hence the power law creep compliance function was converted to an equivalent five term exponential series of the form

given by Eq. (3.5). The five constant coefficents for this series were obtained by means of fitting a curve to the aforementioned power law function and then minimizing the error in a least-squares sense. The exponential series form of the compliance function is presented in Table 7 and it is plotted against the power law curve in Fig. 26 for comparison.

Figure 27 shows the geometry of the tensile dogbone specimen used to carry out the creep and creep recovery tests. This geometry is identical to the one used by Rochefort and Brinson [61]. Due to the symmetry of specimen geometry and applied load, only the upper right hand quadrant of the specimen was analyzed. The finite element discretization consists of two elements along the length of the specimen and one element in the width direction. Eight-node quadrilateral plane stress elements are used for this analysis. A constant tensile load is applied on the specimen for the first 30 min. followed by creep recovery over an equal length of time. The procedure is repeated for three different stress levels at a fixed temperature of 30°C.

The stress input for a uniaxial creep and creep recovery test is given by,

$$\sigma(t) = \sigma_o H(t) - \sigma_o H(t - t_1) \qquad (5.3)$$

where $H(t - t_1)$ is the unit step function, and t_1 is the time at which stress is removed.

Substitution of Eq. (5.3) into Eq. (3.1) coupled with a power law representation for the compliance yields,

$$\varepsilon_c(t) = [g_o D_o + C g_1 g_2 (\frac{t}{a_\sigma})^n]\sigma_o \tag{5.4}$$

and

$$\varepsilon_r(t) = \frac{\Delta\varepsilon_1}{g_1}[(1 + a_\sigma\lambda)^n - (a_\sigma\lambda)^n] \tag{5.5}$$

for the creep and creep recovery strains respectively. In the above expression,

$$\lambda = \frac{t - t_1}{t_1} \tag{5.6}$$

is a nondimensional parameter, and

$$\Delta\varepsilon_1 = \varepsilon_c(t_1) - \varepsilon_o = C\sigma_o g_1 g_2 (\frac{t_1}{a_\sigma})^n \tag{5.7}$$

represents the transient component of creep strain just prior to unloading. Hence, Eqs. (5.4) to (5.7) provide a closed form solution to Schapery's nonlinear single integral law for the simple load history involving creep and creep recovery given by Eq. (5.3).

Figures 28 a, b, and c show the results of the finite element analysis plotted along with the curve representing the closed form analytical solutions for applied stress levels of 21, 17 and 14 MPa respectively. The finite element predictions are in excellent agreement with the closed form solutions except at the beginning of creep and again at the onset of creep recovery. This discrepancy is clearly due to the discrepancy between the power law and the exponential series representation of the creep compliance function $\Delta D(\psi)$, as shown in Fig. 26. The presence of too many data points in the far field region has

caused the least square curve fit to give less weight to the initial data points and therefore overlook the error present near the beginning of the time axis. The complete agreement between the closed form solution and the finite element prediction for large values of time corroborates this fact. From Fig. 28 it is also evident that the error in the predicted value of strain decreases as the applied stress is reduced. This is exactly what is expected since the stress dependent nonlinear parameters g_1 and g_2 act as scale factors on the transient component of the creep strain. Thus, a reduction in the applied stress causes the values of g_1 and g_2 to reduce, which results in a proportionate reduction in the error magnitude.

5.7 Linear and Nonlinear Viscoelastic Analysis of a Model Joint

The loading, boundary conditions and specimen geometry used in this analysis is the same as the one used in the earlier model joint (see Fig. 18). In addition, the same nine parameter solid model was used in this analysis. A linear viscoelastic finite element analysis was carried out over a period of one hour at a constant applied load of 3336 N. The results for the linear analysis are shown in Figs. 29-30. The sharp peak at the left hand edge is due to the singularity caused by the presence of a re-entrant corner and dissimilar materials. All stress plots show the same basic trend in that the stresses are attempting to redistribute themselves to achieve a more uniform distribution.

For the nonlinear viscoelastic analysis of the model joint, the same specimen geometry and material properties were employed. However, the nonlinearizing parameters and the shift function were no longer held constant, but were allowed to change with the current stress state within the adhesive layer. The results from this analysis are presented in Figs. 31 and 32. It is immediately apparent that the effect of the nonlinearity causes a 'softening' of the adhesive, leading to a response that is less stiff compared to the linear case. Hence, even though the applied load is the same, the shearing strain for the nonlinear case is significantly larger as compared to the linear case (Figs. 30 and 32). Moreover, the increment in creep strain for the nonlinear case is 0.0058 as compared to 0.0041 for the linear case over the same period of time. This is exactly what is expected since the nonlinear model takes into account the acceleration of creep caused by the stresses within the adhesive.

The effect of the nonlinearity on the stress curves (Figs. 29 and 31) is to create a more uniform stress distribution by reducing the stress peaks near the edges while increasing the stresses at the mid-section of the overlap. The significant reduction of the stress peaks effected by the nonlinear model is very important from a design point of view since the reduction of stress levels at the critically stressed regions results in an improved joint efficiency.

5.8 Elastic Analysis of a Composite Single Lap Joint

Renton and Vinson [37] used a closed form elastic solution to conduct a parametric study of the effect of adherend properties on the peak stresses within the adhesive in a composite single lap joint. A similar parametric study was carried out using the finite element program NOVA. The geometry, finite element discretization and boundary conditions for the composite lap joint are shown in Fig. 33. For the sake of simplicity, only identical adherends are considered. Each adherend is made up of seven laminas of equal thickness. The orthotropic material properties for a lamina are given in Table 8. In order to maintain material symmetry about the laminate mid-plane and thus eliminate bending-stretching coupling, a $\theta^0/0^0/-\theta^0/0^0/-\theta^0/0^0/\theta^0$ ply orientation was selected for the analysis. Note that this type of ply orientation places the θ^0 ply immediately adjacent to the adhesive layer. The adhesive used is FM-73 and its isotropic linear elastic properties are listed in Table 9. The adhesive layer is modeled using sixteen eight-noded quadrilateral elements along its length and two elements through its thickness. A series of elastic finite element analyses is performed to study the effect of ply orientation, lamina primary modulus (Q_{11}), and geometric nonlinearity on the peak stresses in the adhesive.

In order to study the influence of ply orientation on the adhesive stress distribution, stress analyses were performed for $\theta = 0°$, $\theta = 15°$, $\theta = 45°$, and $\theta = 90°$ respectively. The results are shown in Figs. 34

and 35. The plots show the variation of stresses along the upper bondline of the overlap. The parameter x/c is the normalized distance from the bond centerline such that the value x/c = -1 corresponds to the left-hand free edge of the bond overlap. It is evident from these figures that an increase in the ply orientation angle θ, causes the peak stresses to increase near the free edge of the bond overlap. The adherend with a 0°/90° ply orientation (cross-ply) shows a 28% increase in peel stress and a 17% increase in shear stress over the corresponding values for a 0° (unidirectional) ply orientation. This is not surprising since a cross-ply adherend has a lower bending stiffness which results in a larger lateral deflection causing higher stress concentrations at the overlap ends.

The influence of the lamina primary modulus (Q_{11}) on adhesive peel and shear stresses can be seen in Figs. 36 and 37 respectively. A 0° (unidirectional) adherend ply orientation is used for this analysis. The two figures show a significant increase in the peak adhesive stress as the value of Q_{11} decreases. This is understandable as a more flexible adherend would undergo larger bending and hence produce higher stress concentrations at the overlap ends.

Harris and Adams [65] conducted large displacement finite element analyses on a single lap joint with aluminum adherends and observed significant reduction in peak stresses at the edge of the adhesive as compared to linear results. In order to observe the effect of geometric nonlinearity on a single lap joint with laminated composite adherends, a

large displacement analysis was performed using the program NOVA. Due to its greater susceptibility to bending, cross-ply laminated adherends were used for this analysis. The results can be seen in Figs. 38 and 39. The geometrically nonlinear analysis results in a 30% reduction in the peak peel stress and a 15% reduction in the peak shear stress. The horizontal shifting of the nonlinear curves is due to the configuration coordinate update required by the large displacement analysis.

5.9 Nonlinear Viscoelastic Analysis of a Composite Single Lap Joint

A nonlinear viscoelastic analysis of a lap joint made of composite material was carried out over a time period of forty hours using NOVA. The specimen geometry and the finite element discretization are the same as for the elastic analysis as shown in Fig. 33. However, instead of a uniform end traction, a uniform end displacement of 0.363 mm is applied to the end of the joint and is held constant with time. The adherends are made of symmetric cross-ply laminates whose properties are given in Table 8, while the adhesive used is FM-73 and its creep compliance and Schapery parameters can be found in Table 5.

Figures 40 and 41 show the variation of shear stress and shear strain respectively across the entire bond length over a period of 40 hours. The sharp peak on the left-hand edge is due to the presence of a re-entrant corner and also due to the difference in material properties. Figures 42 and 43 provide a close-up view of the shear stress and strain gradients at the free edge. As might be expected, the shear stress

undergoes relaxation which results in a 36% decrease in the peak value at the left hand edge. The stresses have been normalized with respect to an average shear stress value of 4.5 N/mm^2. The peak shear strain, however, shows an increase of 35% over the same period of time. Similarly, Figs. 44 to 47 reveal that while the peak values of the peel and axial stresses decrease by 26% and 32% respectively, the corresponding strains show a respective increase of 63% and 6%. The reason that the strains increase with time even though the joint end deflection remains fixed, is because the adherends are modeled as elastic continuums. As the stresses in the adhesive relax with time, the elastic adherends deform to attain a new equilibrium configuration and this leads to an altered state of strain within the adhesive. Hence, it is very important that the elastic nature of the adherends be taken into account in an analysis. Also, the significant increase in adhesive strains with time is a viscoelastic phenomenon and therefore it cannot be predicted by means of a purely elastic analysis. This fact emphasizes the need to model the adhesive layer as a viscoelastic medium in order to be able to predict the long-term durability of a bonded joint.

5.10 Nonlinear Fickean Diffusion in Polystyrene

In order to validate the diffusion model implemented in NOVA and discussed in Chapter 4, results from a nonlinear diffusion analysis presented in [66] are used. The test problem involves unsteady sorption of a penetrant in a semi-infinite medium for a diffusion coefficient

that is an exponential function of penetrant concentration, that is, $D = D_0 \exp(kC/C_0)$. Finite element predictions were obtained for k = 0.614 and k = 3.912 and the results were compared with the published results represented by the solid lines in Fig. 48. Excellent agreement is observed for the two values of the coefficient k.

Levita and Smith [67] conducted experiments to study gas transport in polystyrene and found that the diffusion coefficients for gases decreased with time when the polystyrene film was subject to a constant uniaxial strain. This effect was attributed to the continuous free volume recovery (densification) in the polystyrene specimen at constant strain. The study also indicated that larger free volume elements decrease in size faster than the smaller ones as volume recovery progresses. Using the results published in [67] as a guideline, NOVA was used to study the time dependence of the diffusion coefficient for carbon-dioxide gas in a polystyrene film at constant strain. For this case, the temprature and moisture concentration effects presented in Eq. (4.9) were neglected, resulting in a diffusion coefficient that is solely a function of the transient component of the dilatational strain which, in turn, is a measure of the change in the free volume. Figure 49 shows the variation of the diffusion coefficient with time for three different strain levels. The material properties for polystyrene which were obtained from [68] are given in Table 10. From Fig. 49 it is evident that, independent of the strain level, the diffusion coefficient reaches a peak value t = 1 at hour and then slowly decays to the

reference value, D_o. This behavior can be attributed to an initial increase in free volume due to the application of the uniaxial strain, followed by a continuous recovery in free volume (densification) at a constant strain as the polystyrene film undergoes relaxation. A larger applied strain produces larger initial dilatation, and this results in a higher peak in the diffusion coefficient. Figure 49 also reveals that the time rate of free volume recovery, and hence the time rate of decrease in the diffusion coefficient, is proportional to the applied strain level.

The influence of penetrant molecule size on the diffusion coefficient for gases in polystyrene was studied by varying the magnitude of the material parameter B in Eq. (4.9). The temperature and strain were held constant at 50°C and 1.8% respectively. The prediction obtained from NOVA are shown in Fig. 50 for two values of B. The faster rate of decrease in the diffusion coefficient for a higher value of B implies that the larger free-volume elements decrease in size faster than the smaller ones as volume recovery progresses. The NOVA predictions are qualitatively in good agreement with the results presented in [67].

When a polymeric material is in the rubbery state, equilibrium is reached very rapidly in response to variations in temperature, stress and penetrant conentration. By contrast, a material in the glassy state is not in thermodynamic equilibrium and the response of the free volume to changes in external conditions is delayed. This metastable state

causes the free volume to slowly collapse with time until equilibrium is reached. This phenomenon is known as physical aging and causes relaxation processes to take place over a longer time. Struik [69] proposed that for a material in the glassy state, effective time λ is related to actual time t by,

$$\lambda = \int_0^t \left(\frac{t_e}{t_e + \xi}\right)^{\mu} \cdot d\xi \qquad (5.8)$$

where t_e is the aging time at the start of service life or testing and μ is a constant such that $0 \leq \mu \leq 1$. For such a material, the definition of reduced time given by Eq. (3.2) is no longer valid and should be modified to,

$$\psi^{\lambda} = \int_0^{\lambda} (a^s_{\sigma T})^{-1} ds \qquad (5.9)$$

where $a^s_{\sigma T}$ is the shift factor.

The effect of physical aging on the diffusion coefficient for carbon-dioxide gas in polystyrene was studied by implementing Eqs. (5.8) and (5.9) in NOVA. The values of temperature, strain and t_e were set at 50°C, 1.8% and 24 hours respectively. Figure 51 shows that an increased physical aging denoted by a higher value of the parameter μ, causes the diffusion coefficient to decay slower than the one for which μ is lower. This behavior is expected since increased physical aging causes the free volume recovery to take place over a longer period of time. Note that when there is no physical aging, μ and t_e are equal to zero and λ is identically equal to t.

5.11 Linear Elastic Analysis of a Butt Joint

Aivazzadeh et al. [31] used special linear elastic interface elements to study the effect of adhesive thickness and adhesive Young's modulus on the stresses within a bonded butt joint. A similar parametric study was carried out using NOVA where both the adhesive and adherend were assumed to be linearly elastic. The specimen geometry and loading are shown in Fig. 52. Due to symmetry, only a quarter of the butt joint was modeled. The finite element discretization is shown in Fig. 53, together with the boundary conditions. The various adhesive and adherend properties used in the parametric study are given in Table 11. A plane stress elastic finite element analysis was performed and the normalized shear and normal stresses plotted along the interface close to the free edge. Figures 54 and 55 show the influence of the ratio b/e (where b is the width of the butt joint and e is the thickness of the adhesive layer) on the adhesive shear and normal stresses respectively. It is observed that the maximum value of shear stress and the minimum value of normal stress are nearly equal for different joint thicknesses. The influence of the ratio of adhesive to adherend Young's moduli on adhesive stresses are shown in Figs. 56 and 57. As this ratio increases, the maximum shear stress and the maximum normal stress increase in value for b/e = 60.

5.12 Nonlinear Viscoelastic Analysis of a Butt Joint Including Moisture Diffusion

The effect of a change in the free volume of a polymer on its viscoelastic response was discussed by Knauss and Emri [27]. They used the unifying concept of the free volume by considering that fractional free volume depends on three variables: temperature T, moisture concentration c, and mechanically induced dilatation θ. Lefebvre et al. [51] extended the free volume concept to define a nonlinear diffusion coefficient, which results in a coupling between the viscoelasticity and the diffusion boundary value problems (see Section 4.1). The influence of this coupling on the viscoelastic response and moisture diffusion within the adhesive layer of a butt joint was investigated by using the program NOVA. The specimen geometry and finite element discretization are the same as shown in Figs. 52 and 53, respectively. However, instead of a uniform end traction, a uniform axial displacement of 0.1 mm is applied at the end of the joint and is held constant with time. The adherends are made of aluminum and the adhesive used is polystyrene. The various material properties are listed in Tables 10 and 11. The selection of polystyrene as an adhesive was prompted by the fact that it is one of the few polymeric materials that have their viscoelastic properties and diffusion parameters adequately documented. The normalized moisture concentration at the free edge of the adhesive layer is unity, and the initial concentration throughout the adhesive layer is zero. The tests are conducted at the reference temperature of 50°C.

Figure 58 shows the moisture concentration profiles within the adhesive layer at three different times when there is no coupling. In this case the diffusion coefficient remains constant with time, that is, $D = D_0$. Fig. 59 shows the moisture concentration profiles for the case where there is viscoelastic coupling only, that is, when the diffusion coefficient depends on the transient component of the dilatational strain. Fig. 60 depicts the case where there is full coupling, that is, the diffusion coefficient is a function of the dilatational strain and the moisture concentration at any given point in the adhesive. Conversely, the viscoelastic shift factor is now a function of the dilatational strain and the moisture concentration (see Eq. 4.12). Fig. 61 presents the results for each of these three cases for comparison at time t = 8 hours. From these figures it is evident that the effect of coupling is to accelerate moisture diffusion in the adhesive. The mechanically induced dilatation together with the swelling due to moisture sorption results in a higher free volume fraction within the adhesive which, according to Eq. 4.9, causes diffusion to proceed faster over the same period of time. It is to be noted that in Fig. 61, the curves become less concave as the coupling increases, which is in good agreement with the results published in [66].

Figures 62 to 65 show the variation of the stresses and strains with time within the adhesive layer in the butt joint when there is no coupling due to moisture induced swelling. Mathematically, this implies that $\gamma = 0$ in equations 4.9 and 4.12. From Figs. 62 and 63 it is evident

that the stresses do not relax significantly over the time period of the analysis. This is because the elastic adherend acts as a spring causing the adhesive to creep even though the joint end displacement remains fixed. However, there is a slight relaxation in the normal stress as one moves towards the center of the bond. The large increase in the strains, as shown in Figs. 64 and 65, is due to the creep caused by the strain recovery in the elastic adherend. This observation is supported by Fig. 66 which shows that the normal strain in the adherend immediately adjacent to the interface undergoes significant reduction with time. The decrease in the adherend normal stress, as shown in Fig. 67, reflects the concurrent stress relaxation that occurs in the adhesive and triggers the strain recovery in the adherend.

Figs. 68 to 71 show the effect of moisture induced swelling on the viscoelastic stresses and strains in the adhesive layer. Mathematically, this means γ has a nonzero value in Eqs. 4.9 and 4.12. The actual value of γ selected for this study is 0.001. For this value of γ, the moisture absorbed causes large swelling strains within the adhesive, which increase in magnitude as the diffusion progresses. This moisture induced swelling strain causes a reduction in the mechanically induced normal strain and hence a lower value for the normal stress in the adhesive. This effect can be observed in Fig. 68 where progressive swelling has caused a 25% reduction in the peak normal stress over a period of 8 hours. It is interesting to note that the difference between the two stress curves diminishes as one moves towards the center

of the bond. This behavior is expected since there is very little moisture near the center of the bond and so the stress reduction is primarily due to viscoelastic relaxation. The large increase in the adhesive strains, as seen in Figs. 70 and 71, is due to the adherend acting as a elastic spring.

Fig. 72 shows the influence of the moisture coefficient γ, on the normal stress in the adhesive layer after eight hours of sorption. As can be seen, the swelling induced for $\gamma = 0.001$ results in a significantly lower normal stress near the free edge as compared to the case where $\gamma = 0$. Away from the free edge, the two stress curves appear to merge as one moves towards the interior of the bond. This is because the low moisture concentrations present in the bond interior is insufficient to cause any significant reduction in the normal stress due to swelling.

5.13 Delayed Failure of a Butt Joint

The theory presented in Secs. 4.3 and 4.4 was applied to predict viscoelastic creep failure within the adhesive in a butt joint. The specimen geometry and the finite element discretization are the same as shown in Figs. 52 and 53, respectively. The adherend is made of aluminum and its material properties are given in Table 11. The adhesive used is FM-73 and its tensile creep compliance is listed in Table 5. The failure parameter (R) for FM-73, also known as the resilience, was obtained by computing the area under the stress-strain curve presented in [70]. This procedure yielded a value of the

resilience as 1.3 N.mm/mm^3. Note that the area under the visco-plastic yield plateau was not included in computing the value of R. According to the Reiner-Weisenberg theory, failure occurs when the stored energy per unit volume in the body reaches the resilience R, for the material. Using this postulate as a failure criterion, NOVA was utilized to predict failure in the adhesive layer of the butt joint subject to a constant uniaxial tension. The influence of applied stress level on delayed failure was studied by using a stress level of 69, 60, and 54 MPa respectively. In all three cases, failure was initiated in the adhesive element located right at the free-edge and immediately adjacent to the interface. It was also observed that the direction of the plane of failure was always inclined at an angle of 18°, counter-clockwise to the x-axis. Since the direction of failure coincides with the direction of principal stress, it is evident that a multiaxial state of stress exists near the free edge, even though the applied stress is uniaxial. This observation is in agreement with the results presented in Secs. 5.11 and 5.12. Fig. 73 shows the variation of normal (or creep) strain with time at 30°C for the element in which failure is first initiated. The right hand termination point on the curves indicate the point at which failure occured. It is observed that for an applied stress level of 69 MPa, the time to failure (t_F) is 1.5 secs. In other words, for this stress level, failure occurs almost instantaneously. For an applied stress of 60 MPa, t_F increases to 400 secs. Reducing the applied stress to 54 MPa results in a time to failure of approximately

10 hours. These results are qualitatively in good agreement with the results presented by Brüller [45] for PMMA.

From the above observations it is clearly evident that for viscoelastic polymers like FM-73, the time to failure depends strongly on the applied stress level. Fig. 74 shows the evolution of stored energy with time for different stress levels. For very high applied stress levels, almost all the strain energy is conserved as stored energy and failure occurs almost immediately. For intermediate levels of applied stress, viscoelastic creep causes a part of the strain energy to be dissipated. As a result, only a fraction of the total strain energy is conserved as stored energy. Consequently, the stored energy builds up slowly, analogous to a "leaking vessel", resulting in delayed failure. For an applied stress level that is below a certain threshold value for a given material, the dissipated energy may constitute a large fraction of the total strain energy. In that case, the stored energy would increase too slowly to exceed the resilience of the material over any realistic length of time, and hence there would be no failure even if the applied stress acts indefinitely.

CHAPTER 6

SUMMARY AND CONCLUSIONS

6.1 General Summary

A nonlinear viscoelastic computational model is developed, validated and applied to the stress analysis of adhesively bonded joints. The large displacements and rotations experienced by the adherends and the adhesive are taken into account by invoking the updated Lagrangian description of motion. The adhesive layer is modeled using Schapery's nonlinear single integral constitutive law for uniaxial and multiaxial stress states. The effect of temperature and stress level on the viscoelastic response is taken into account by a nonlinear shift factor definition. Optionally, a nonlinear shift factor definition based on the concept of free volume that was postulated by Knauss is also available. Penetrant sorption is accounted for by a nonlinear Fickean diffusion model in which the diffusion coefficient is dependent on the temperature, penetrant concentration, and the dilatational strain. A delayed failure criterion based on the Reiner-Weisenberg failure theory has also been implemented in the finite element code. The program is validated by comparing the present results with analytical and experimental results available in the literature. Additional results for a bonded cantilever plate, single lap joint, thick adherend specimen, and butt joint are also presented. The program capability has been extended to account for laminated composite adherends and adhesives with a time dependent Poisson's ratio. In

general, the computer program developed herein, named NOVA, is believed to provide accurate predictions over a wide range of specimen geometries, external loads, and environmental conditions.

6.2 Conclusions

The results presented in Ch. 5 underscore the importance of modeling the adhesive in a bonded joint as a viscoelastic material. This allows the analyst to predict the large increments in adhesive strains that occur with time and cannot be predicted by a purely elastic analysis. Furthermore, other events (such as moisture diffusion and delayed failure), that are highly relevant for bonded joint analysis, cannot be accurately predicted unless viscoelasticity is taken into account. At high stress levels, nonlinear viscoelastic effects can produce creep strains that are significantly larger than the linear viscoelastic predictions and such effects, therefore, should be accounted for. The effect of change in Poisson's ratio with time in some polymers have a significant bearing on the final response and must be taken into account in order to obtain accurate results.

The results in Chapter 5 also indicate that the stress boundary conditions at the free edges of the adhesive are not exactly satisfied. This deficiency in the model is expected because a displacement based finite-element formulation satisfies the boundary conditions only in a global sense. Even so, the shear stress, as presented in Chapter 5, shows a tendency to drop towards zero as it approaches the free edge. Any deviations from this behavior can be

attributed to either the presence of a re-entrant corner or the lack of a refined mesh near the free edge.

Table 1. Data for Linear Elastic Analysis.

Adherend (Aluminum)	Adhesive (Araldite)
$E = 10.3 \times 10^6$ psi	$E = 8.19 \times 10^6$ psi
$\nu = 0.3$	$\nu = 0.33$

Table 2. Data for Geometric Nonlinear Analysis of a Lap Joint.

Adherend (steel)	Adhesive (FM-73)
$E = 29.3 \times 10^6$ psi	$E = 0.2437 \times 10^6$ psi
$\nu = 0.33$	$\nu = 0.32$

Table 3. Data for Geometric Nonlinear Analysis of a Bonded Cantilever Plate.

Adherend (Aluminum)	Adhesive
$E = 70 \times 10^3$ MPa	$E = 2.8 \times 10^3$ MPa
$\nu = 0.34$	$\nu = 0.4$

Table 4. Data for Viscoelastic Rod.

$C_1 = 8.86$	$\nu = 0.32$
$C_2 = 101.6$	$E(t) = 5.0E5 + (1.0E6)e^{-t/2}$ psi
$T_r = 120$	$F(t) = 4500 \sin(\frac{\pi t}{2})$ lb.
$T = 123.5734$	$L = 5$ in.
$\alpha_T = 1.0E-4$	$A = 0.3$ in^2.

Table 5. Material Data for FM-73 Unscrimmed at 30°C.

Elastic Compliance, D_0:	360×10^{-6}/MPa
Poisson's Ratio, ν:	0.38
Coefficient of Thermal Expansion, α:	6.6×10^{-5} m/m/°K

Prony Series Coefficients:

$D_1 = 11.05 \times 10^{-6}$/MPa	$\tau_1 = 10$ secs.
$D_2 = 12.27 \times 10^{-6}$/MPa	$\tau_2 = 10^2$ secs.
$D_3 = 17.35 \times 10^{-6}$/MPa	$\tau_3 = 10^3$ secs.
$D_4 = 21.63 \times 10^{-6}$/MPa	$\tau_4 = 10^4$ secs.
$D_5 = 31.13 \times 10^{-6}$/MPa	$\tau_5 = 10^5$ secs.
$D_6 = 41.78 \times 10^{-6}$/MPa	$\tau_6 = 10^6$ secs.

Table 6. Data for Creep and Recovery of FM-73 Adhesive.

$$D(\psi) = D_o + D_c(\psi)$$

$$D_o = 227.573 \times 10^{-6}/\text{MPa}$$

$$D_c(\psi) = c\psi^n$$

$$c = 31.763 \times 10^{-6}/\text{MPa}$$

$$n = 0.151$$

$$a_\sigma = 1 - 3.536 \times 10^{-3}\sigma^{1.74}$$

$$g_o = 1 + 2.247 \times 10^{-2}\sigma^{1.005}$$

$$g_1 = 1 + 6.981 \times 10^{-4}\sigma^{1.88}$$

$$g_2 = 1 + 3.098 \times 10^{-6}\sigma^{4.12}$$

where σ is in MPa.

Table 7. Compliance Data for Creep and Recovery of FM-73.

$$D(\psi) = D_o + D_c(\psi)$$

$$D_o = 227.573 \times 10^{-6}/\text{MPa}$$

$$D_c(\psi) = \sum_{r=1}^{5} [D_r(1 - e^{-\psi/\tau_r})]$$

$D_1 = 19.86 \times 10^{-6}/\text{MPa}$	$\tau_1 = 1$ min.
$D_2 = 28.99 \times 10^{-6}/\text{MPa}$	$\tau_2 = 10$ min,
$D_3 = 17.66 \times 10^{-6}/\text{MPa}$	$\tau_3 = 100$ min.
$D_4 = 36.20 \times 10^{-6}/\text{MPa}$	$\tau_4 = 1000$ min.
$D_5 = 8.51 \times 10^{-6}/\text{MPa}$	$\tau_5 = 10000$ min.

Table 8. Orthotropic Material Properites for Composite Adherend.

$Q_{11} = 46.885 \times 10^3$ MPa

$Q_{12} = Q_{13} = 4.137 \times 10^3$ MPa

$Q_{22} = Q_{33} = 14.962 \times 10^3$ MPa

$Q_{23} = Q_{32} = 2.068 \times 10^3$ MPa

$Q_{44} = Q_{55} = Q_{66} = 3.447 \times 10^3$ MPa

Table 9. Isotropic Linear Elastic Properties for FM-73.

$E = 2.78 \times 10^3$ MPa

$G = 1.01 \times 10^3$ MPa

$\nu = 0.38$

Table 10. Material Properties for Polystyrene at 50°C.

Bulk Compliance:

$M_0 = 1.2 \times 10^{-4}$/MPa

$M_1 = 0.2896 \times 10^{-4}$/MPa	$\tau_1 = 1.515 \times 10^{2}$ sec.
$M_2 = 0.2246 \times 10^{-4}$/MPa	$\tau_2 = 1.515 \times 10^{3}$ sec.
$M_3 = 0.3721 \times 10^{-4}$/MPa	$\tau_3 = 1.515 \times 10^{4}$ sec.
$M_4 = 0.1354 \times 10^{-4}$/MPa	$\tau_4 = 1.515 \times 10^{5}$ sec.

Shear Compliance:

$J_0 = 1.0 \times 10^{-3}$/MPa

$J_1 = 2.16$/MPa	$\eta_1 = 1.515 \times 10^{8}$ sec.
$J_2 = 2.92$/MPa	$\eta_2 = 1.515 \times 10^{10}$ sec.
$J_3 = 1.38$/MPa	$\eta_3 = 1.515 \times 10^{12}$ sec.
$J_4 = 2.88$/MPa	$\eta_4 = 1.515 \times 10^{13}$ sec.
$J_5 = 2.31$/MPa	$\eta_5 = 1.515 \times 10^{14}$ sec.
$J_6 = 3.59$/MPa	$\eta_6 = 1.515 \times 10^{15}$ sec.
$J_7 = 0.648$/MPa	$\eta_7 = 1.515 \times 10^{16}$ sec.

Reference free volume $f_0 = 0.033$

Diffusion coefficient $D_0 = 9 \times 10^{-6}$ mm^2/sec

Table 11. Properties for Elastic Analysis of a Butt Joint.

Materials	E(MPa)	ν
Steel	2.07×10^5	0.29
Aluminum	0.7×10^5	0.33
Eponal	5.8×10^3	0.33
Rigid Epoxy	2.2×10^3	0.33

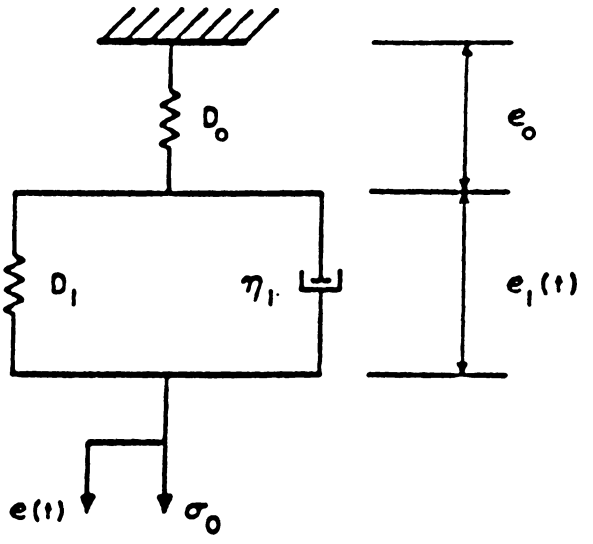

Figure 1. A Single Kelvin Unit Subject to Uniaxial Stress.

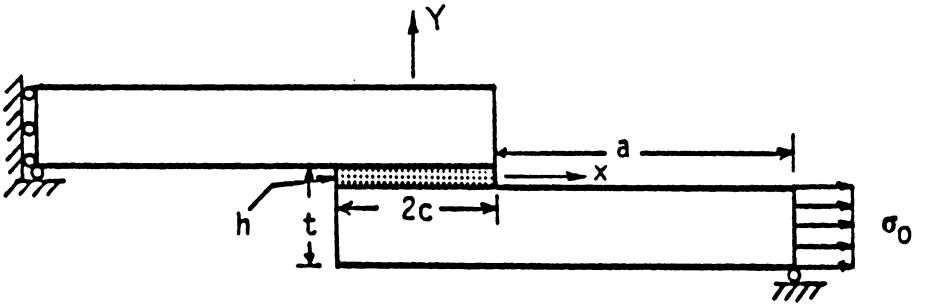

(a) Case 1

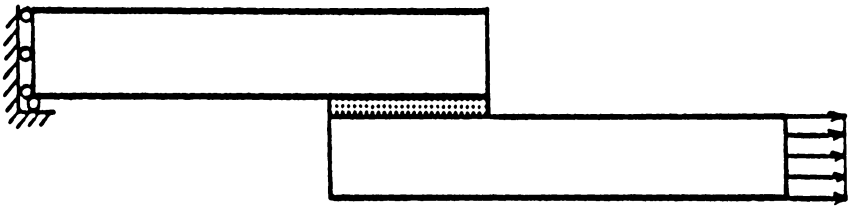

(b) Case 2

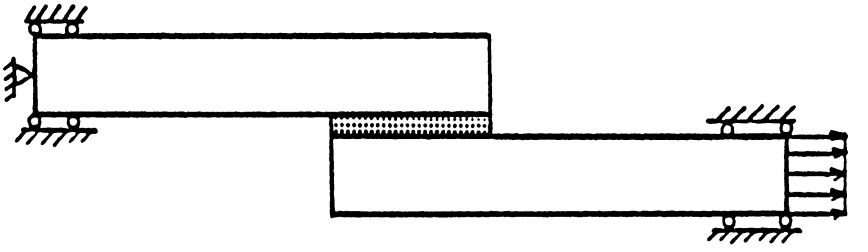

(c) Case 3

Figure 2. Various Boundary Conditions Used in the Linear Elastic Analysis of a Single Lap Joint (a = 1.26, c = 0.315, h = 0.0126, t = 0.063, all dimensions in inches, applied stress = 1423 psi.).

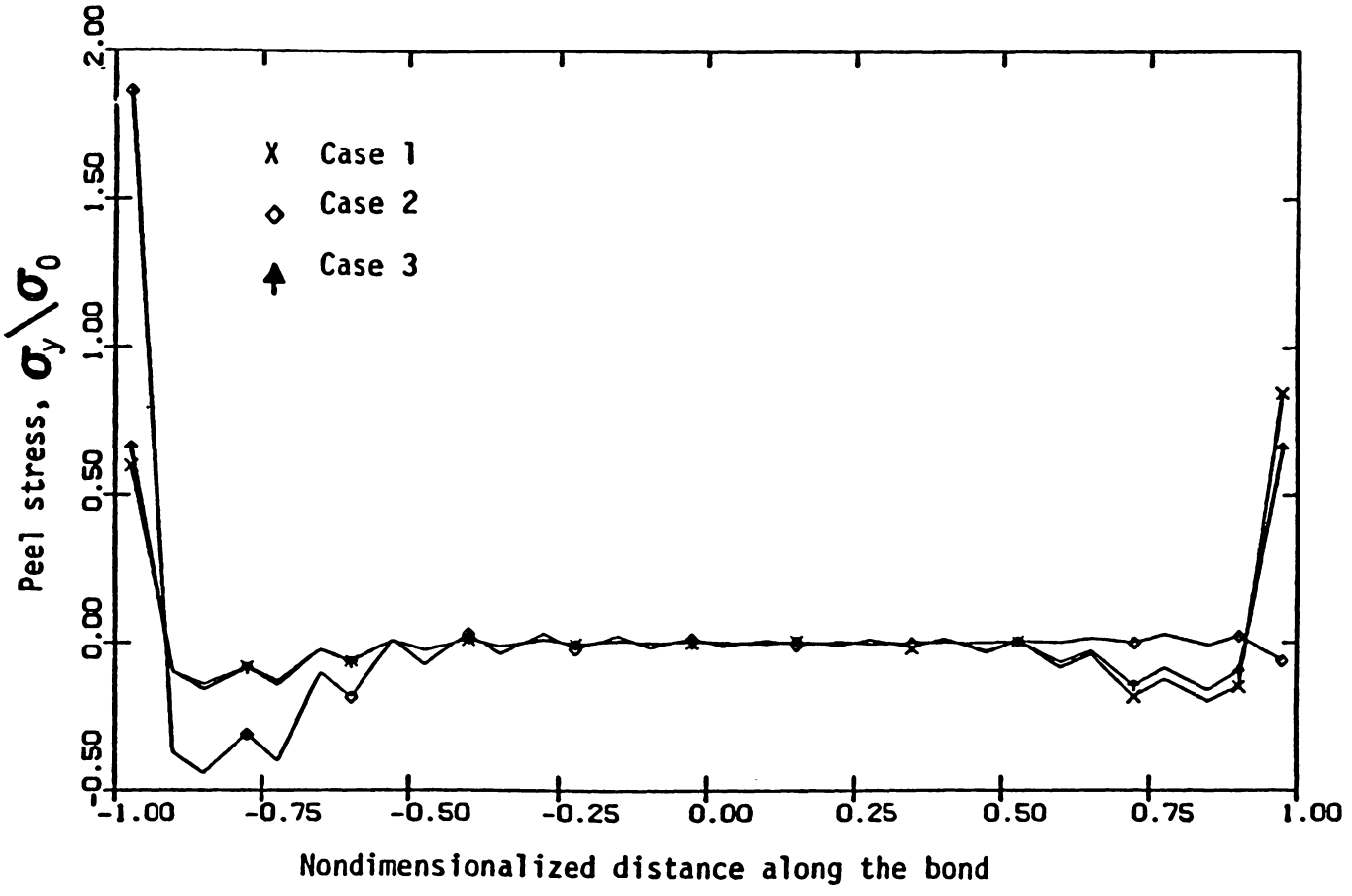

Figure 3. Variation of Peel Stress Along the Bond Centerline (Uniform Mesh).

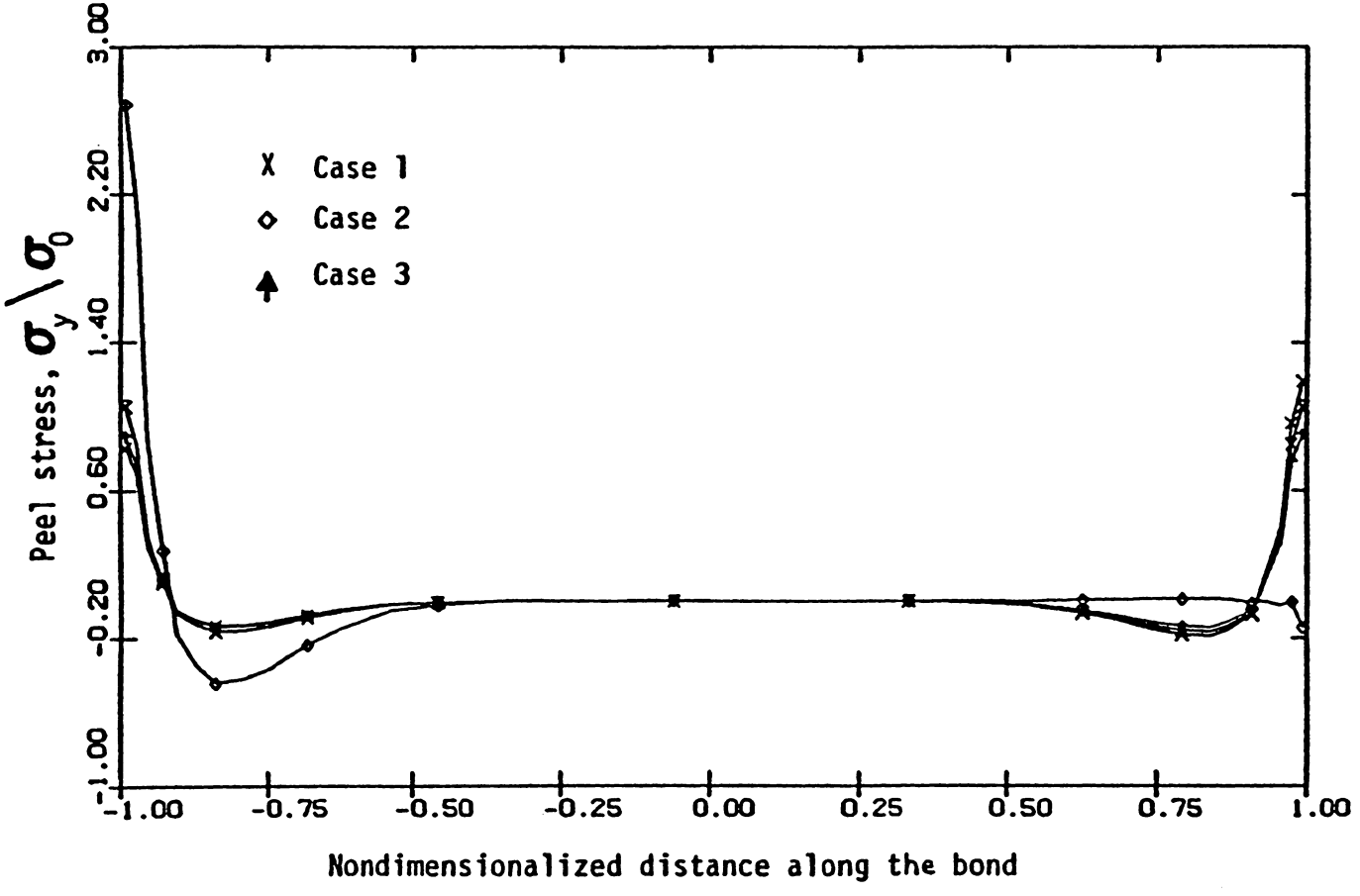

Figure 4. Variation of Peel Stress Along the Bond Centerline (Nonuniform Mesh).

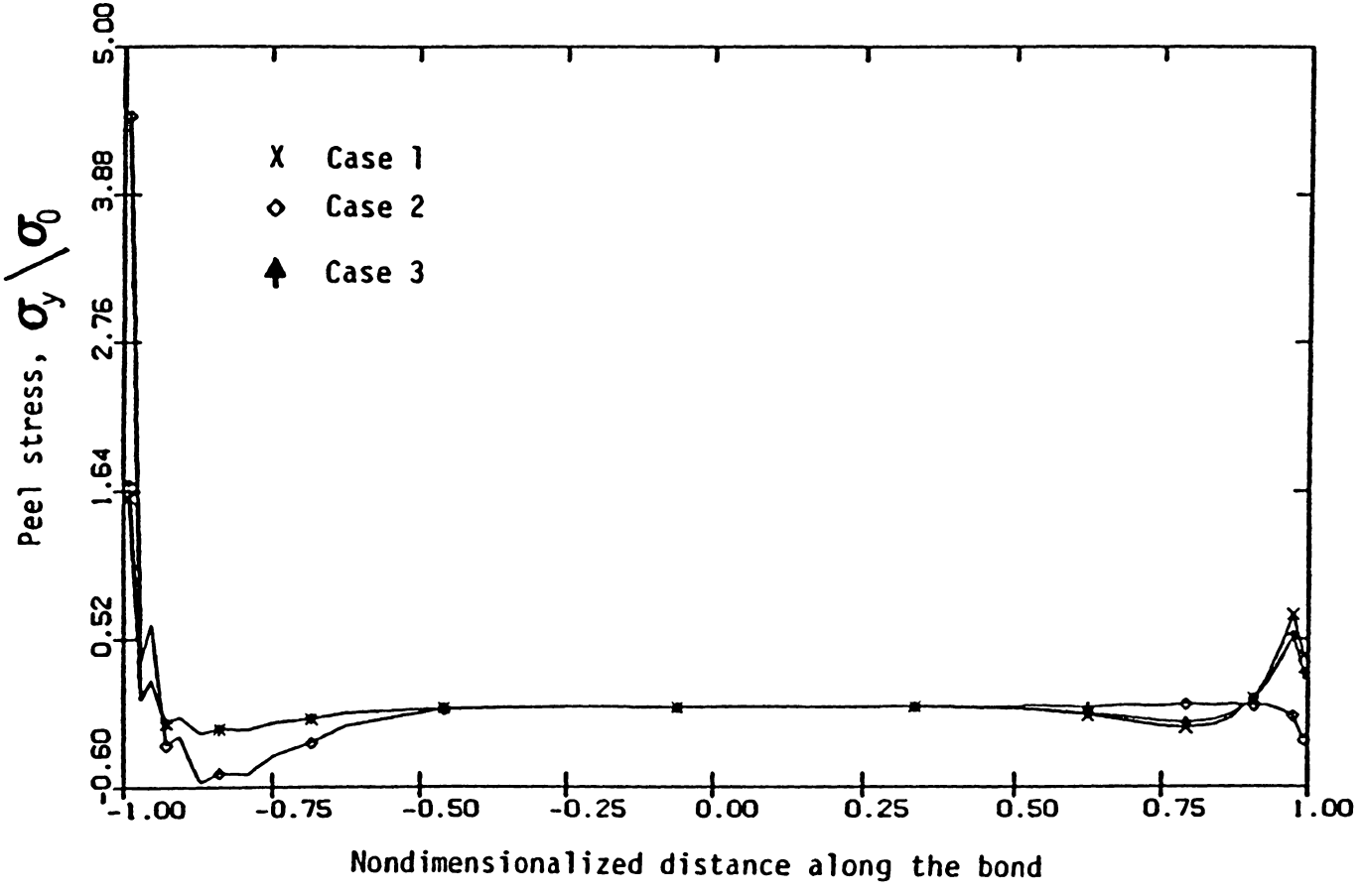

Figure 5. Variation of the Peel Stress along the Upper Bondline.

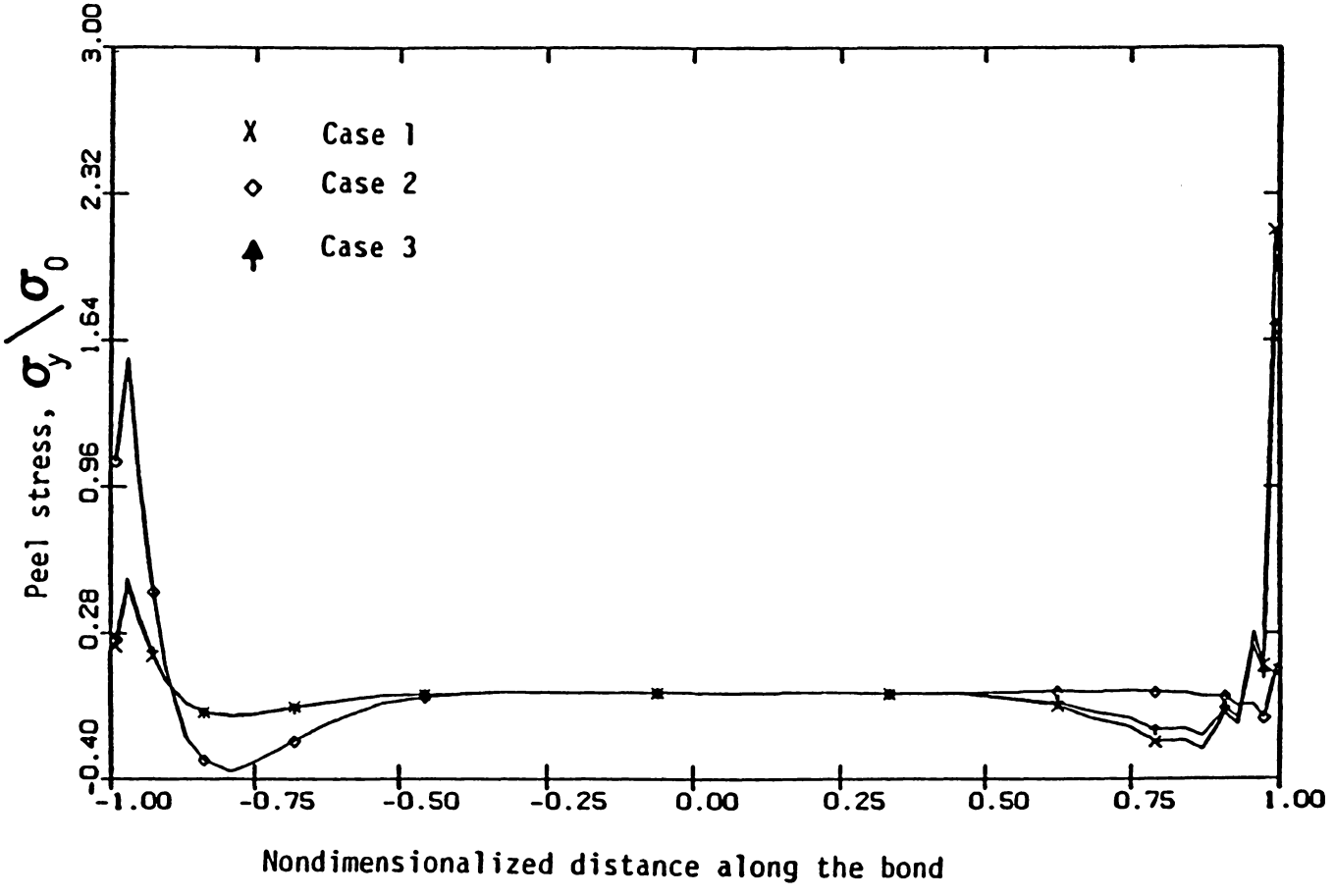

Figure 6. Variation of the Peel Stress along the Lower Bondline.

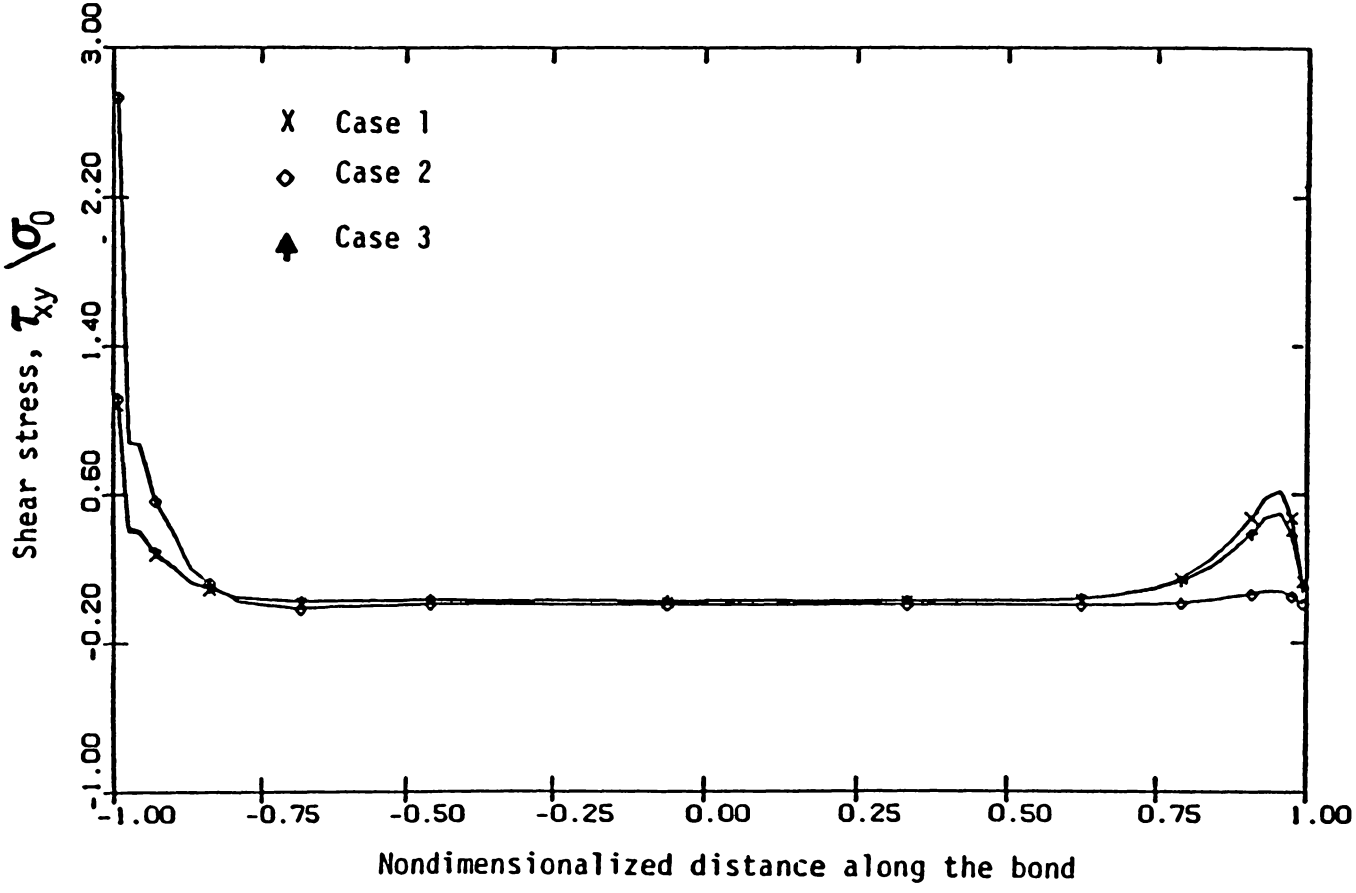

Figure 7. Variation of the Shear Stress along the Upper Bondline.

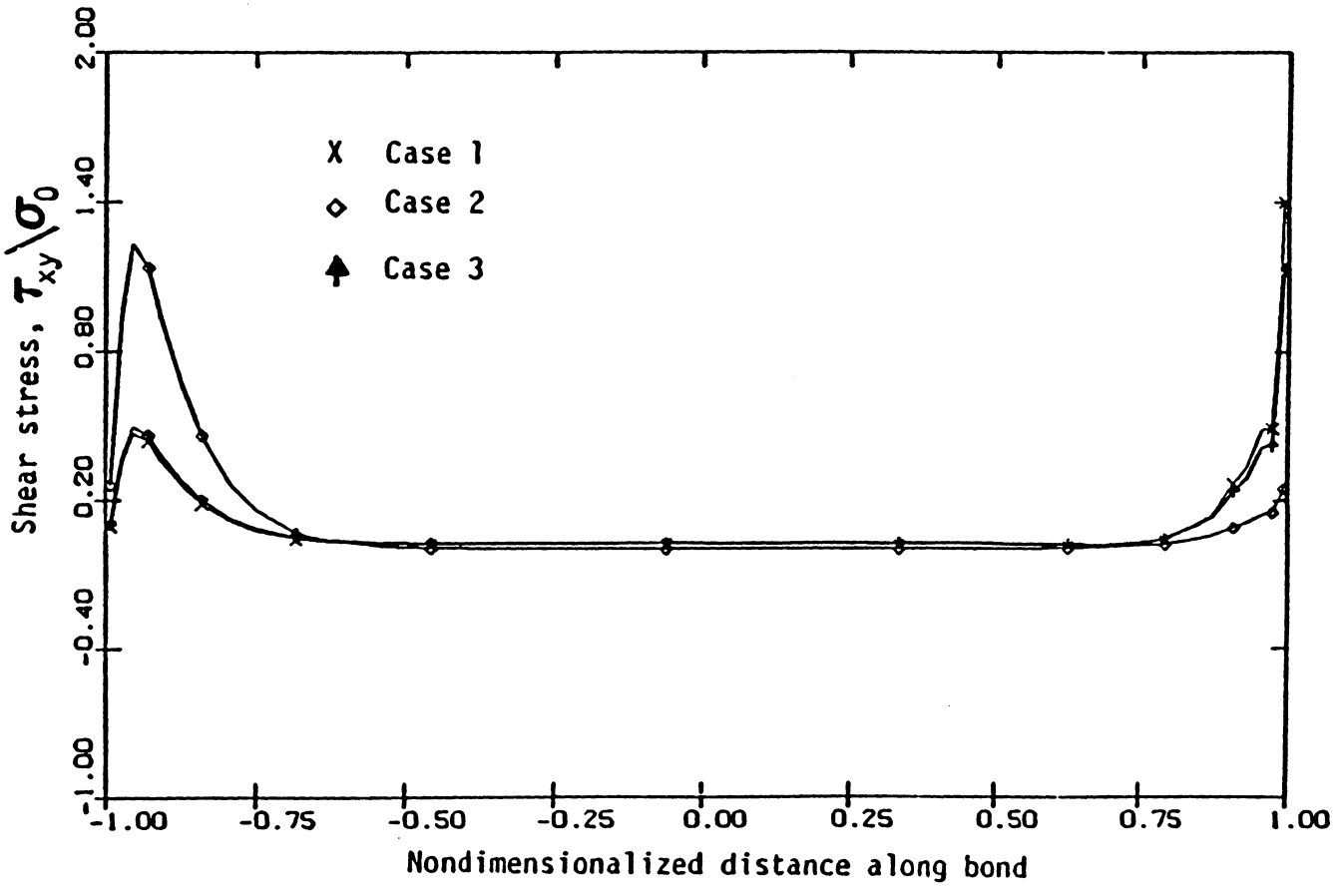

Figure 8. Variation of the Shear Stress along the Lower Bondline.

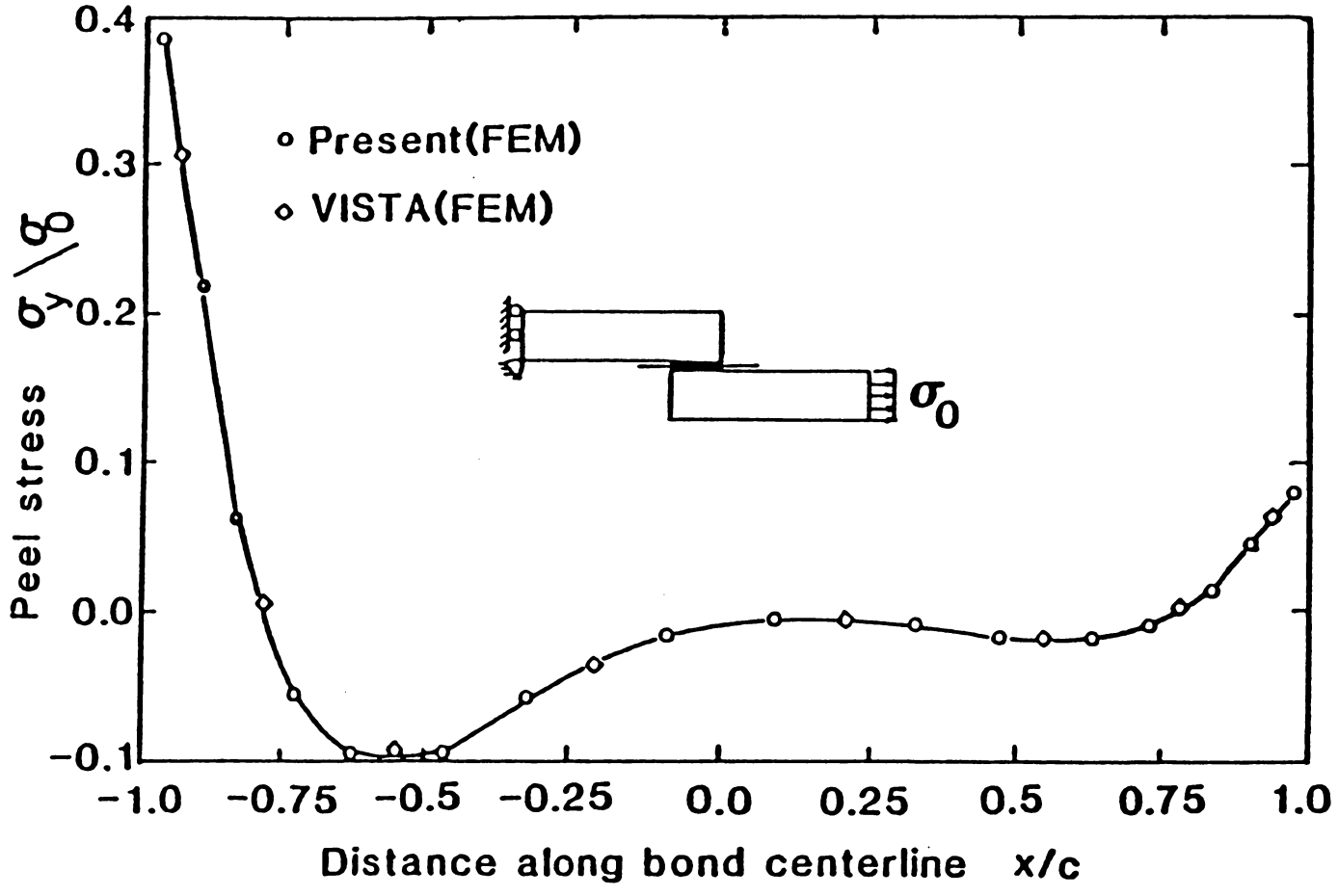

Figure 9. Variation of Peel Stress along the Bond Centerline for Geometric Nonlinear Analysis of a Single Lap Joint.

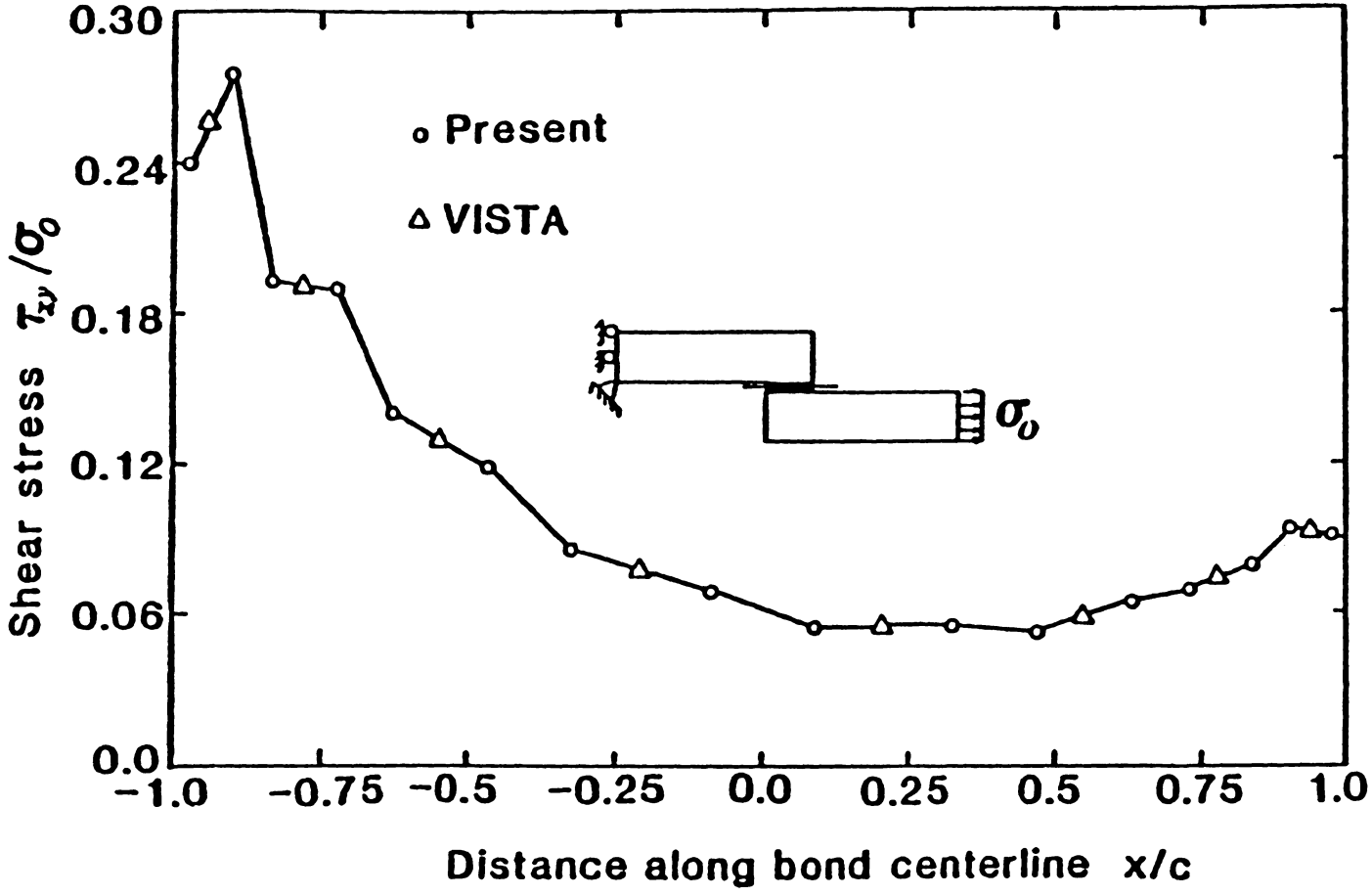

Figure 10. Variation of Shear Stress along the Bond Centerline for Geometric Nonlinear Analysis of a Single Lap Joint.

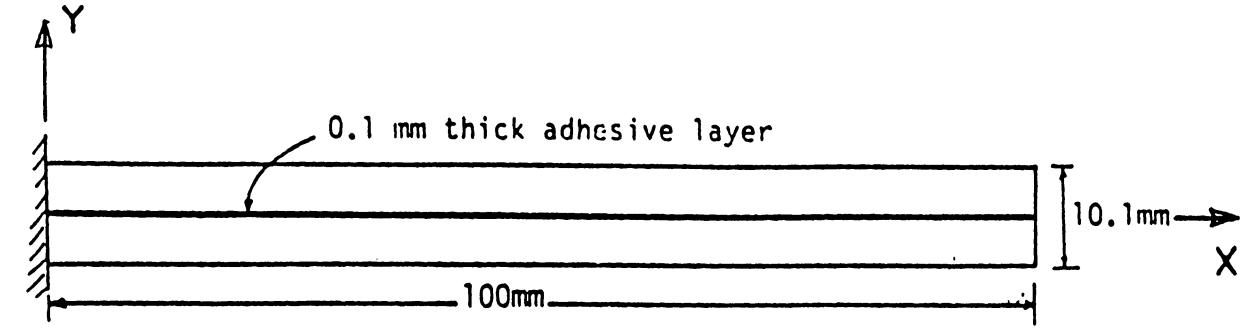

(a) Geometry of the plate

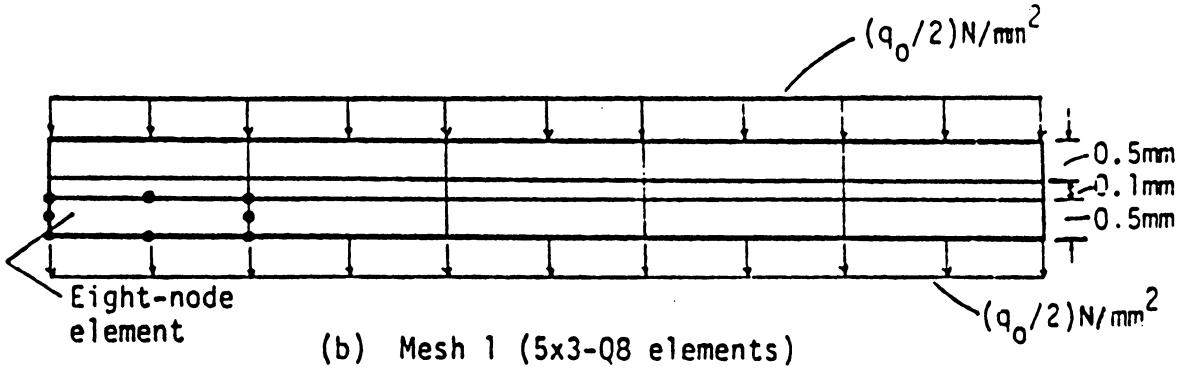

(b) Mesh 1 (5x3-Q8 elements)

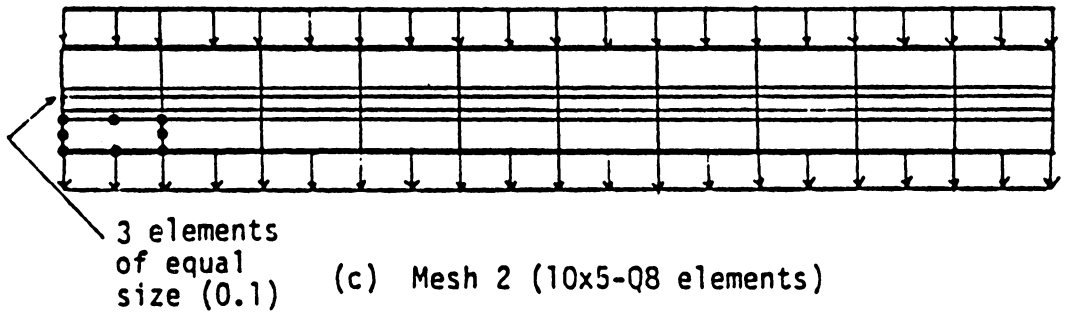

(c) Mesh 2 (10x5-Q8 elements)

Figure 11. The Geometry and Finite Element Discretizations for a Bonded Cantilever Plate.

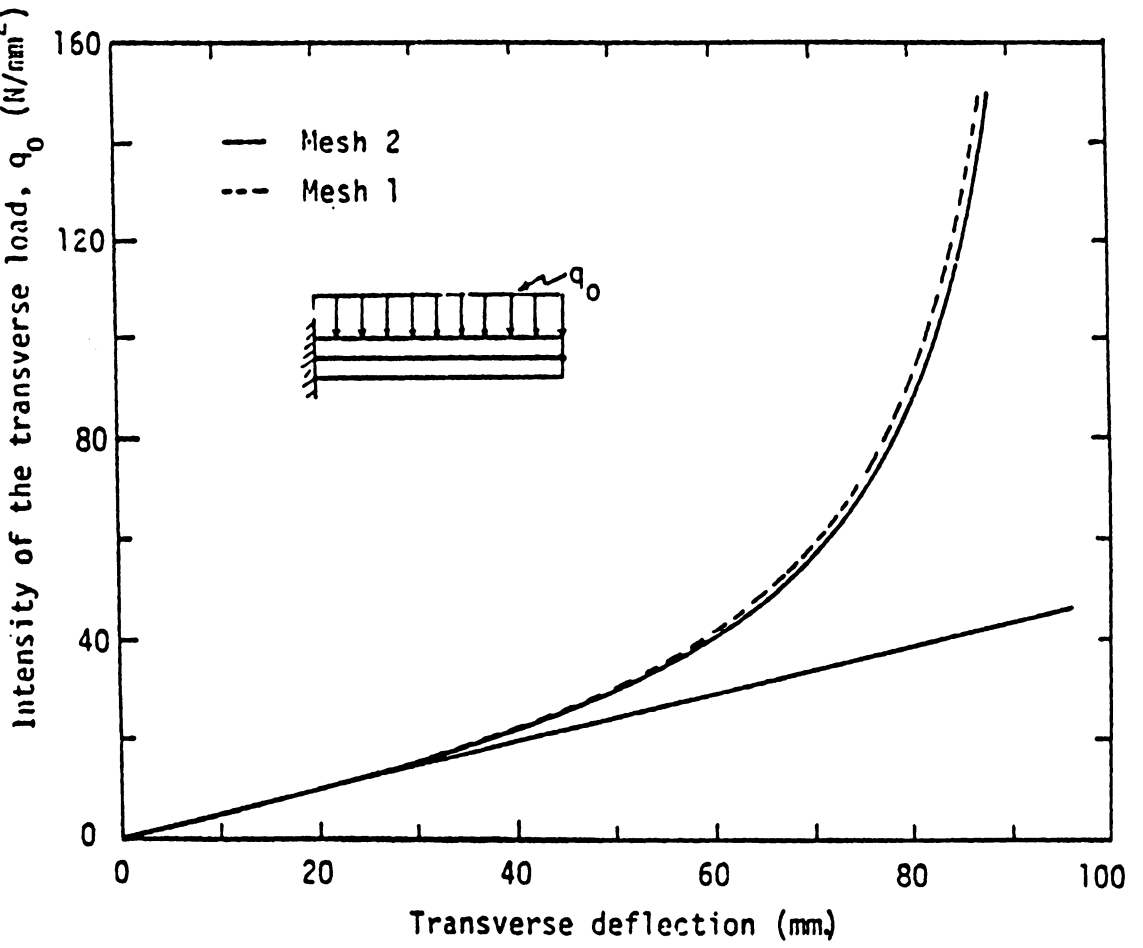

Figure 12. Load - Deflection Curves for a Bonded Cantilever Plate.

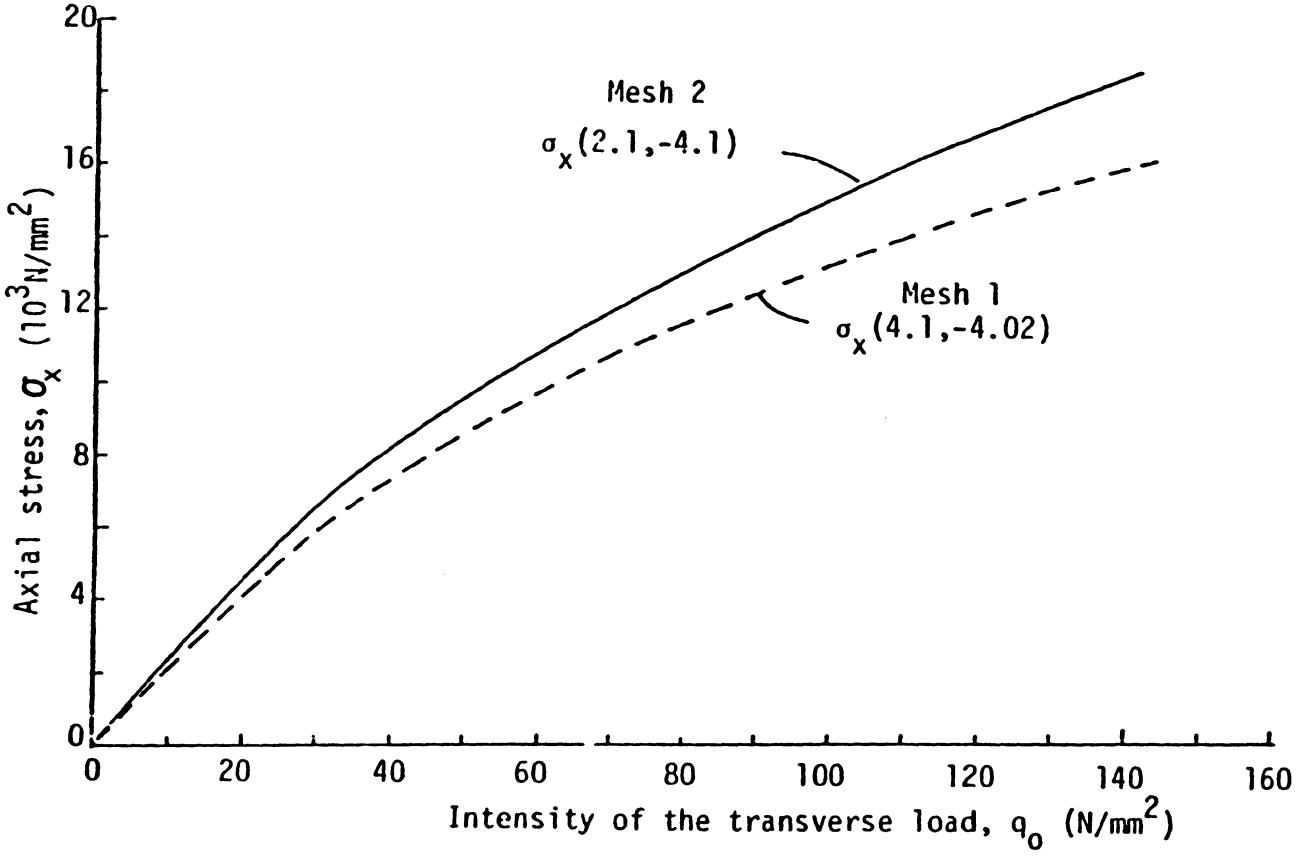

Figure 13. Axial Stress against Load Intensity for a Bonded Cantilever Plate.

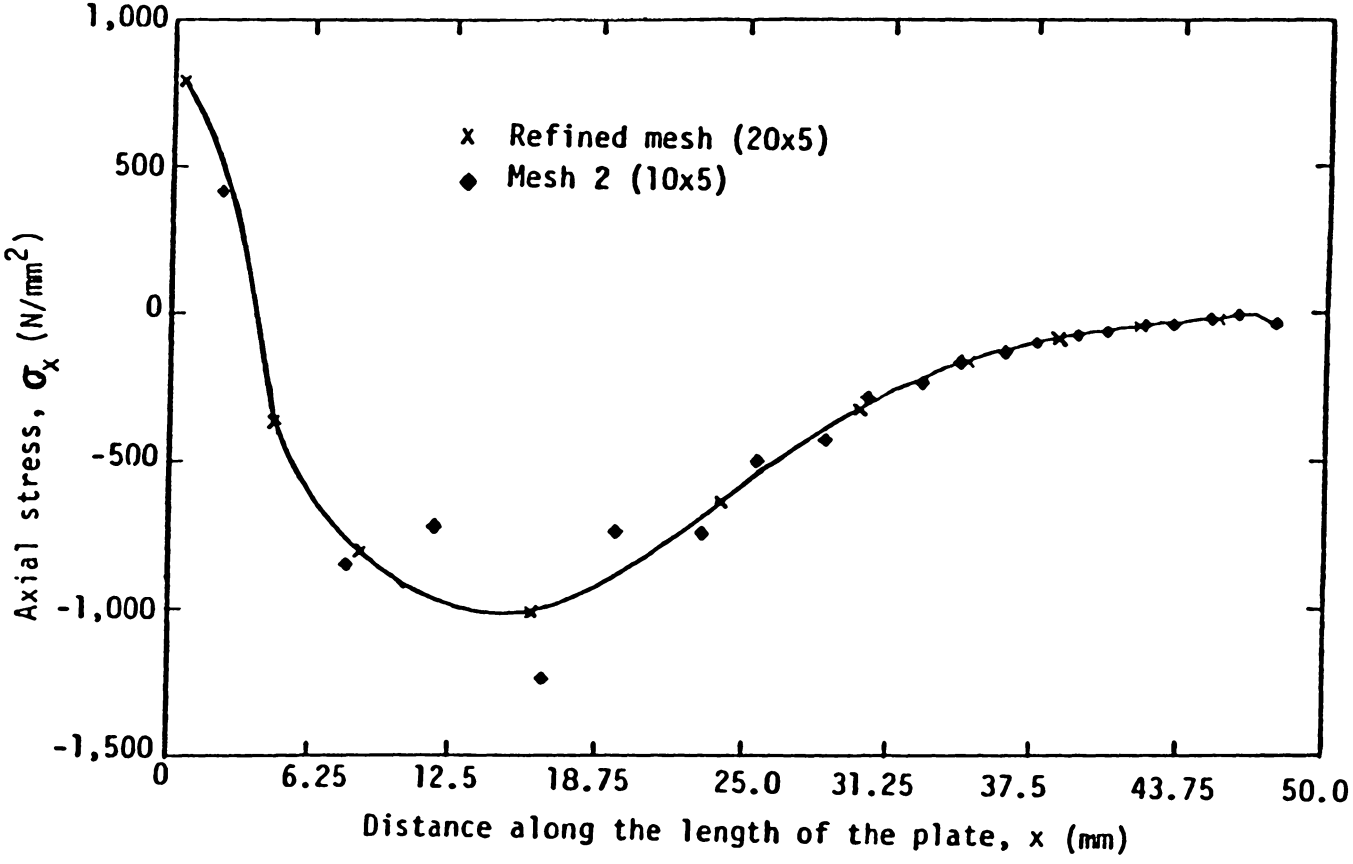

Figure 14. Plot of Axial Stress along the Bondline for a Bonded Cantilever Plate.

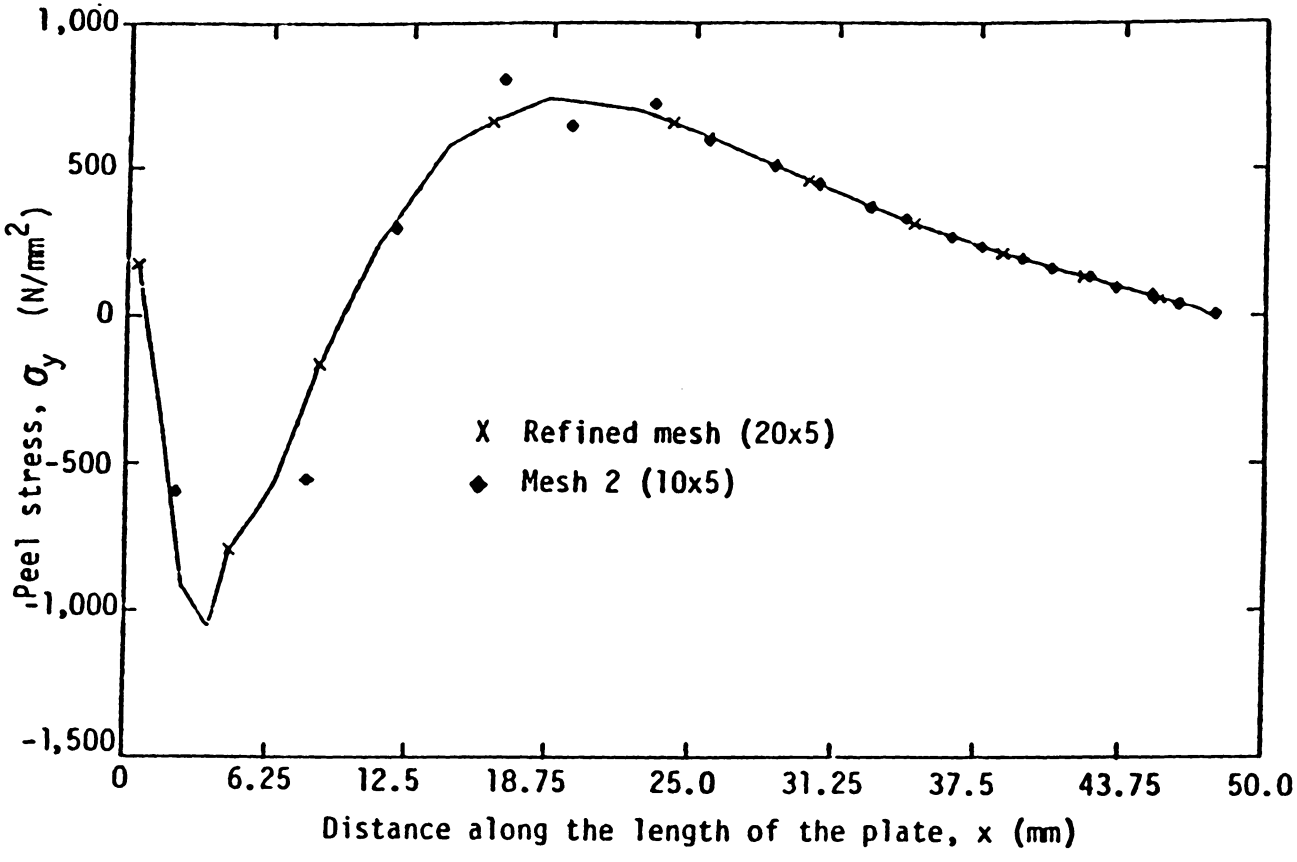

Figure 15. Plot of Peel Stress along the Bondline for a Bonded Cantilever Plate.

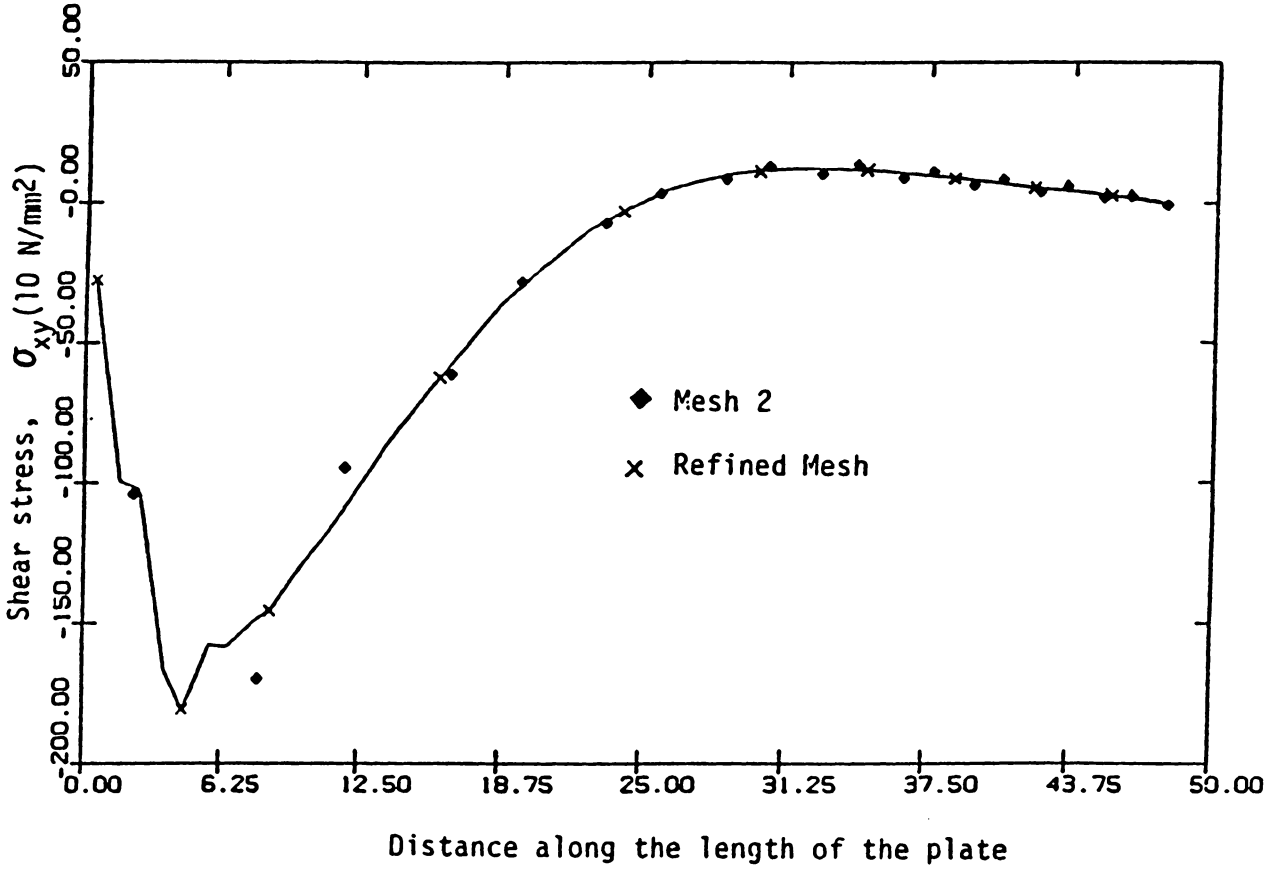

Figure 16. Plot of Shear Stress along the Bondline for a Bonded Cantilever Plate.

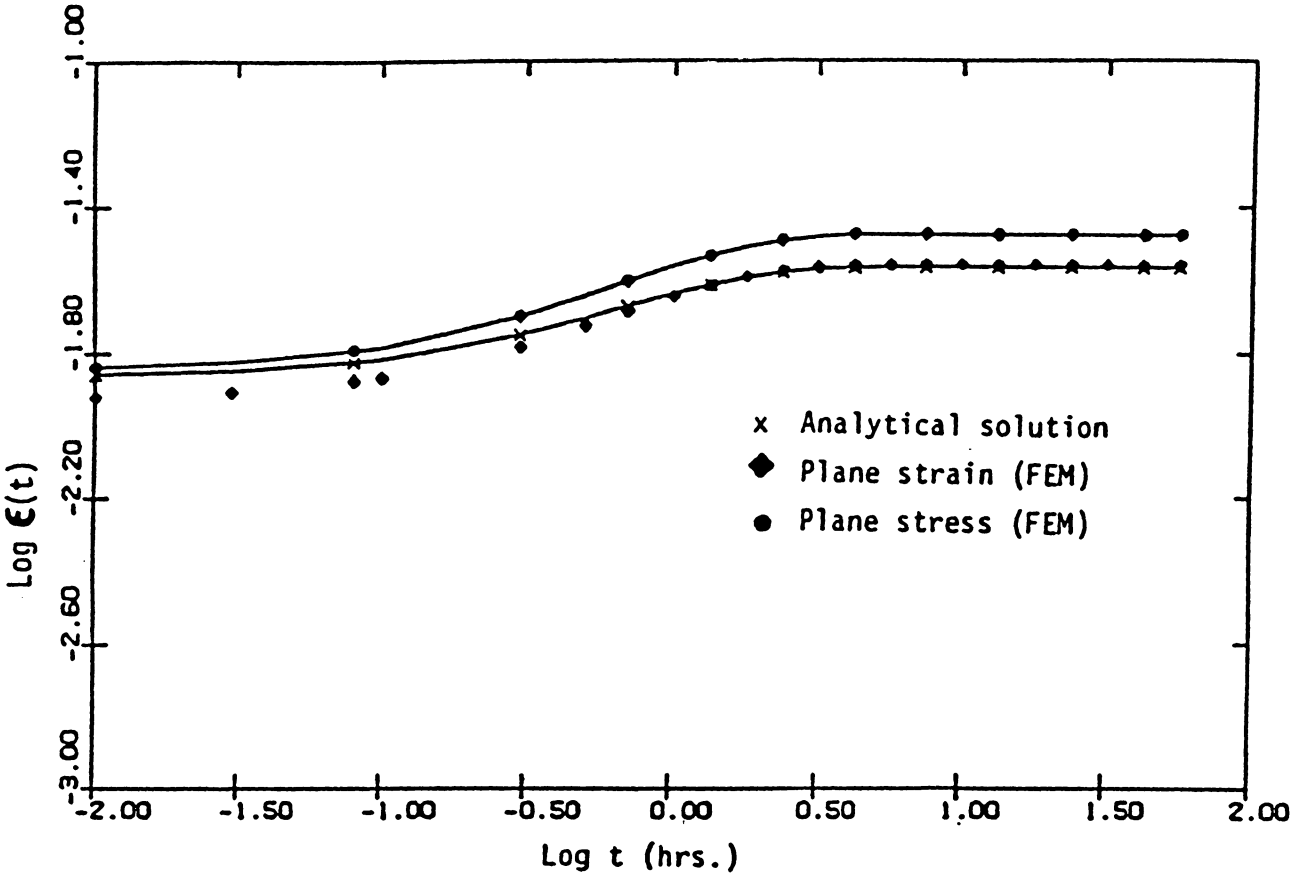

Figure 17a. Variation of Creep Strain with Time for a Poisson's Ratio of 0.417.

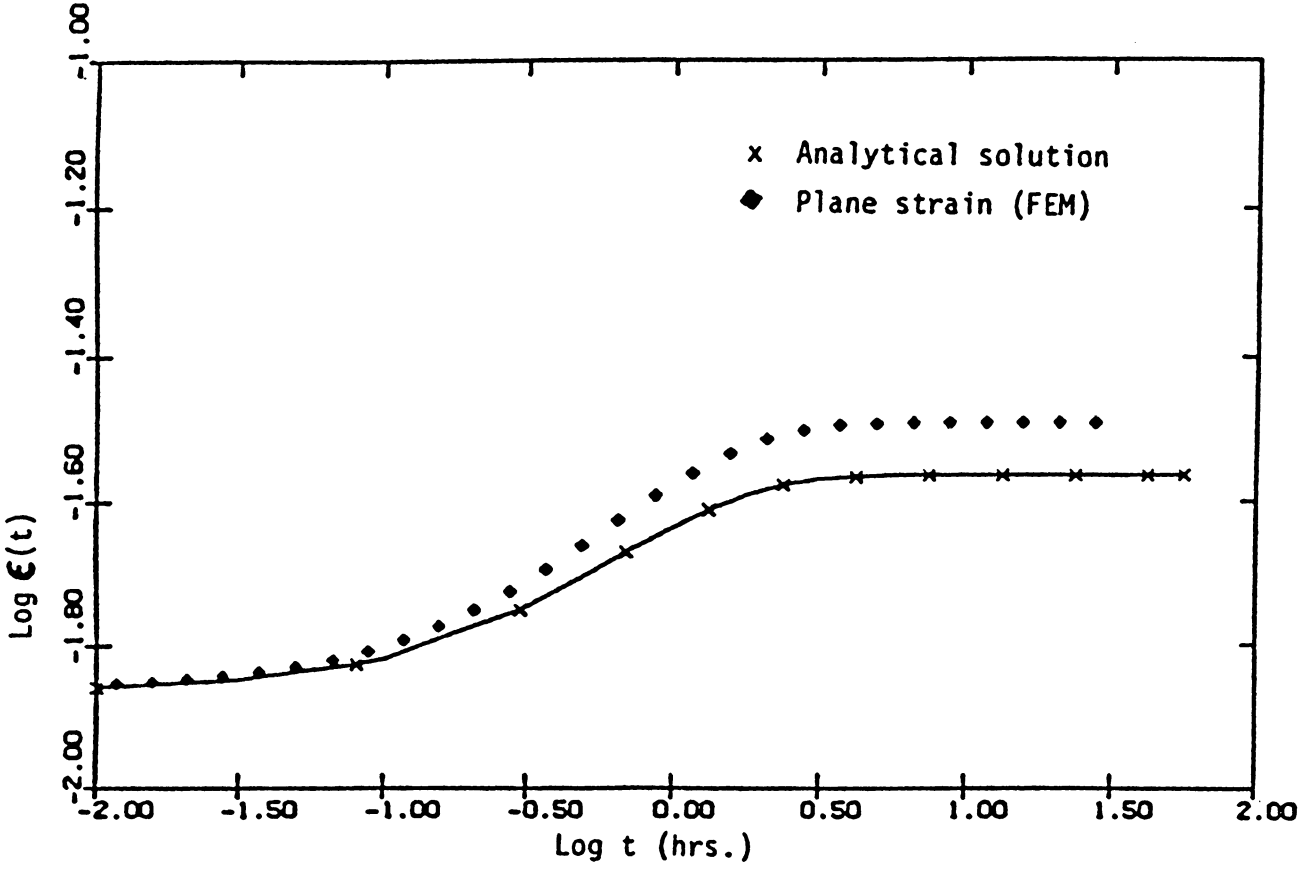

Figure 17b. Variation of Creep Strain with Time for a Poisson's Ratio of 0.32 .

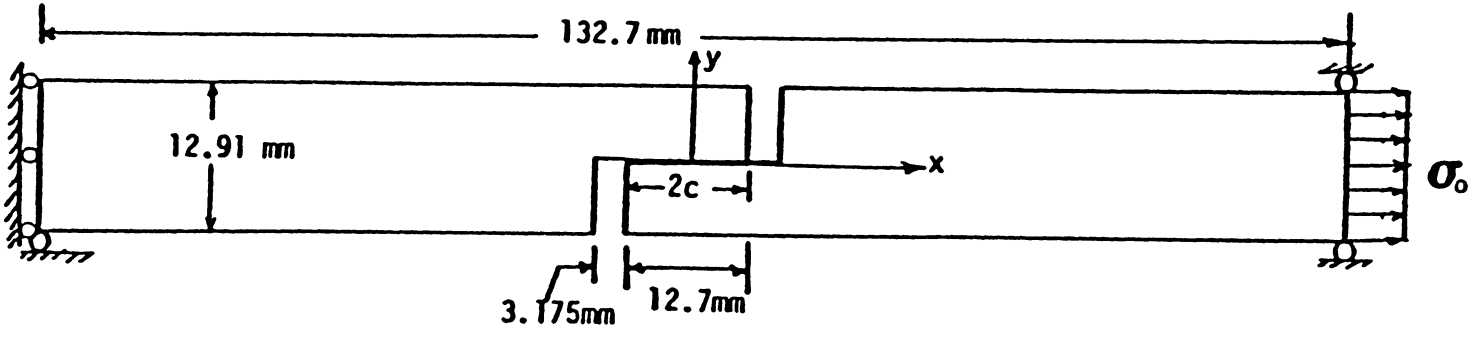

(a)

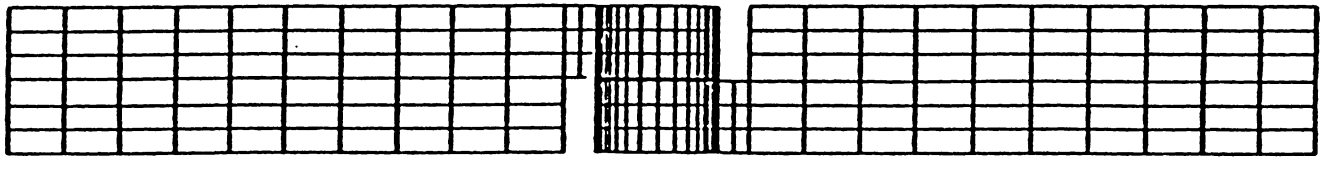

(b)

Figure 18. The Geometry, Boundary Conditions, Loading and Finite Element Mesh used in the Model Joint Analysis.

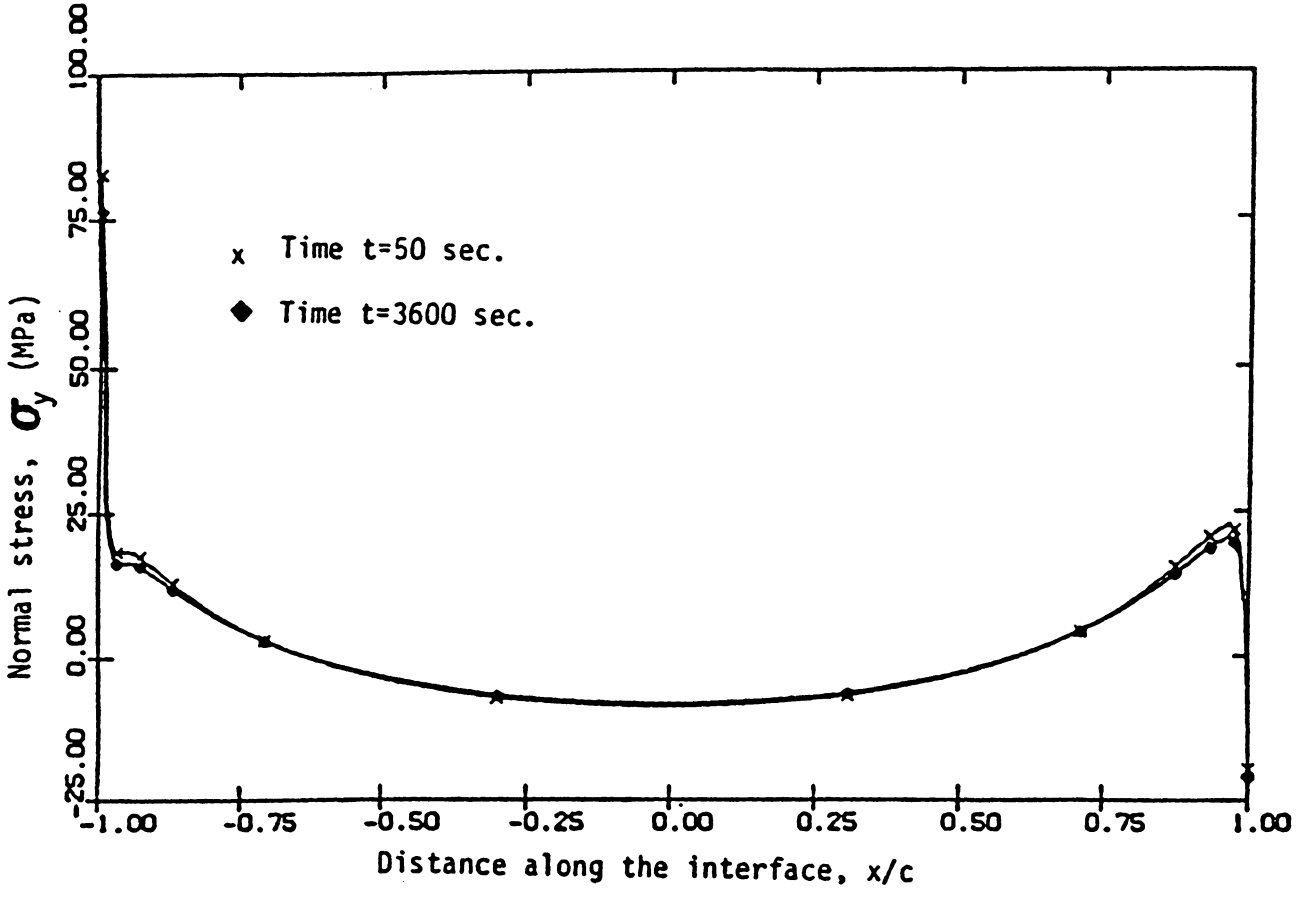

Figure 19. Peel Stress along the Bondline for a Linear Viscoelastic Analysis of a Model Joint.

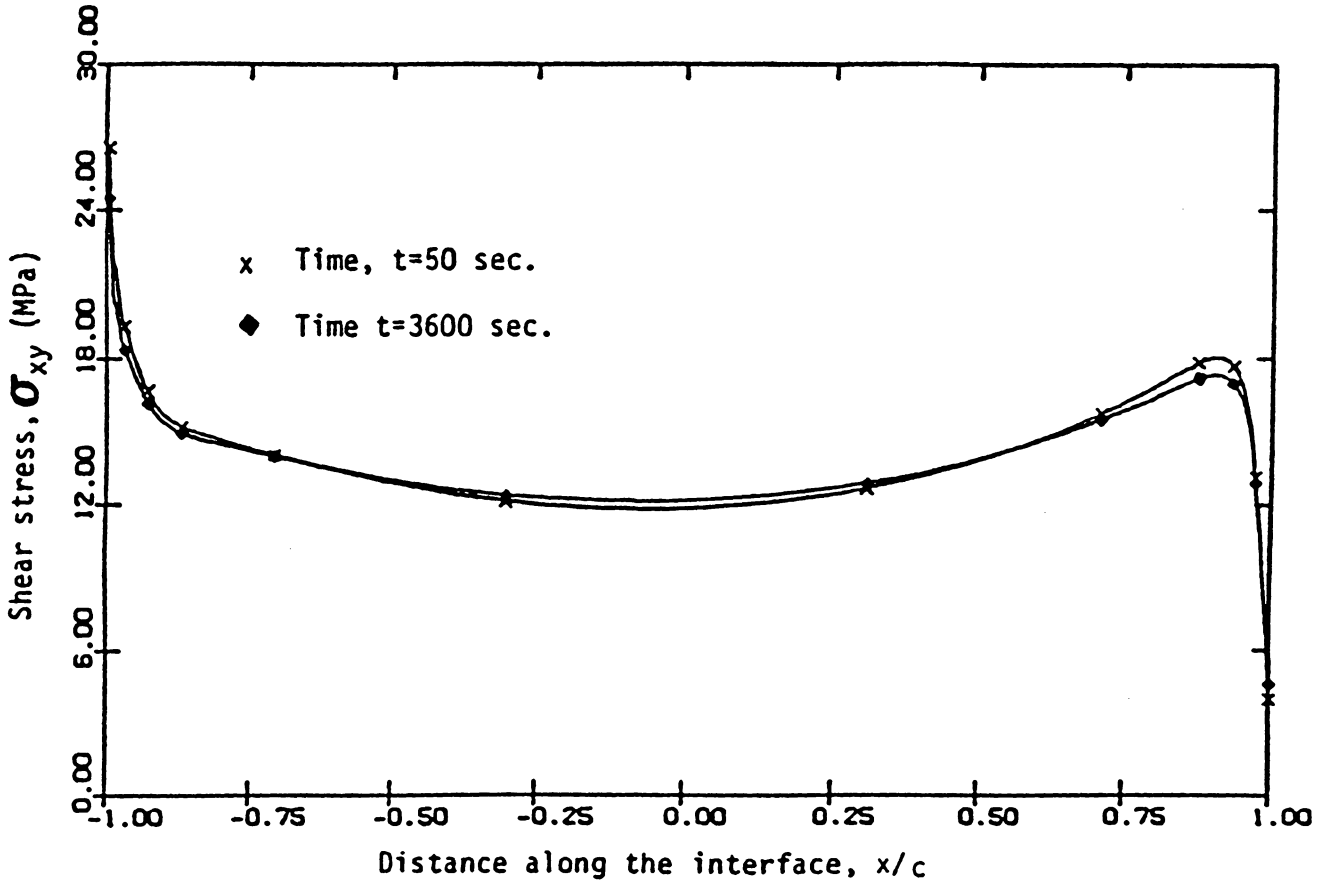

Figure 20. Shear Stress along the Bondline for a Linear Viscoelastic Analysis of a Model Joint.

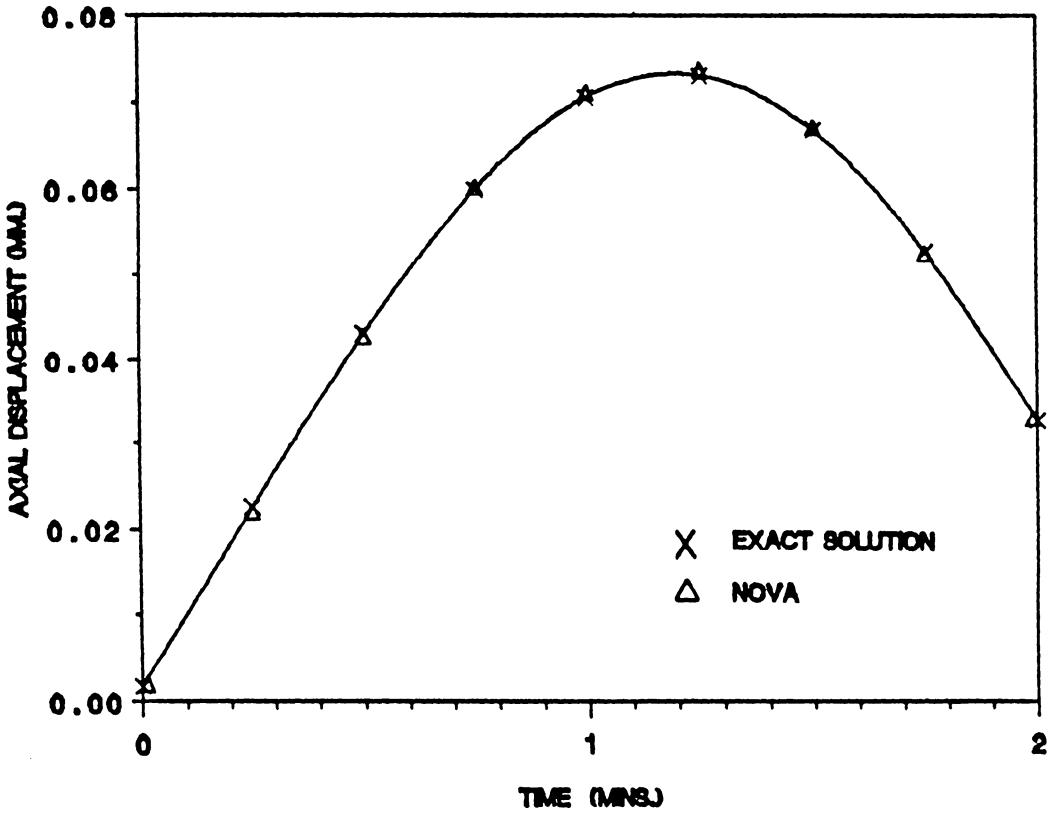

Figure 21. Plot of Axial Displacement against Time for a Viscoelastic Rod.

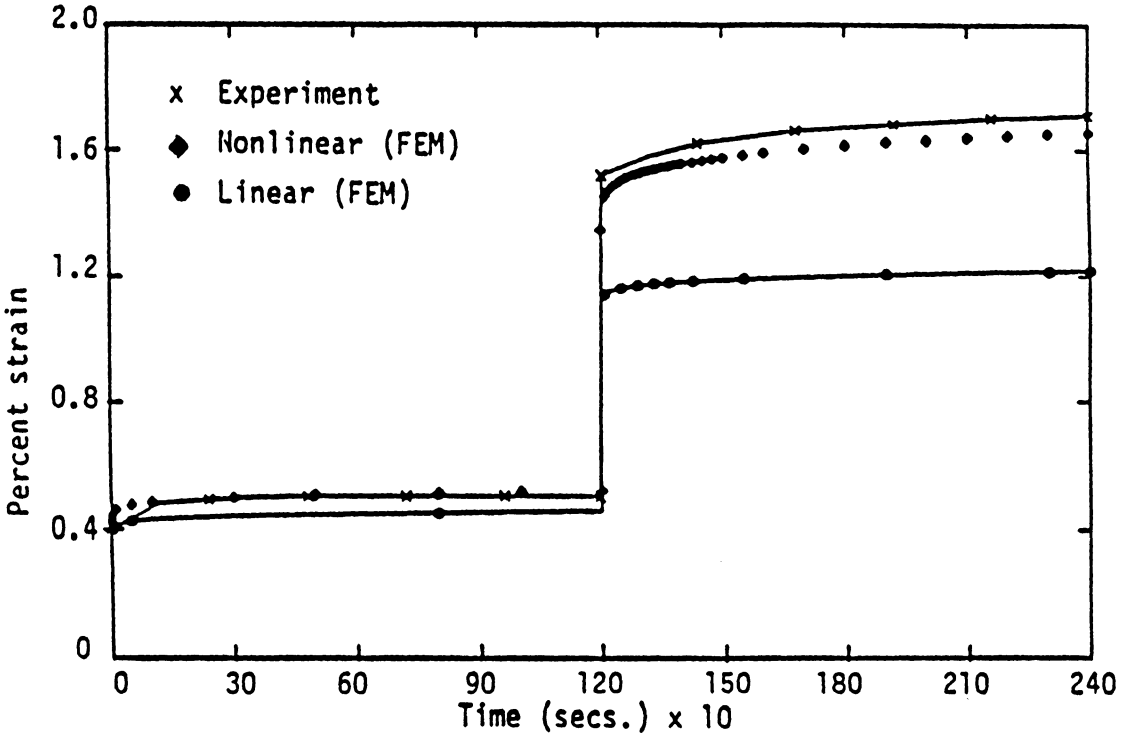

Figure 22. Variation of Creep Strain with Time for a FM-73 Coupon Subject to Step Loads at Constant Temperature.

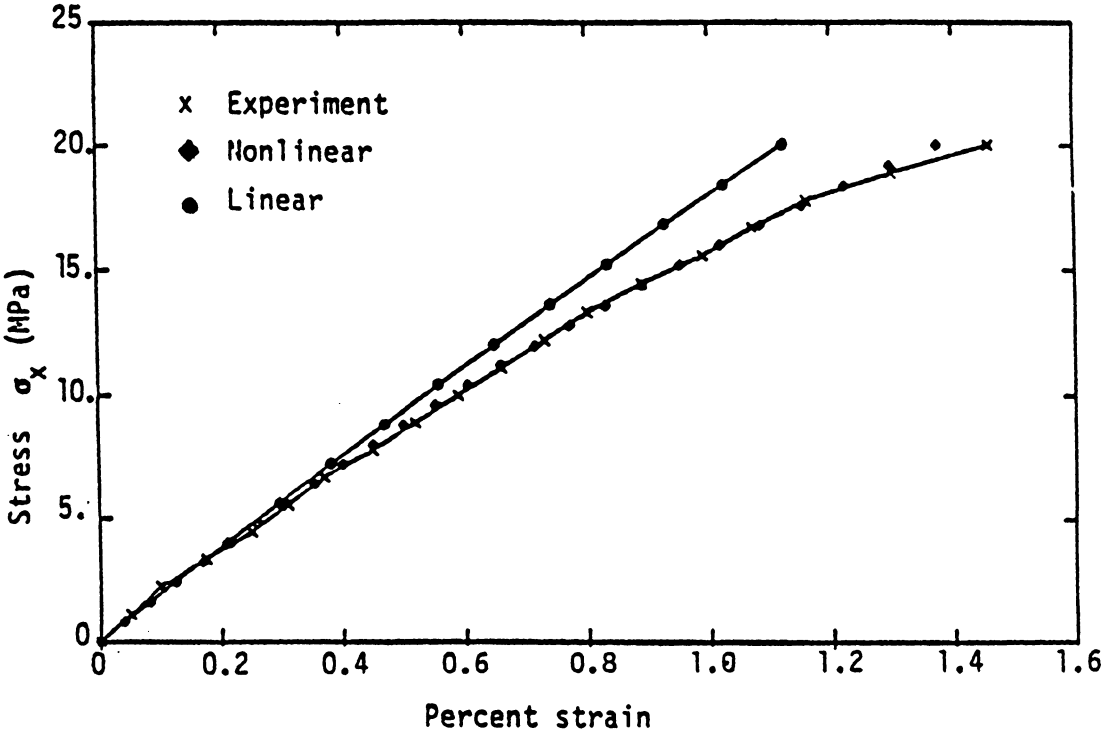

Figure 23. Stress-Strain Curve for a FM-73 Coupon Under Linearly Varying Stress and Temperature.

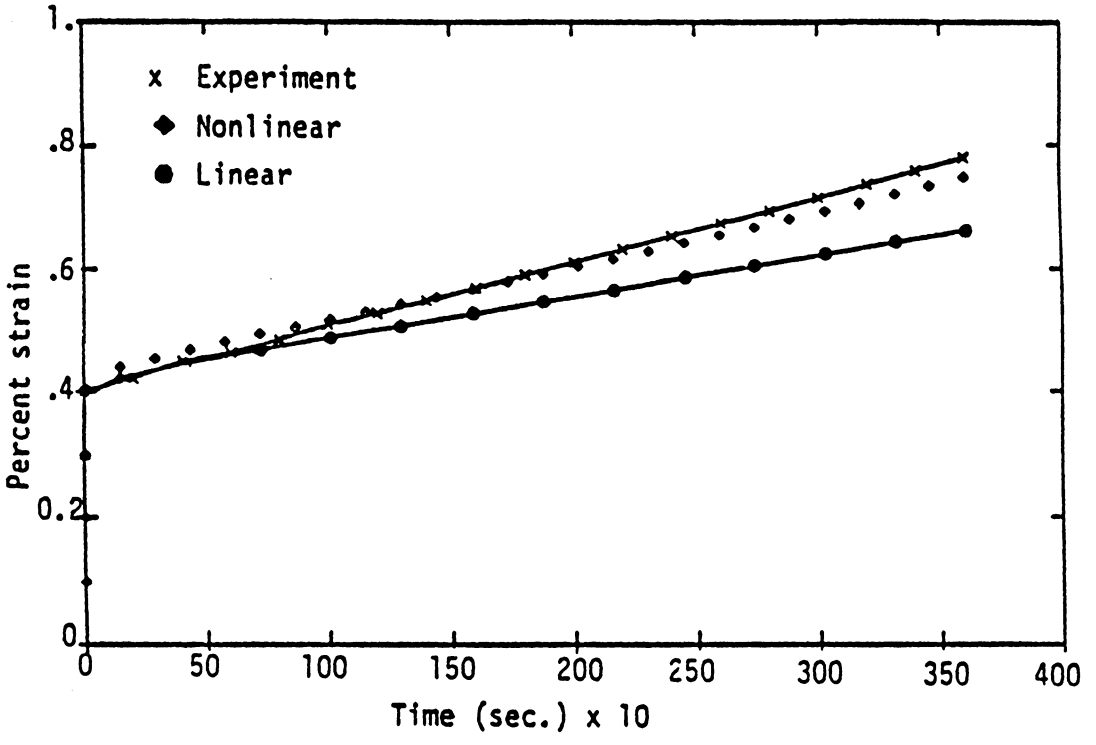

Figure 24. Variation of Creep Strain with Time for a FM-73 Coupon Subject to a Linearly Varying Temperature at Constant Stress.

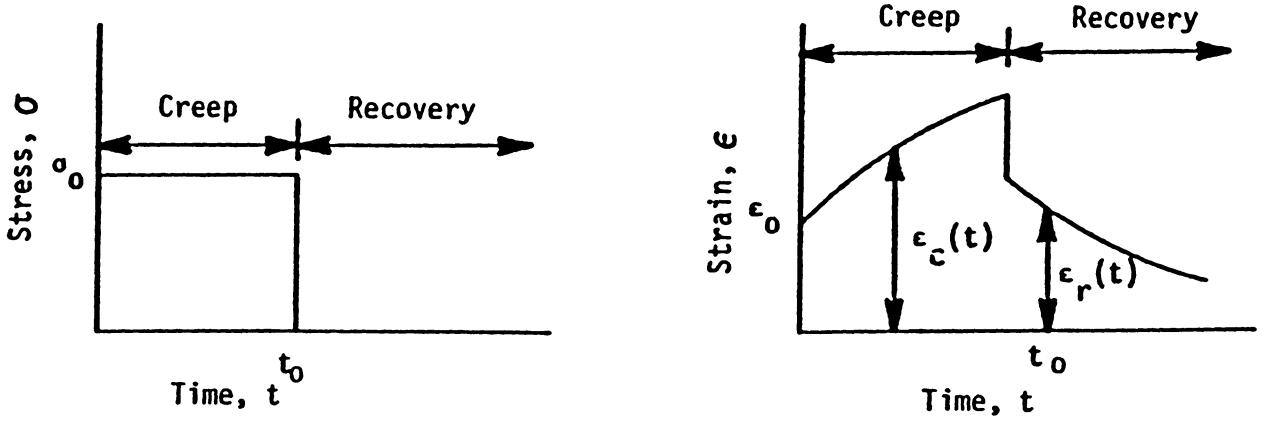

Figure 25. Load and Response for a Creep and Recovery Test.

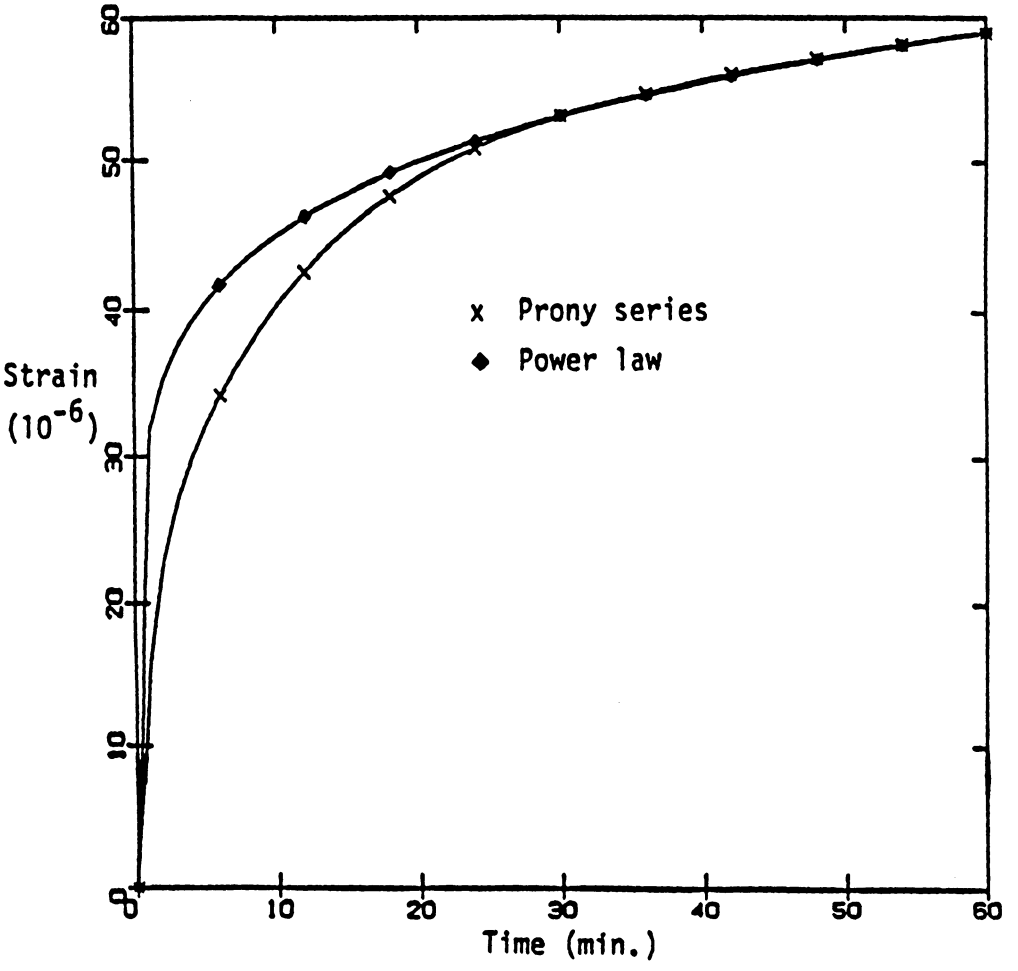

Figure 26. Comparison of Creep Compliances Obtained Using Prony Series and Power Law.

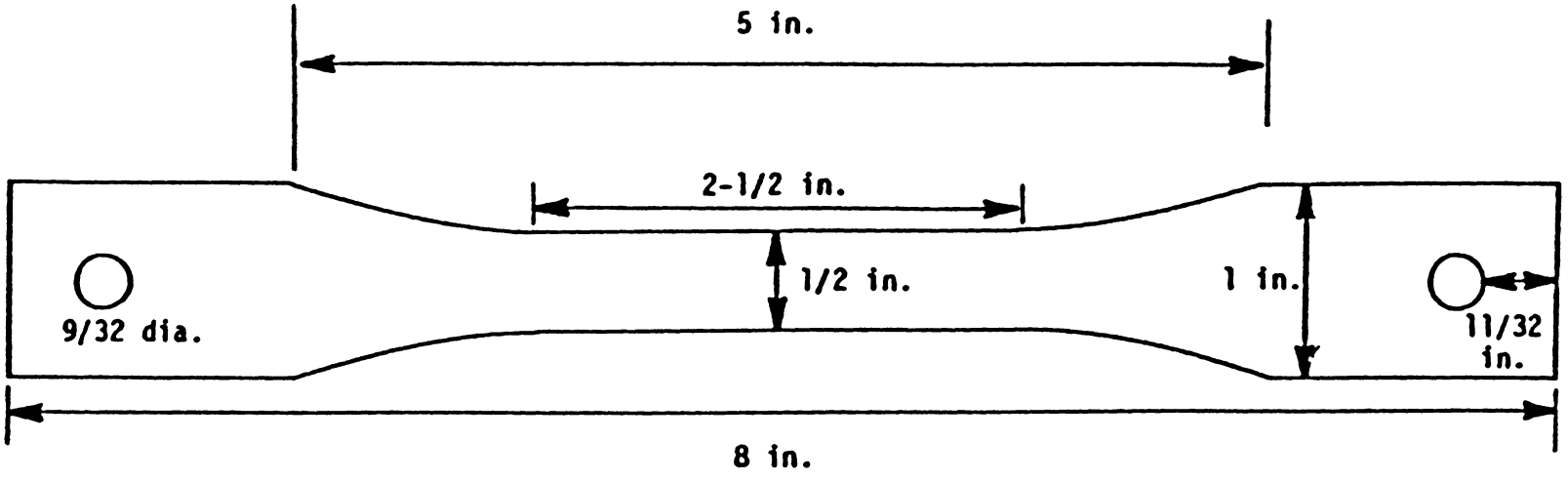

Figure 27. A Tensile Dogbone Test Specimen.

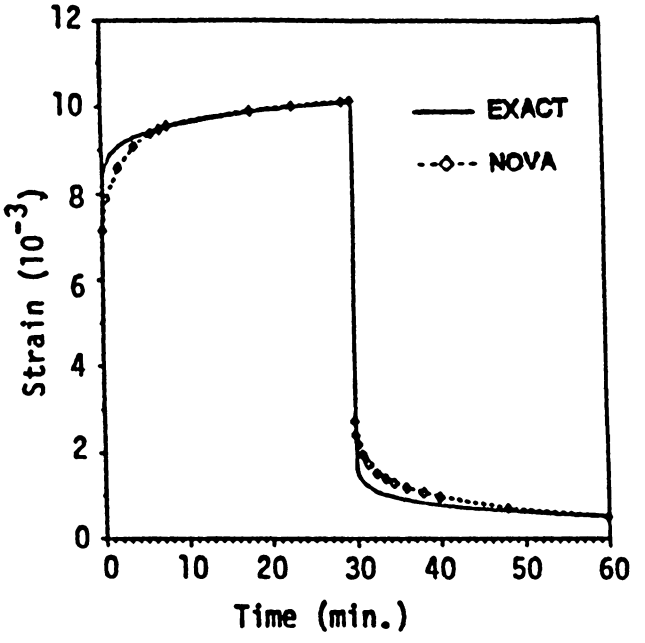

Figure 28a. Creep and Creep Recovery in a FM-73 Adhesive Coupon for an Applied Stress of 21 MPa.

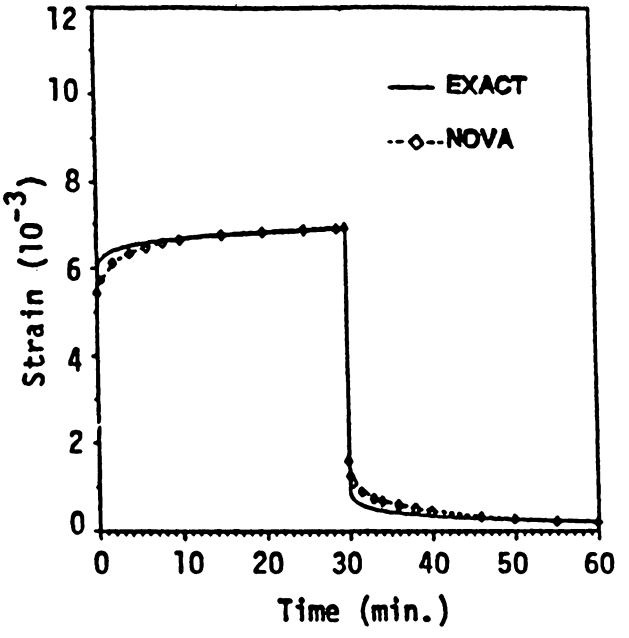

Figure 28b. Creep and Creep Recovery in a FM-73 Adhesive Coupon for an Applied Stress of 17 MPa.

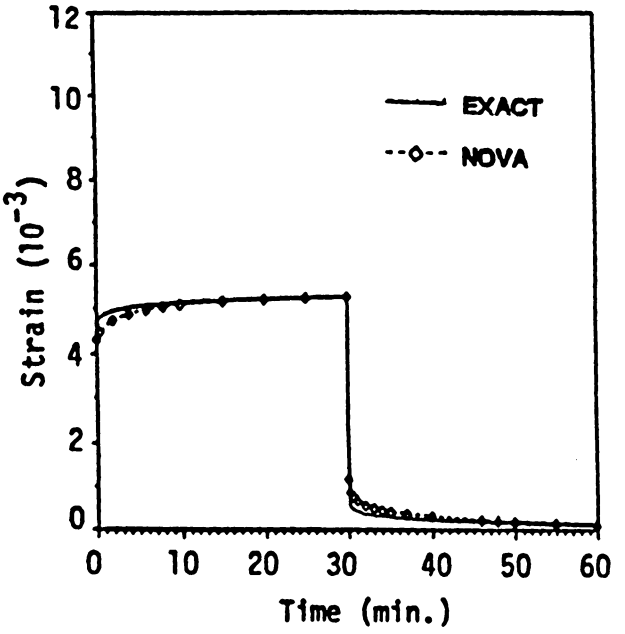

Figure 28c. Creep and Creep Recovery in a FM-73 Adhesive Coupon for an Applied Stress of 14 MPa.

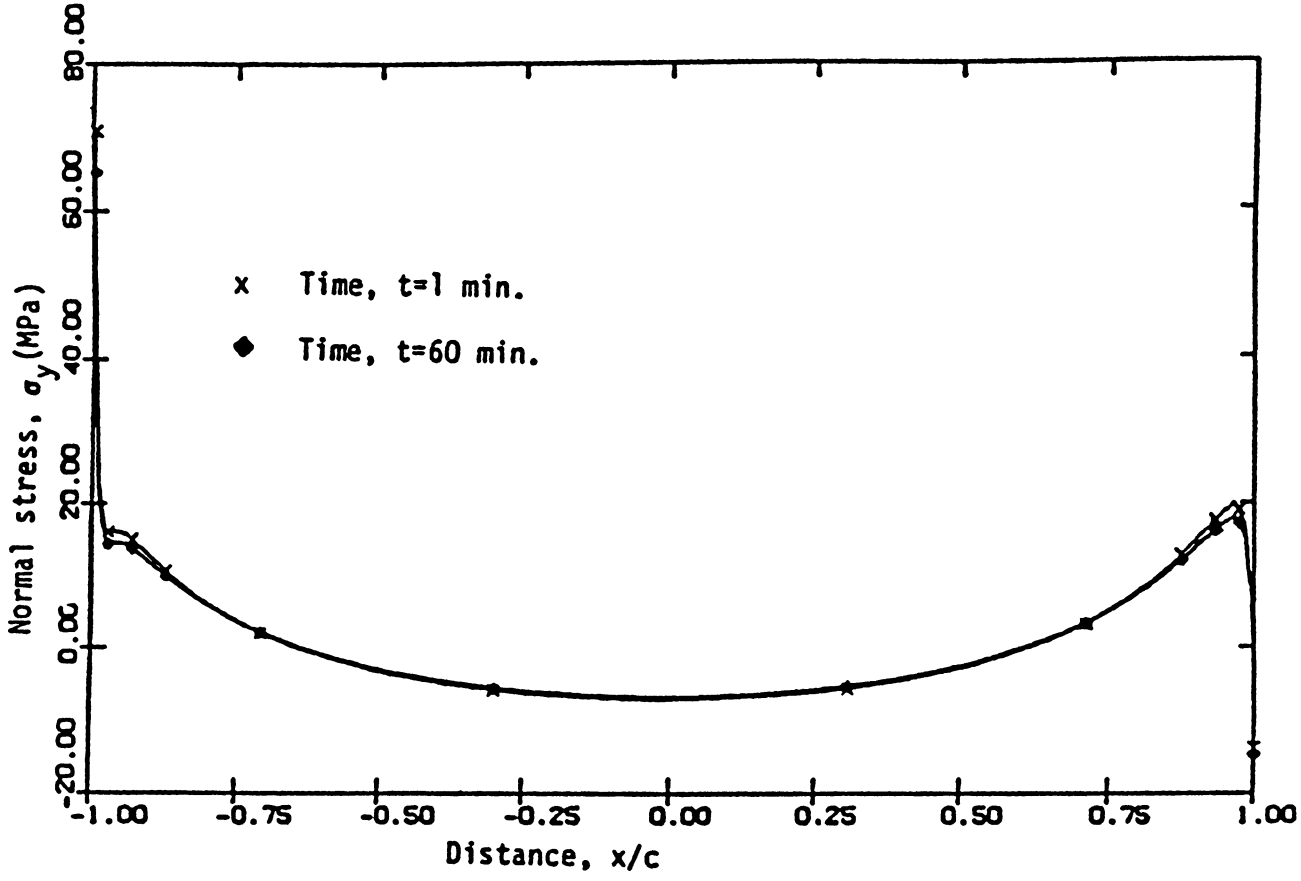

Figure 29a. Peel Stress along the Upper Bondline for Linear Viscoelastic Analysis of a Model Joint.

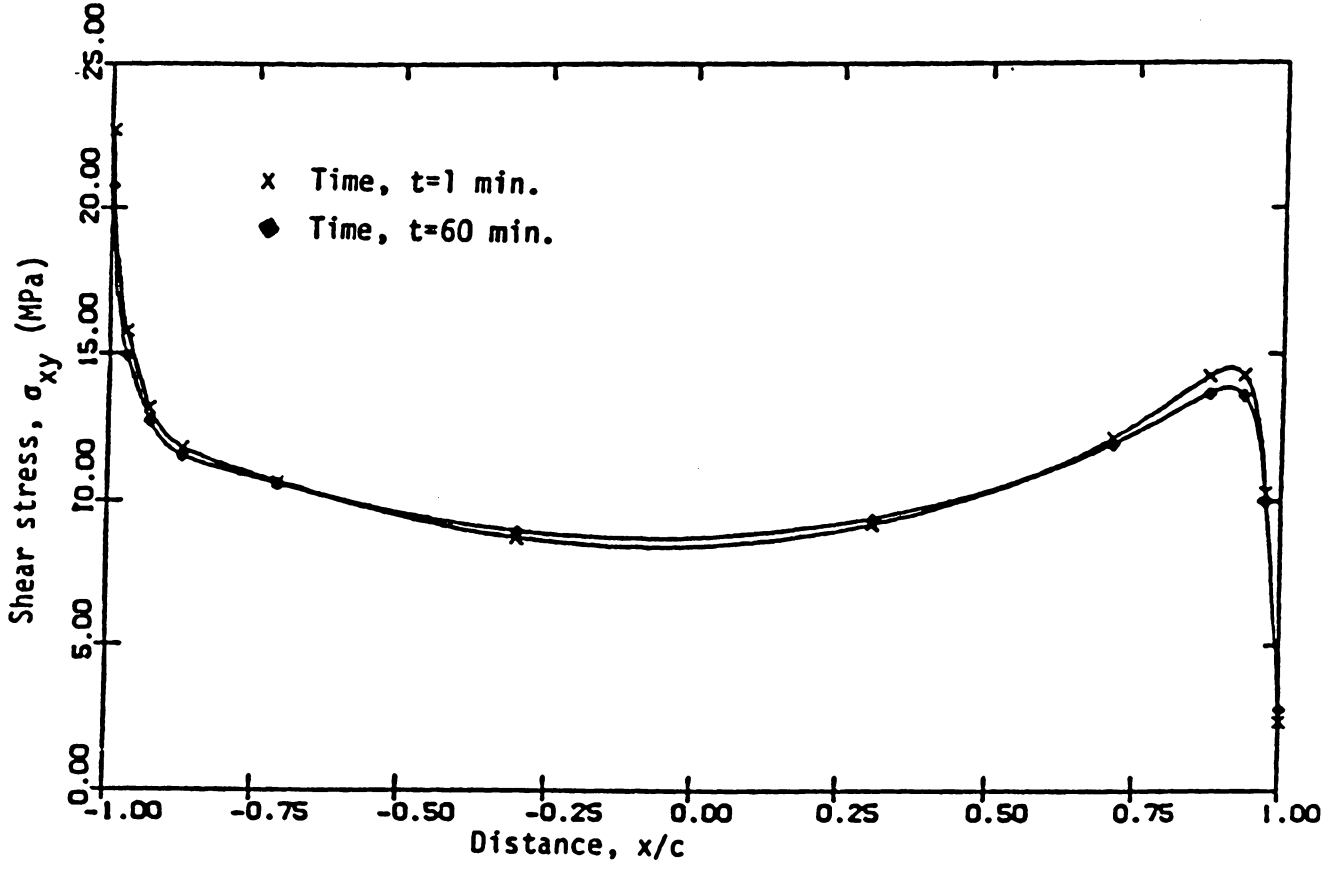

Figure 29b. Shear Stress along the Upper Bondline for Linear Viscoelastic Analysis of a Model Joint.

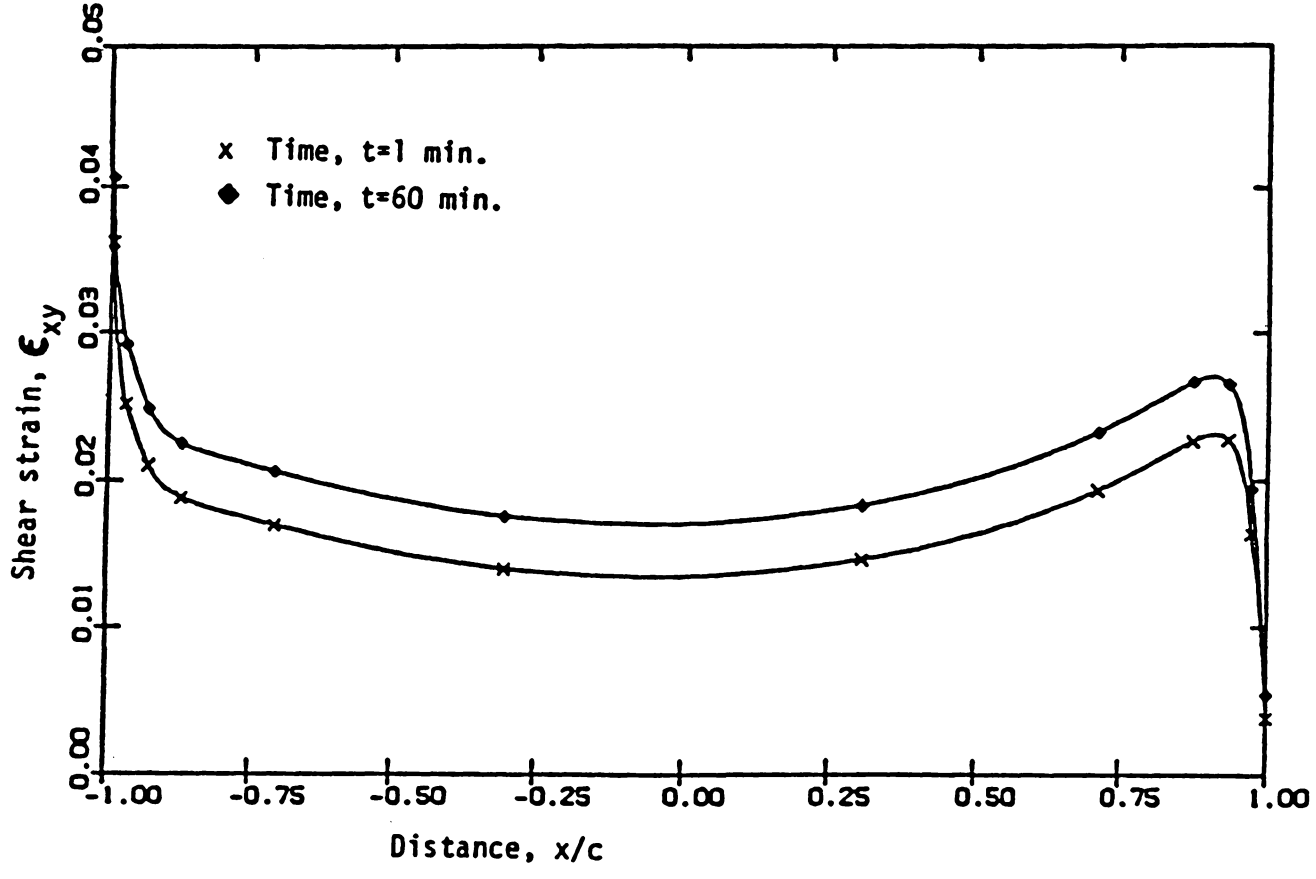

Figure 30. Shear Strain along the Upper Bondline for Linear Viscoelastic Analysis of a Model Joint.

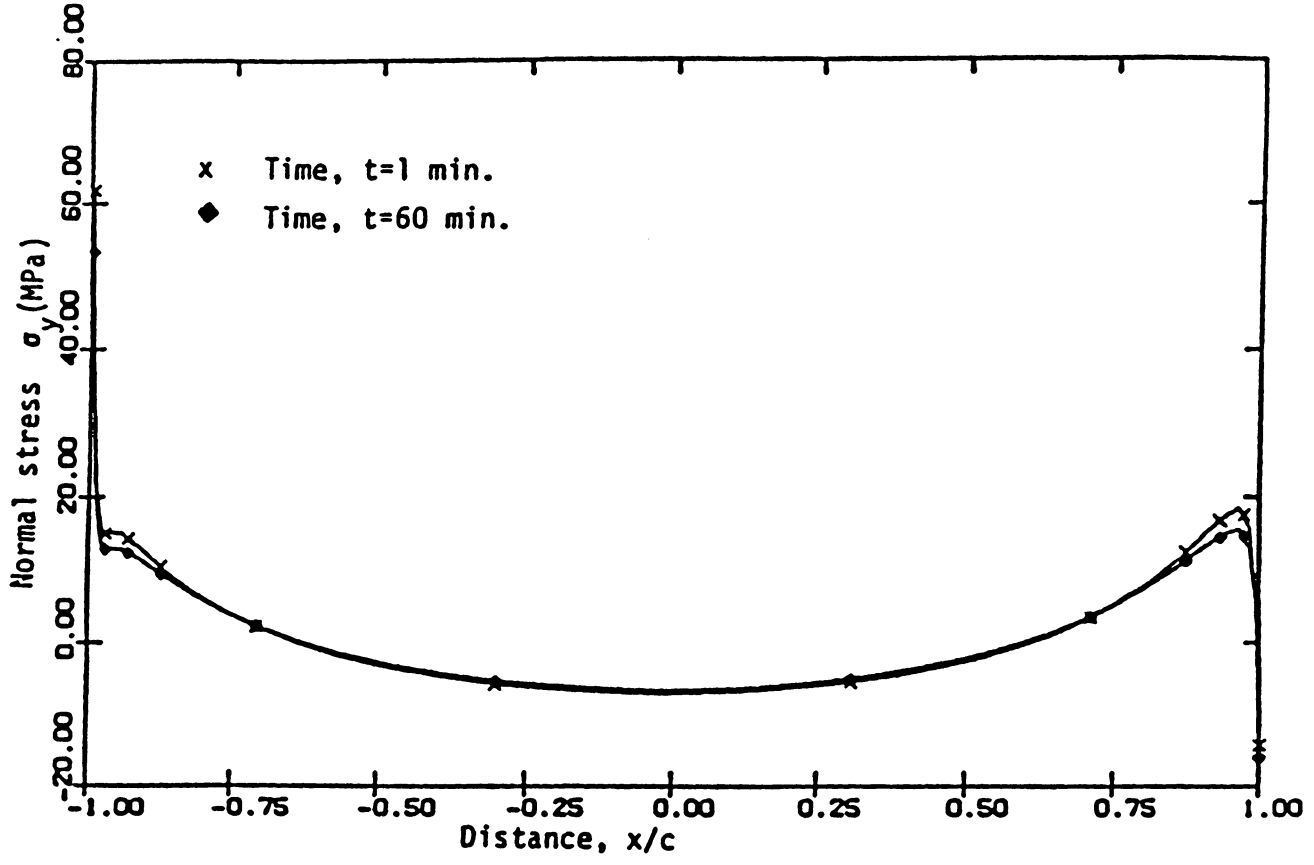

Figure 31a. Peel Stress along the Upper Bondline for Nonlinear Viscoelastic Analysis of a Model Joint.

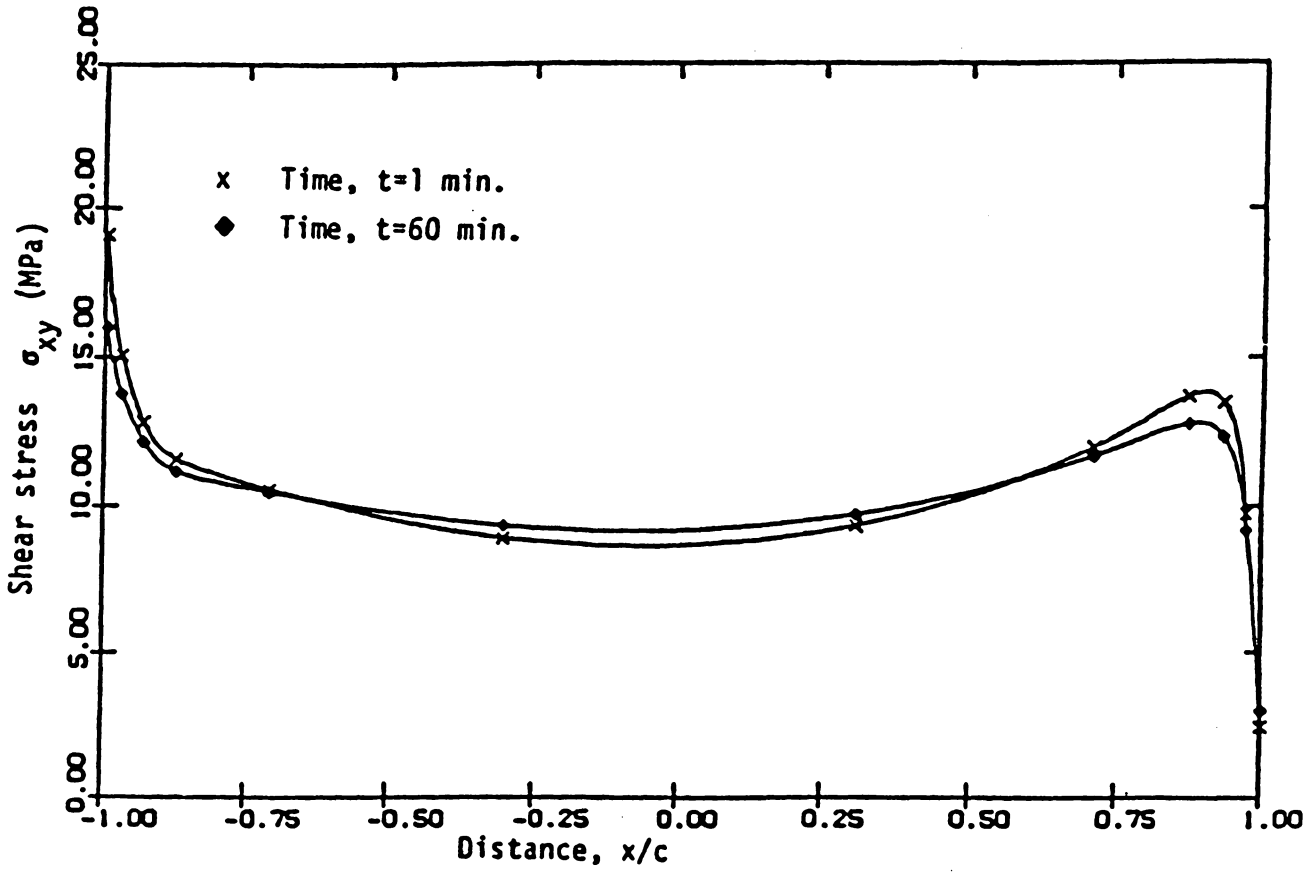

Figure 31b. Shear Stress along the Upper Bondline for Nonlinear Viscoelastic Analysis of a Model Joint.

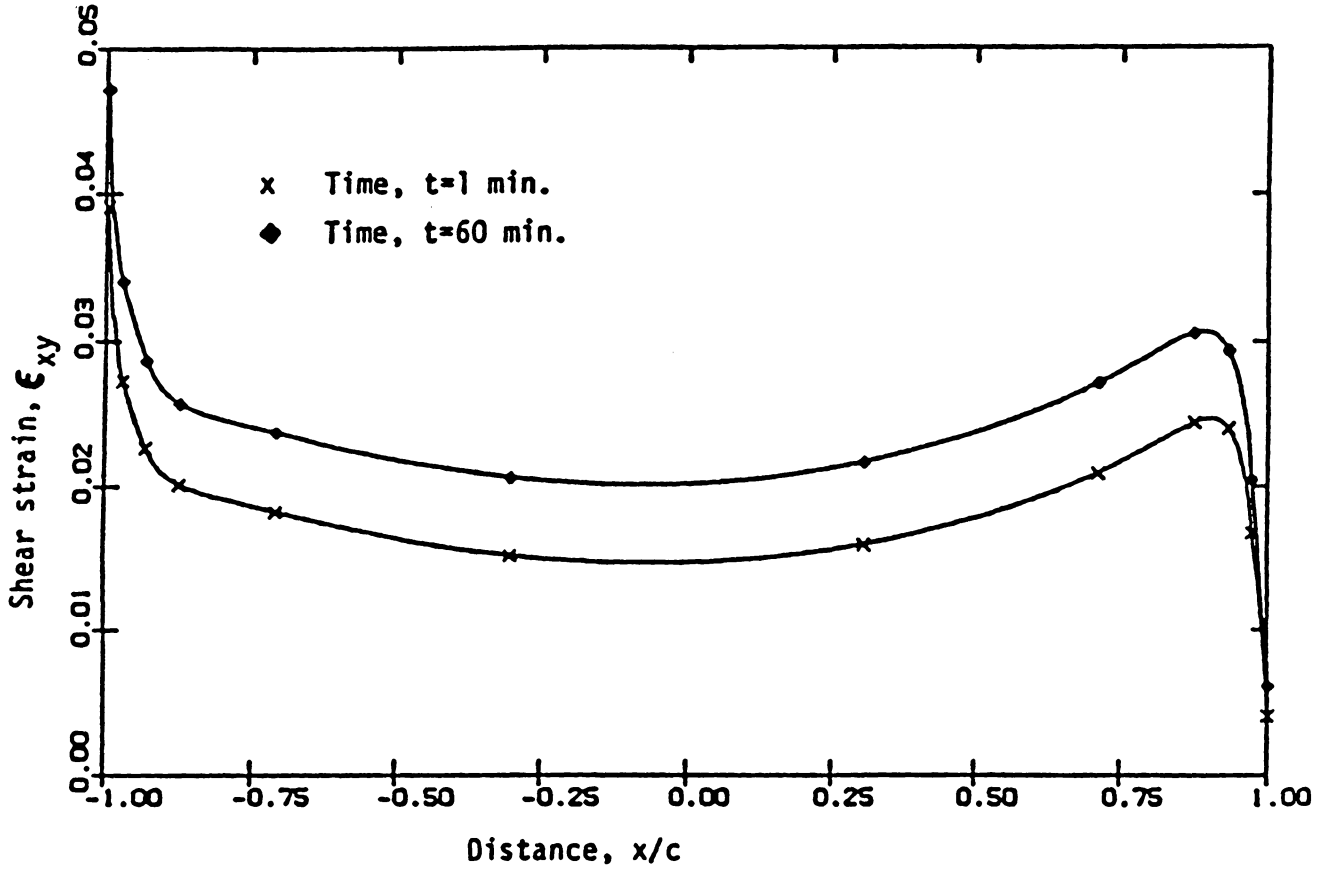

Figure 32. Shear Strain along the Upper Bondline for Nonlinear Viscoelastic Analysis of a Model Joint.

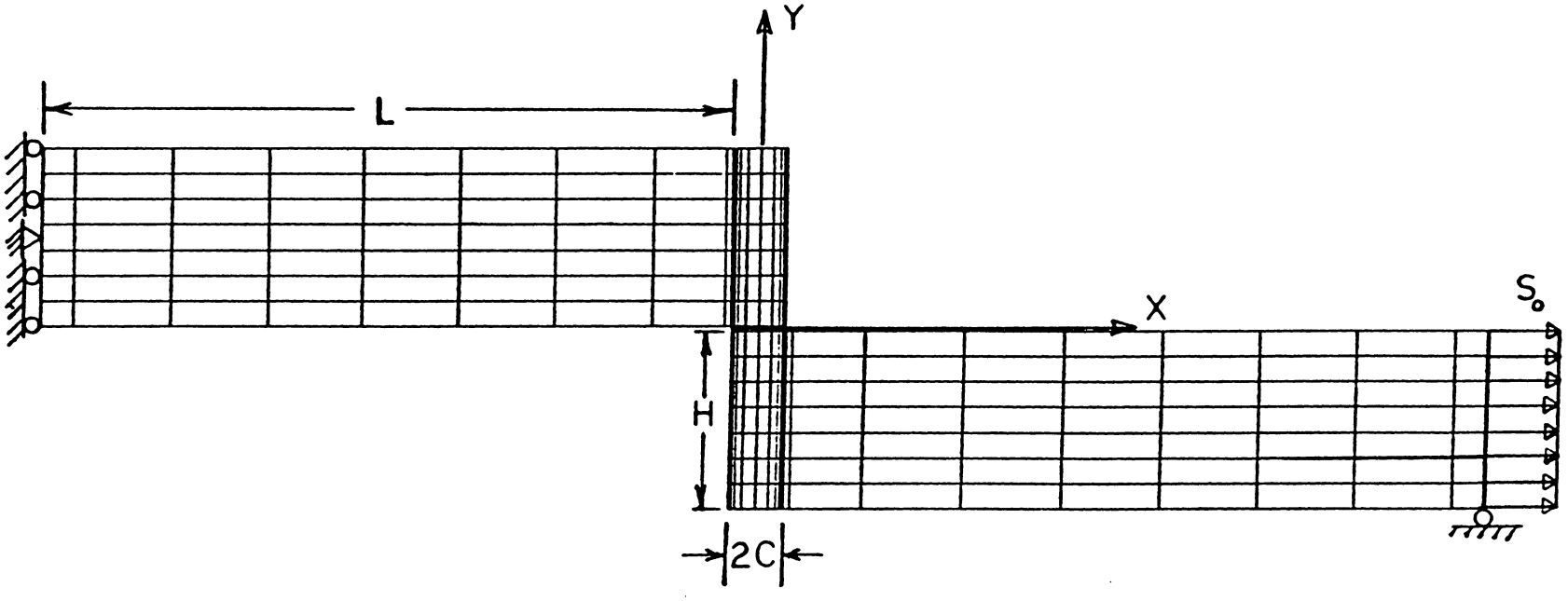

Figure 33. Specimen Geometry, Boundary Condition, and Finite Element Discretization for a Single Lap Joint with Composite Adherends (L = 107.0, H = 1.61, C = 4.0, Thickness of Adhesive Layer = 0.05, all dimensions in mm., Applied Stress = 2763 MPa.).

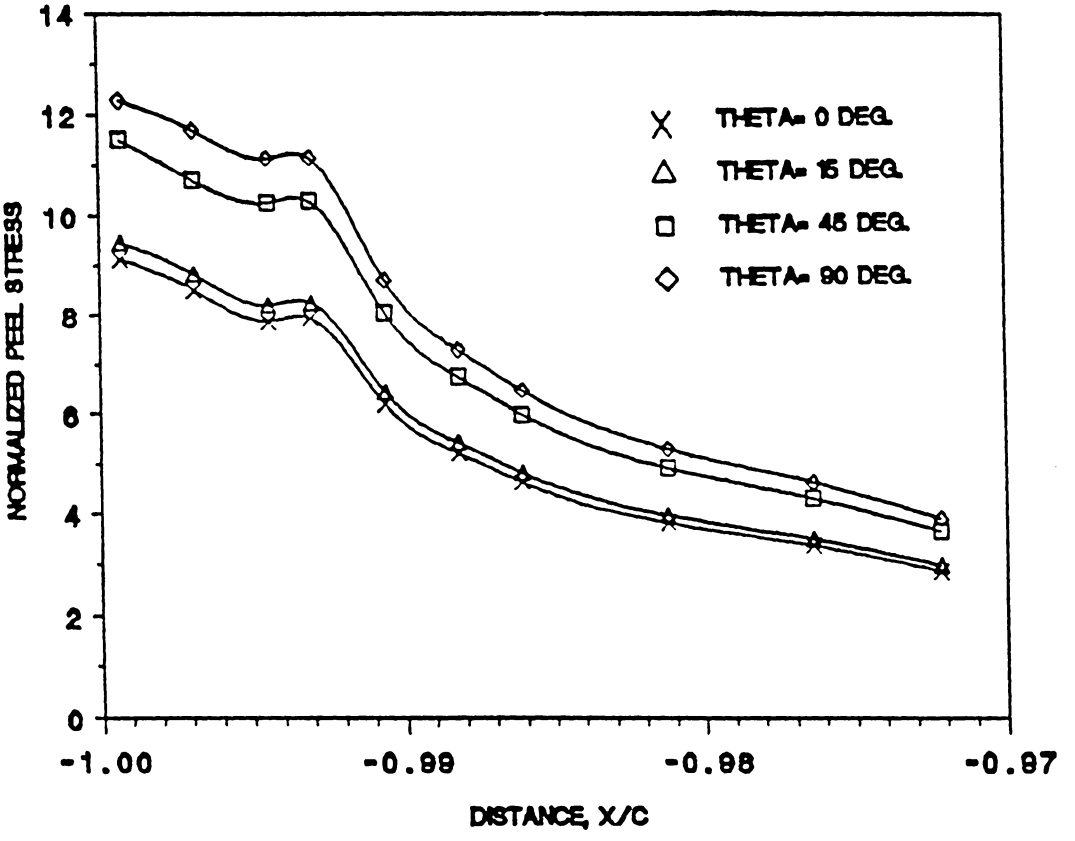

Figure 34. Influence of Ply Orientation on Adhesive Peel Stress.

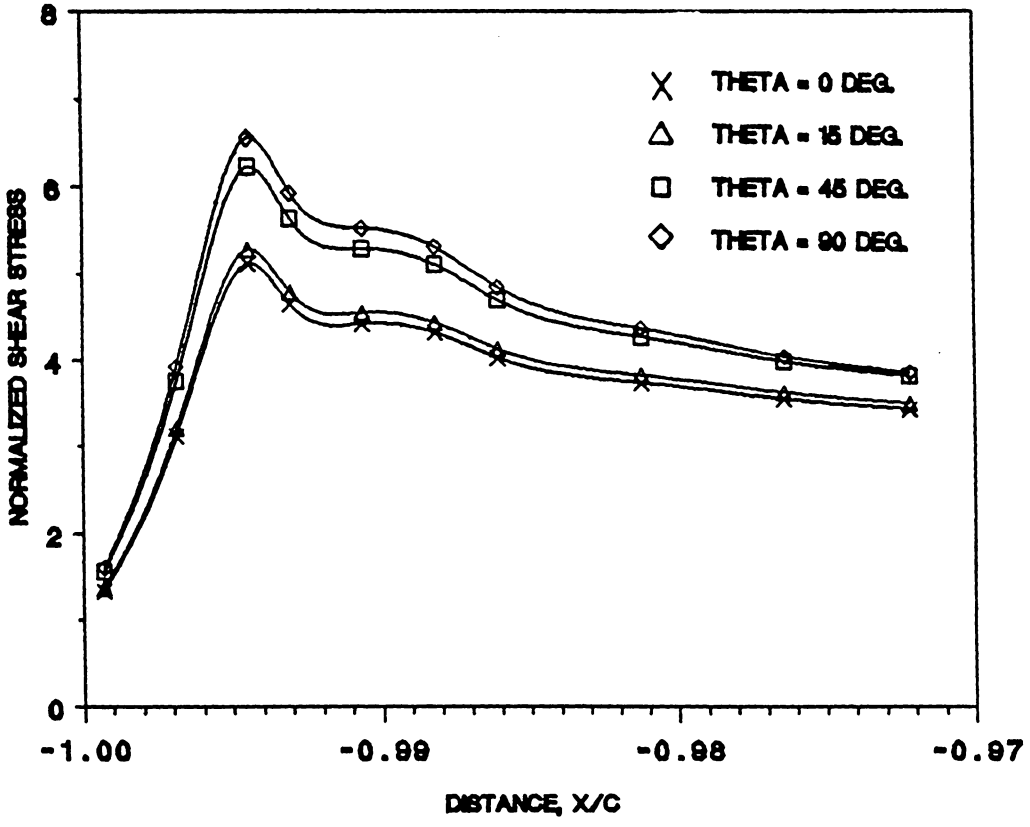

Figure 35. Influence of Ply Orientation on Adhesive Shear Stress.

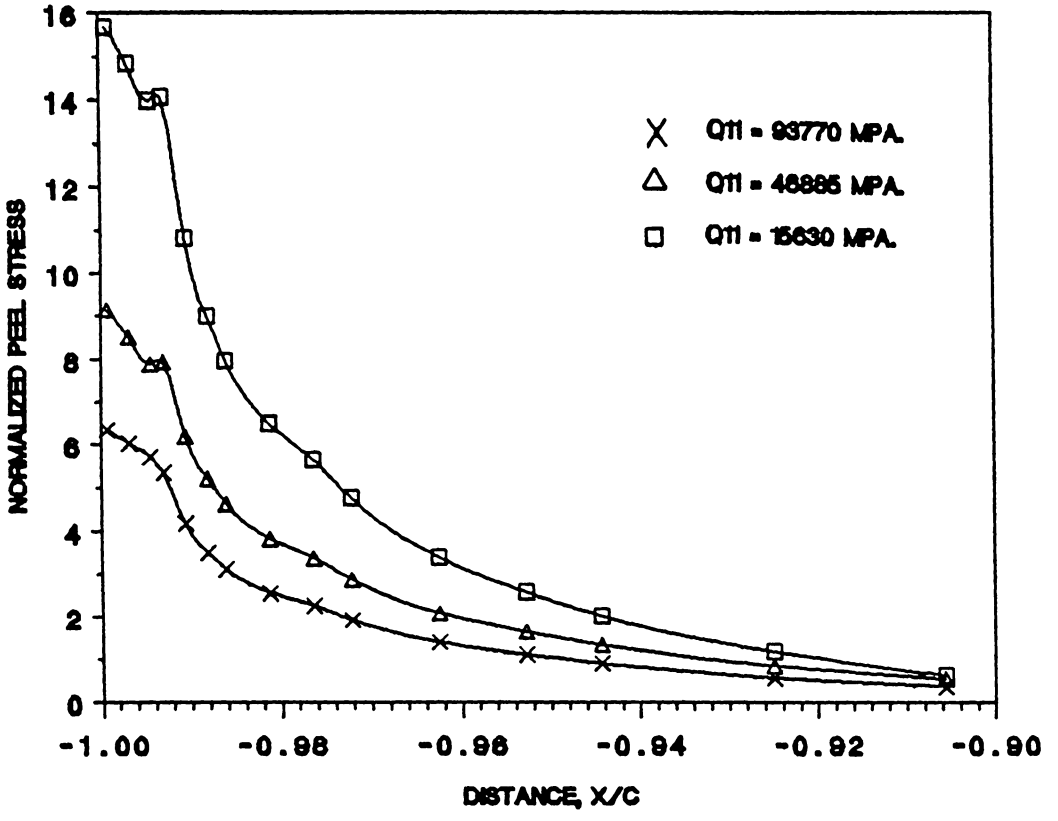

Figure 36. Influence of Q11 on Adhesive Peel Stress.

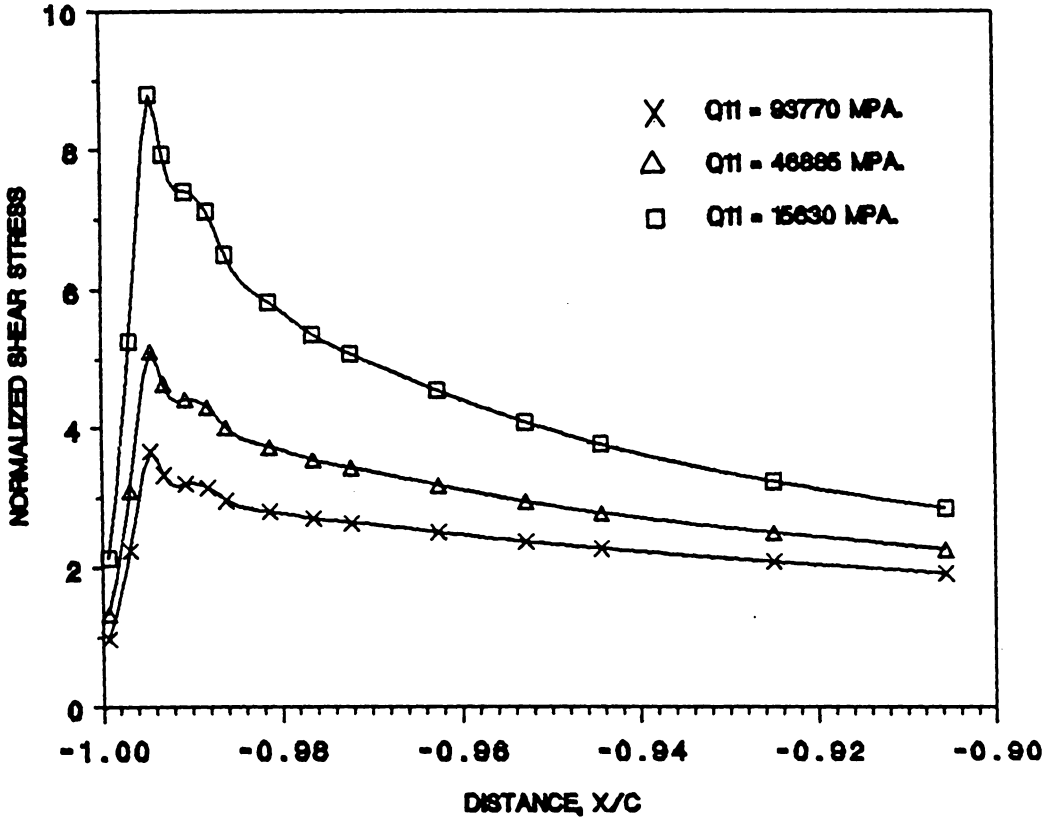

Figure 37. Influence of Q11 on Adhesive Shear Stress.

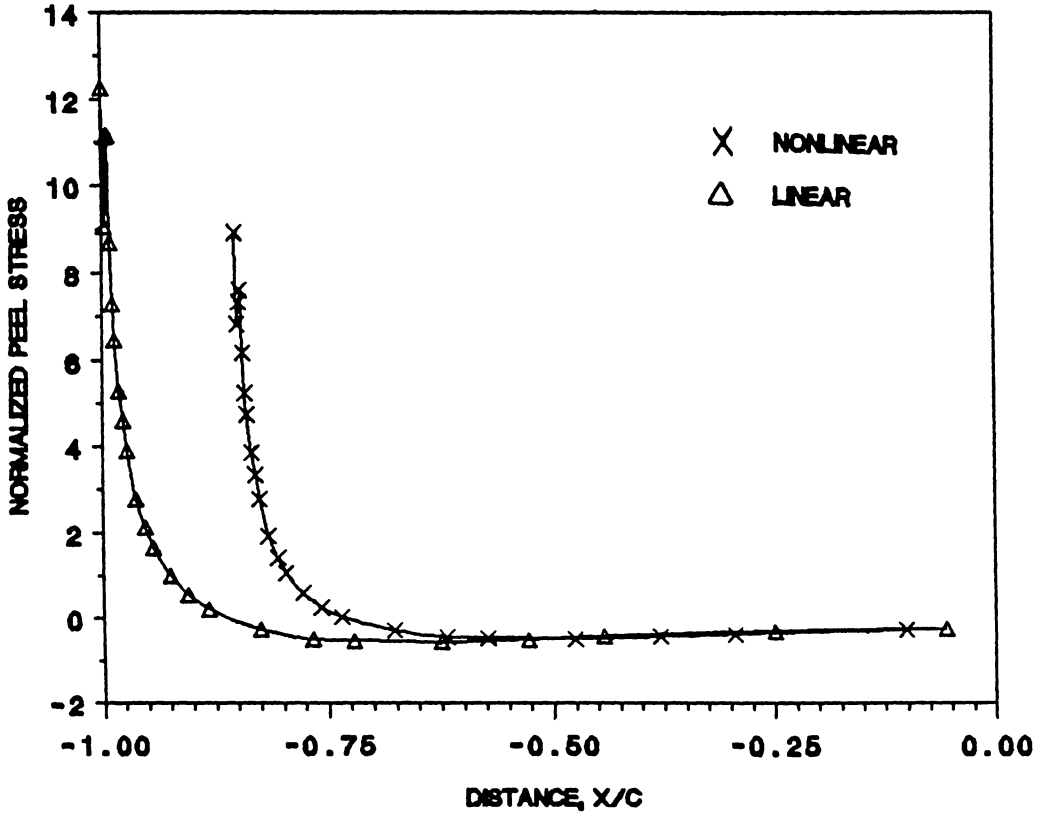

Figure 38. Influence of Geometric Nonlinearity on Adhesive Peel Stress.

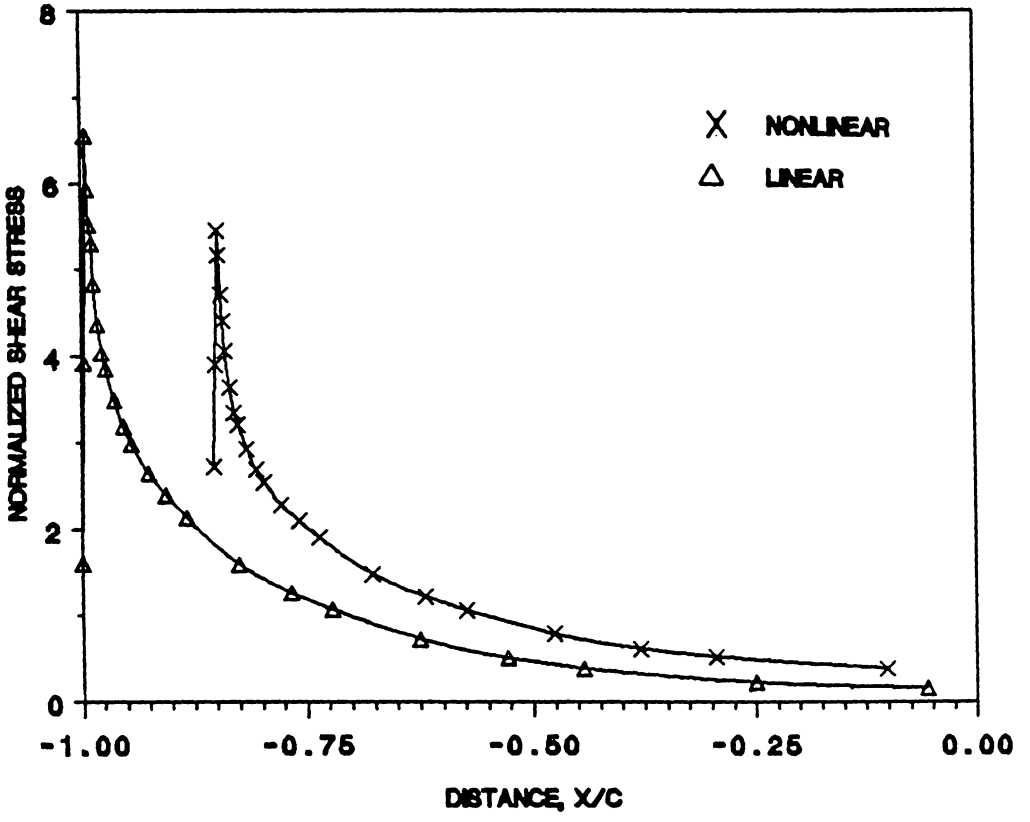

Figure 39. Influence of Geometric Nonlinearity on Adhesive Shear Stress.

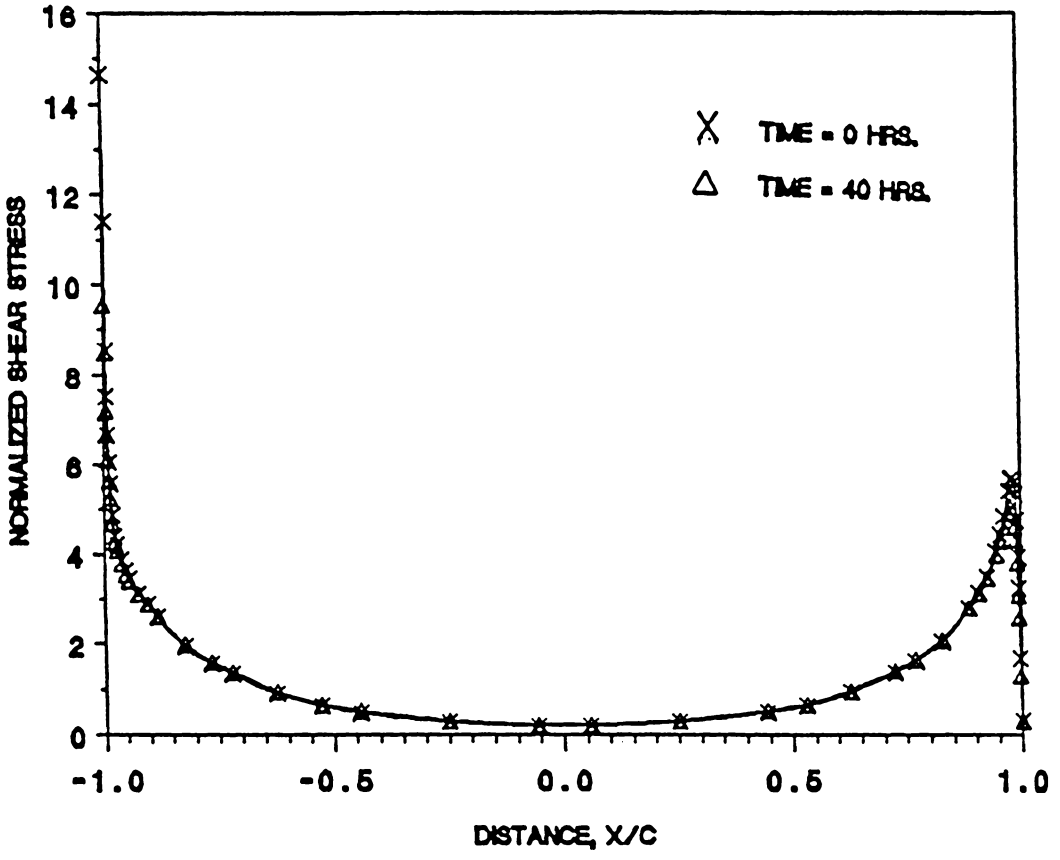

Figure 40. Variation of Shear Stress with Time for Entire Overlap.

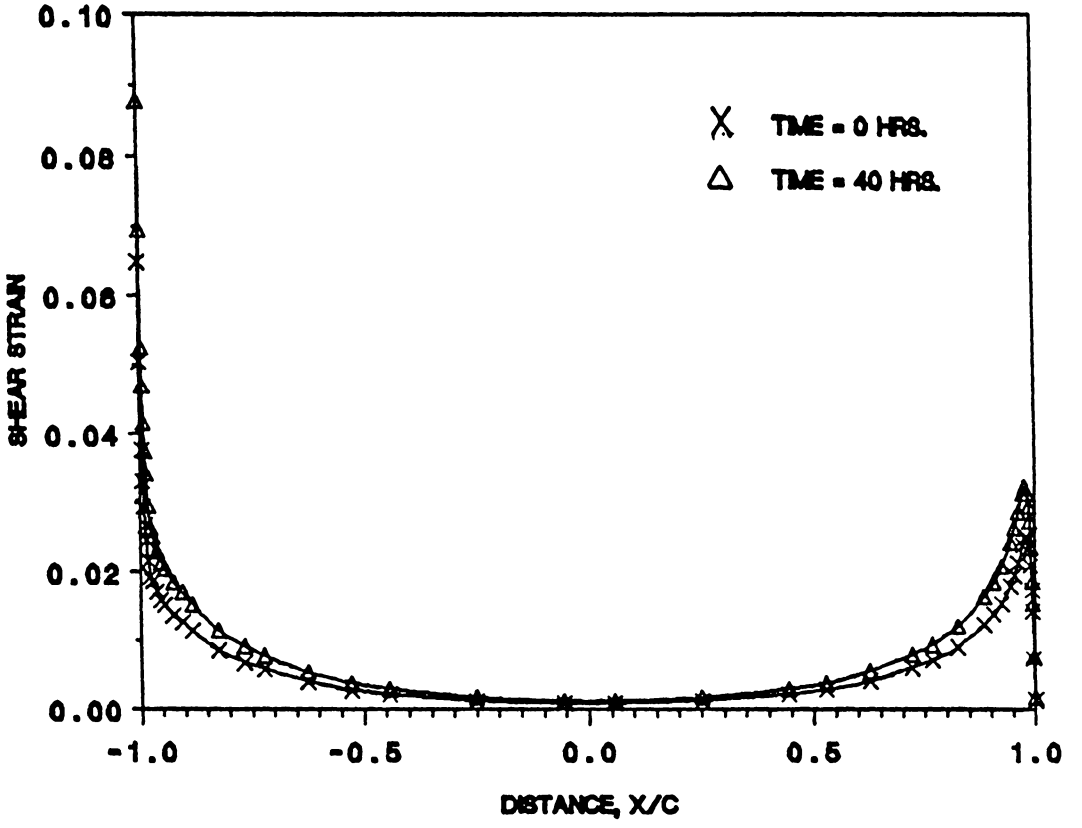

Figure 41. Variation of Shear Strain with Time for Entire Overlap.

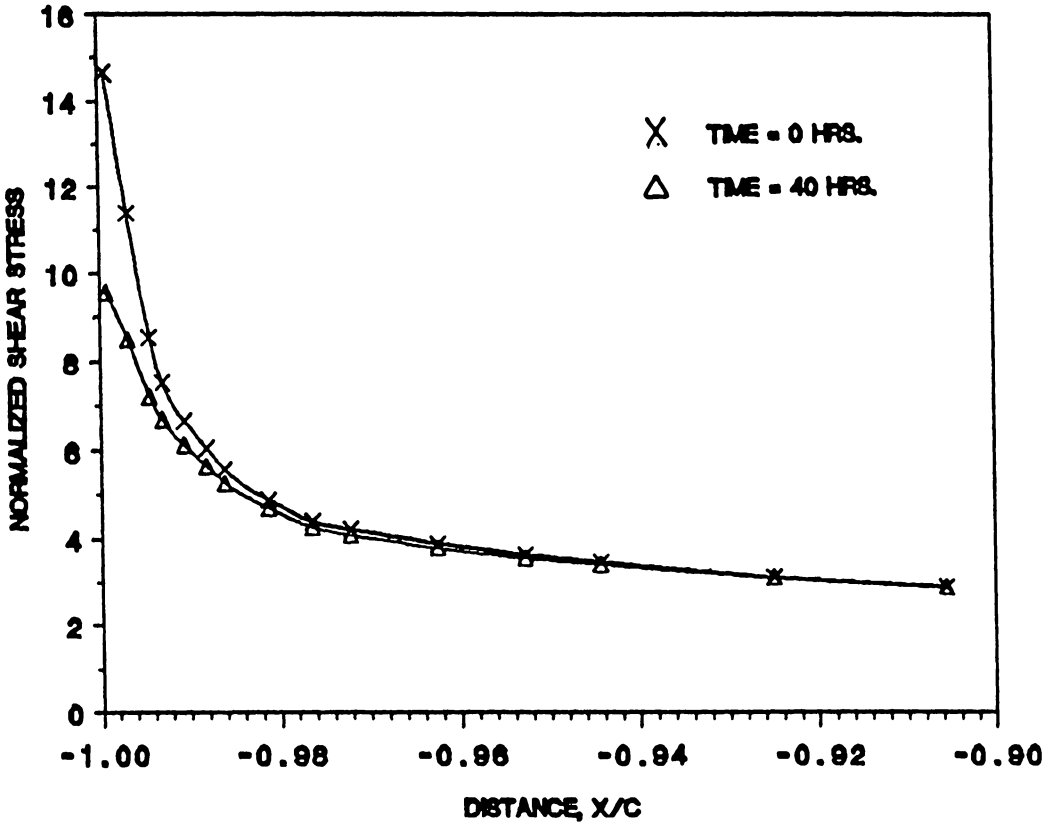

Figure 42. Variation of Shear Stress with Time Near the Free Edge.

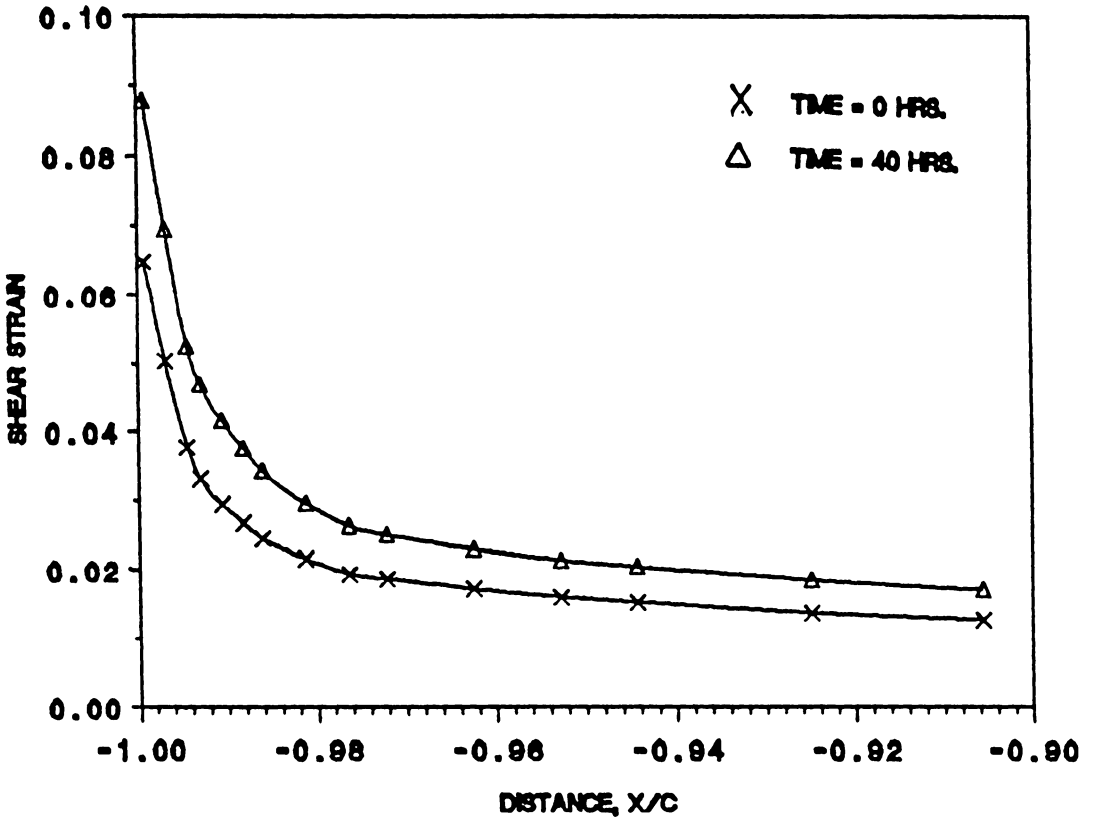

Figure 43. Variation of Shear Strain with Time Near the Free Edge.

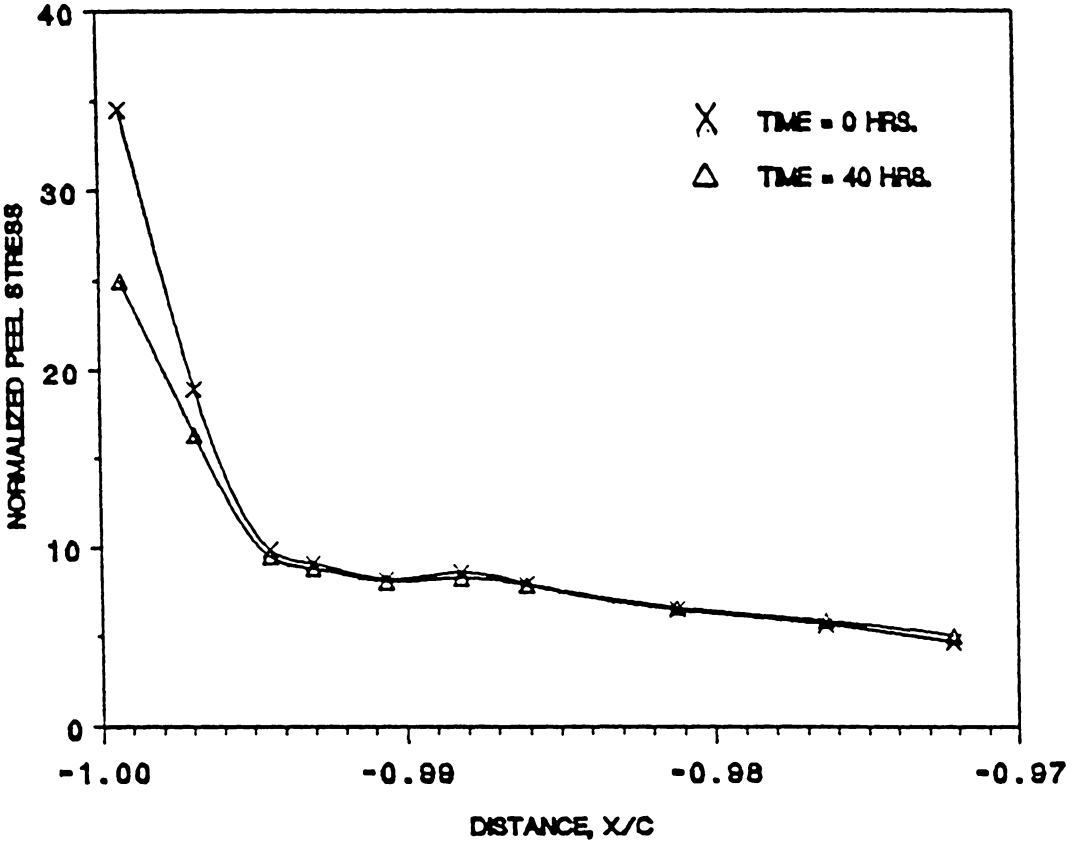

Figure 44. Variation of Peel Stress with Time Near the Free Edge.

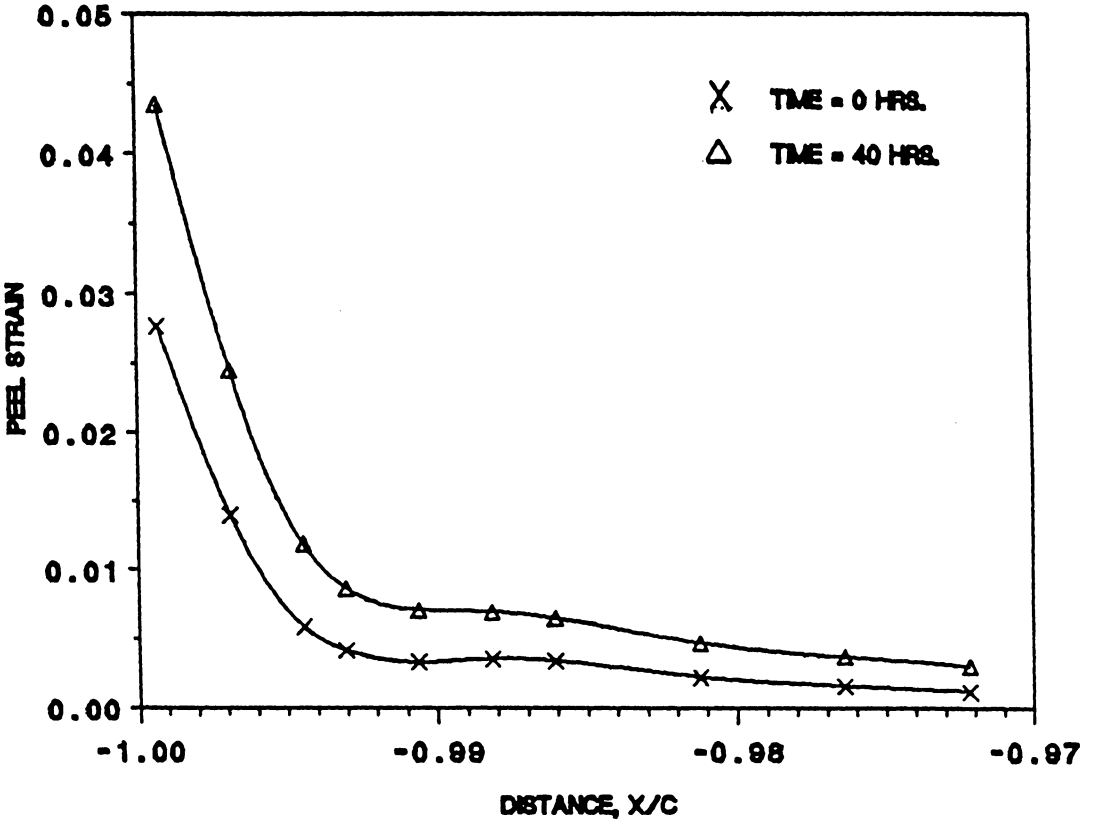

Figure 45. Variation of Peel Strain with Time Near the Free Edge.

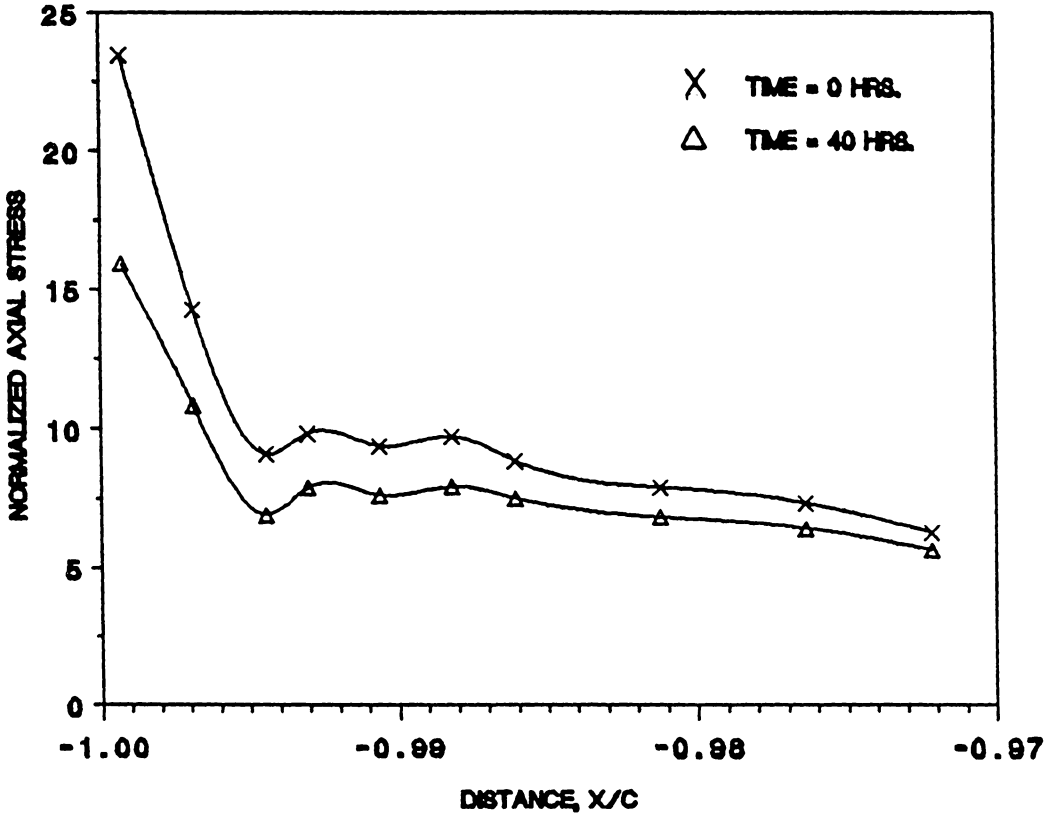

Figure 46. Variation of Axial Stress with Time Near the Free Edge.

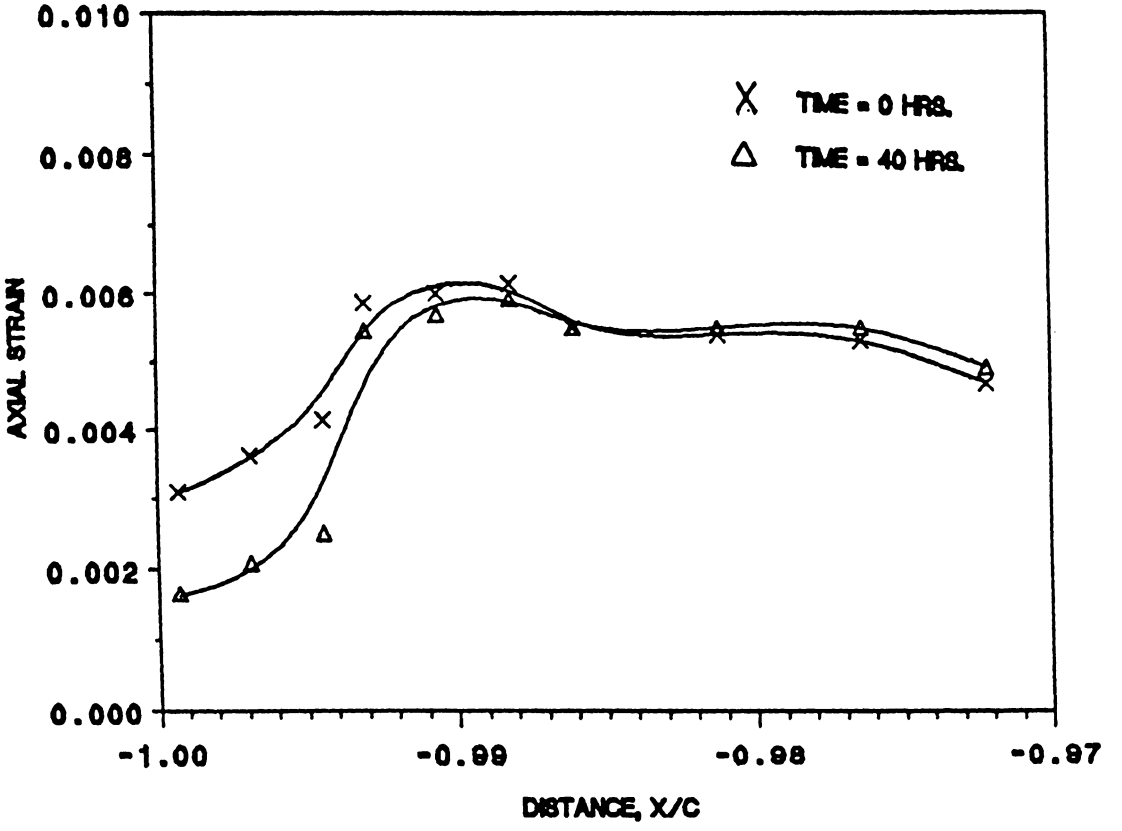

Figure 47. Variation of Axial Strain with Time Near the Free Edge.

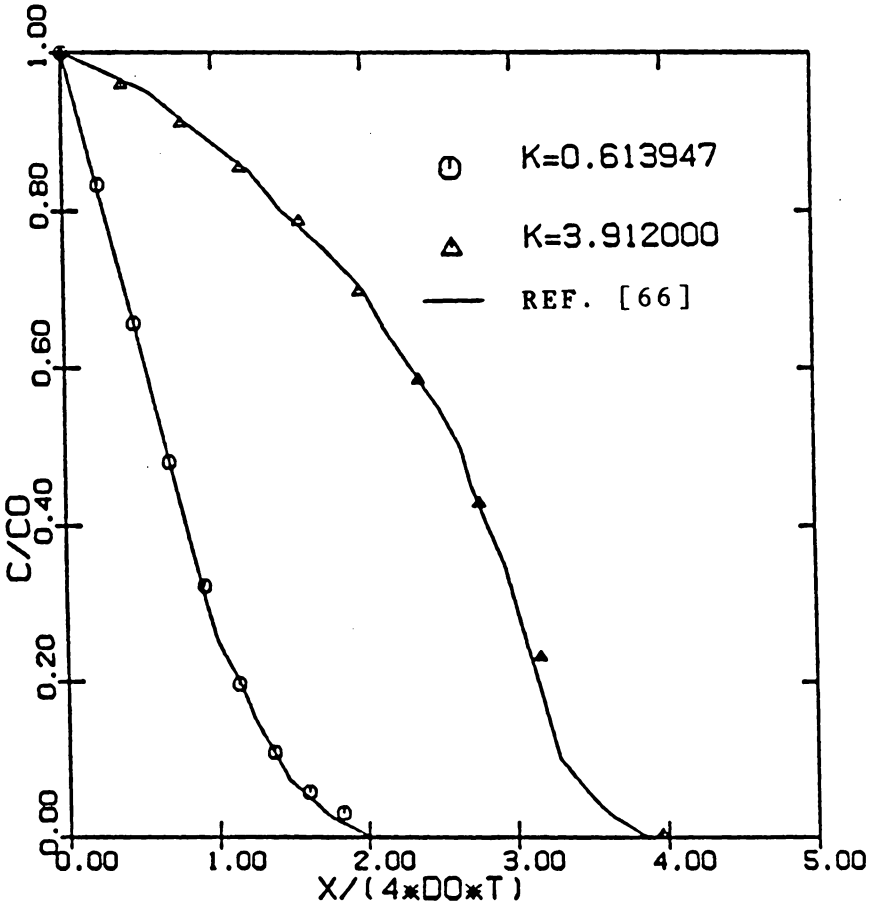

Figure 48. Profiles for the Unsteady Sorption of a Penetrant in a Semi-Infinite Medium.

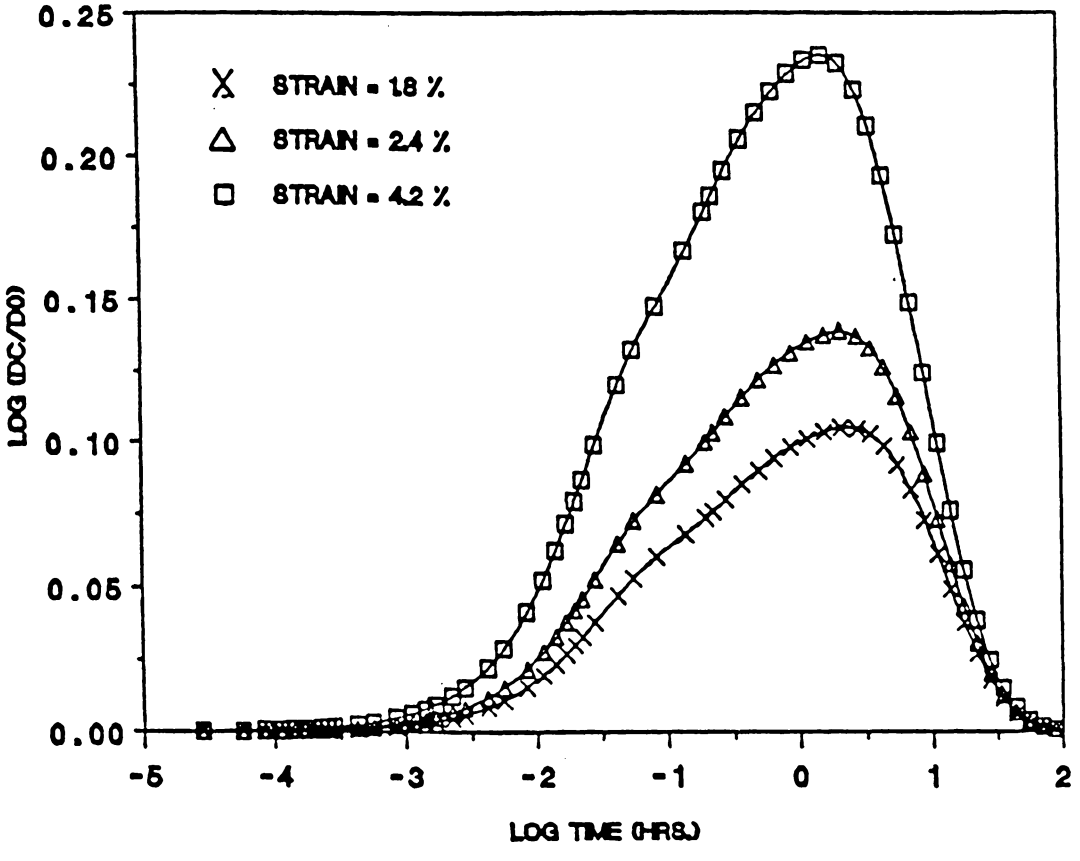

Figure 49. Effect of Mechanical Strain on the Diffusion Coefficient for Polystyrene.

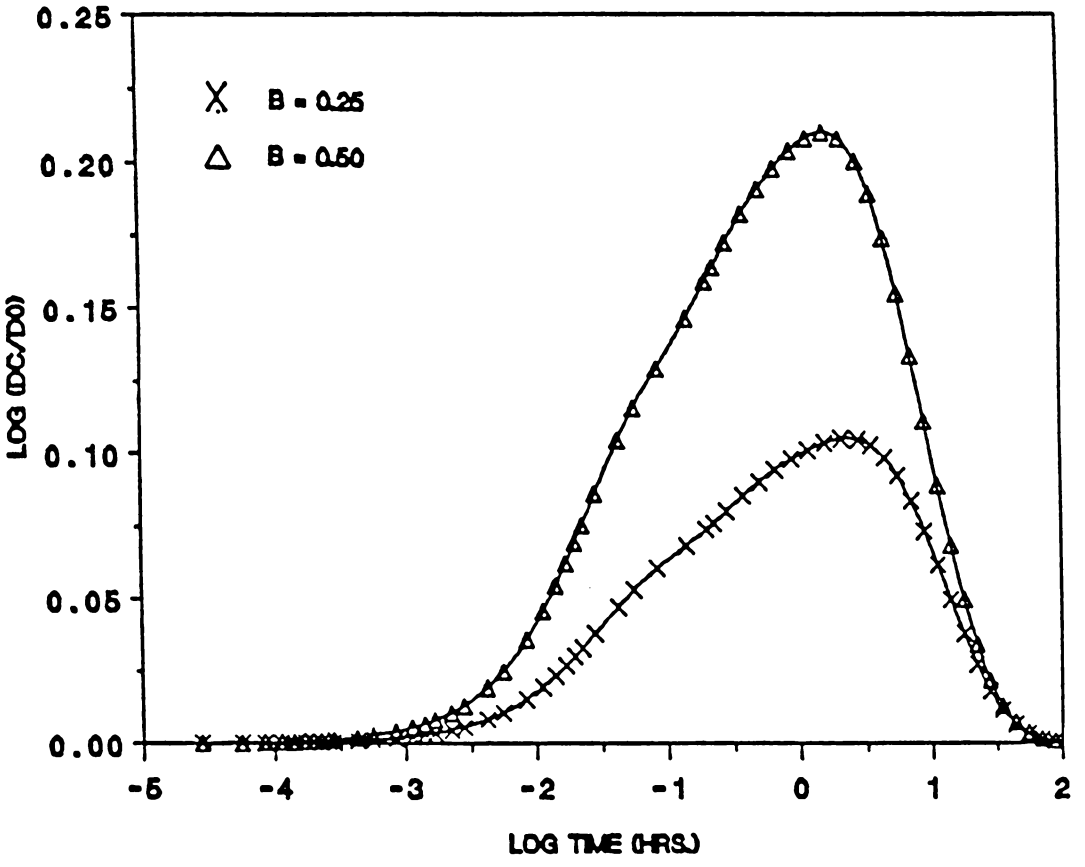

Figure 50. Effect of Material Parameter B on the Diffusion Coefficient for Polystyrene.

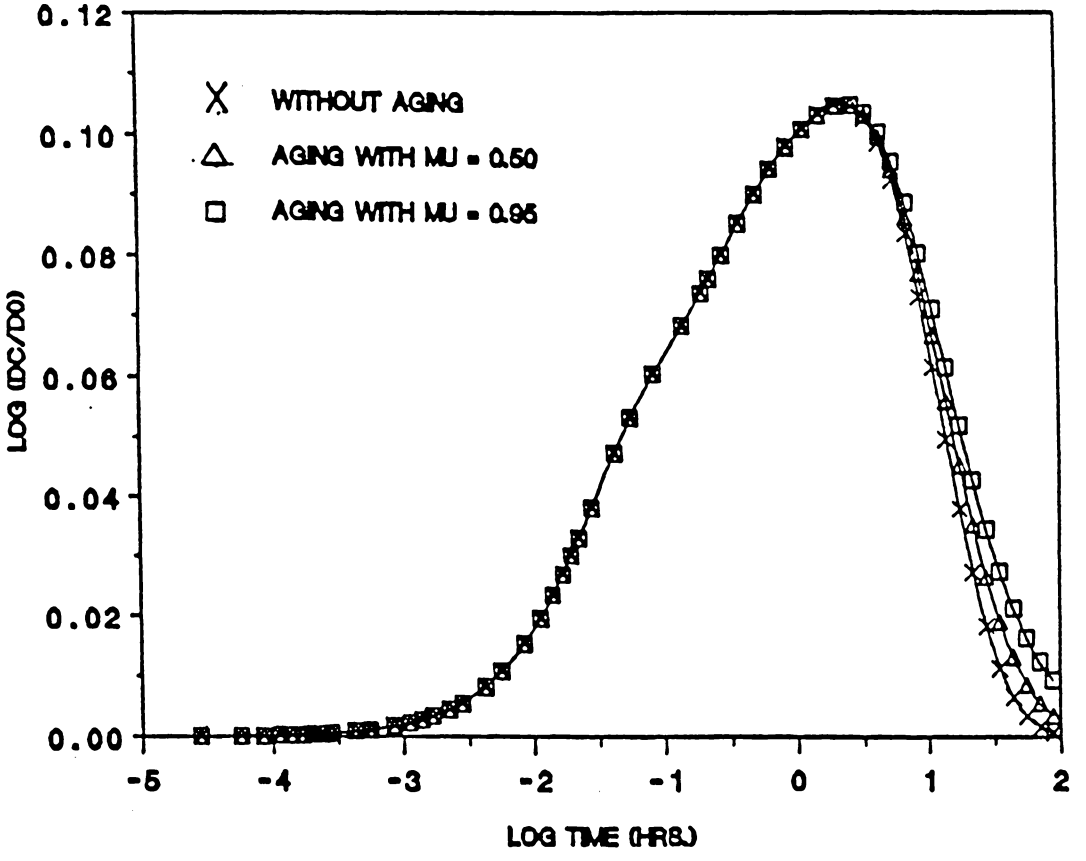

Figure 51. Effect of Physical Aging on the Diffusion Coefficient for Polystyrene.

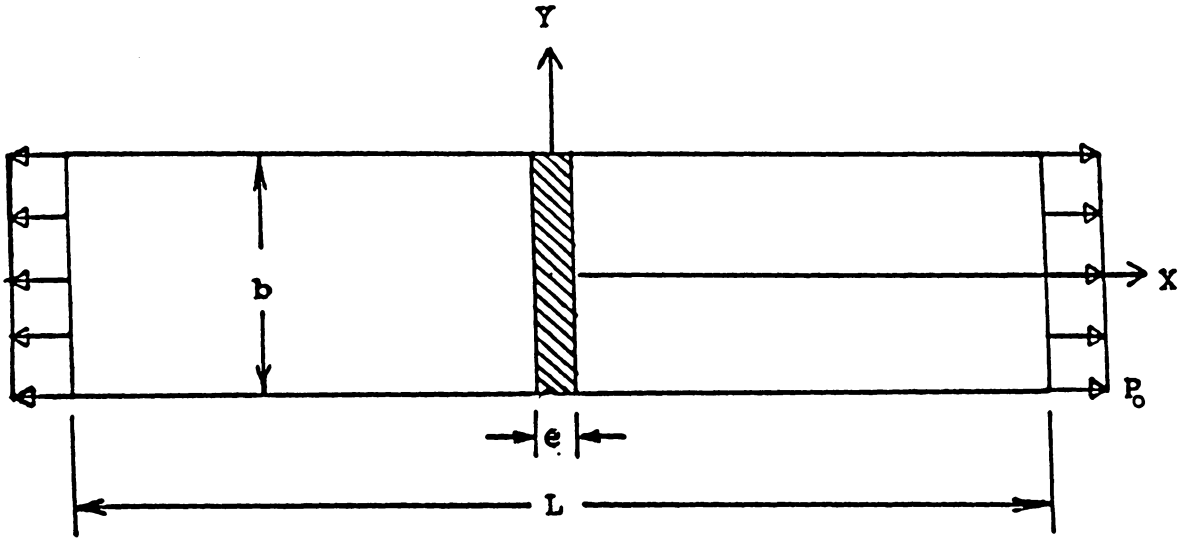

Figure 52. Specimen Geometry and Boundary Conditions for the Analysis of a Butt Joint (L = 200.5, b = 30.0, e = 0.25, all dimensions in mm., Applied Stress = 10 MPa.).

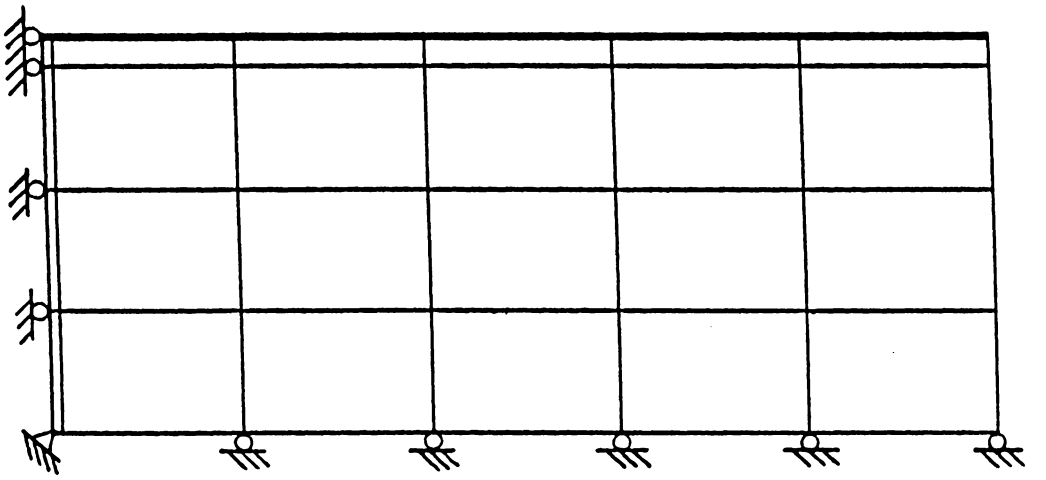

Figure 53. Finite Element Discretization and Boundary Conditions for the Analysis of a Butt Joint.

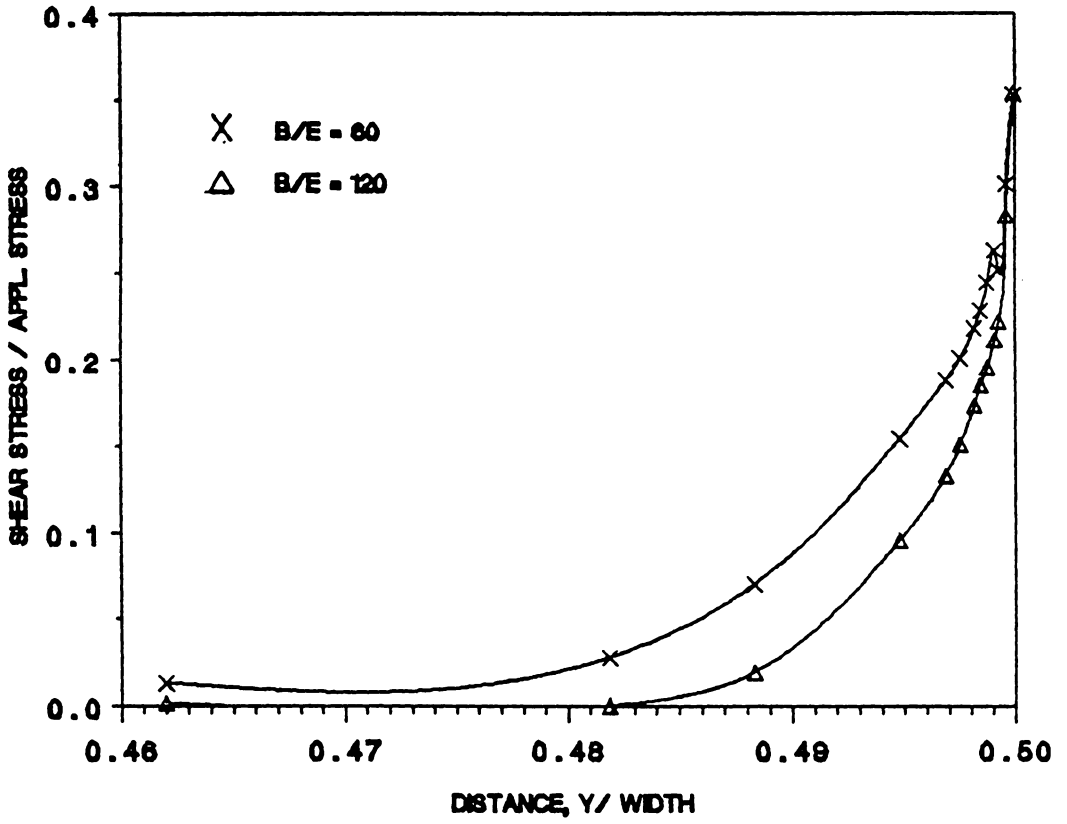

Figure 54. Influence of b/e Ratio on Adhesive Shear Stress.

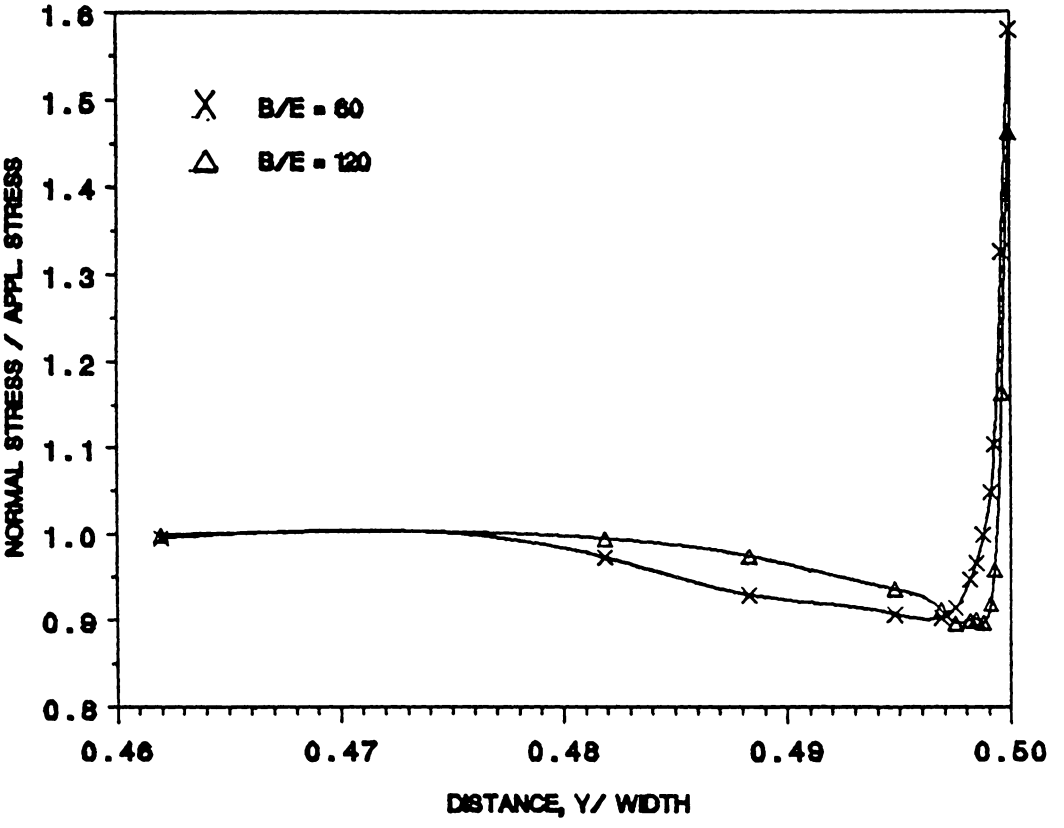

Figure 55. Influence of b/e Ratio on Adhesive Normal Stress.

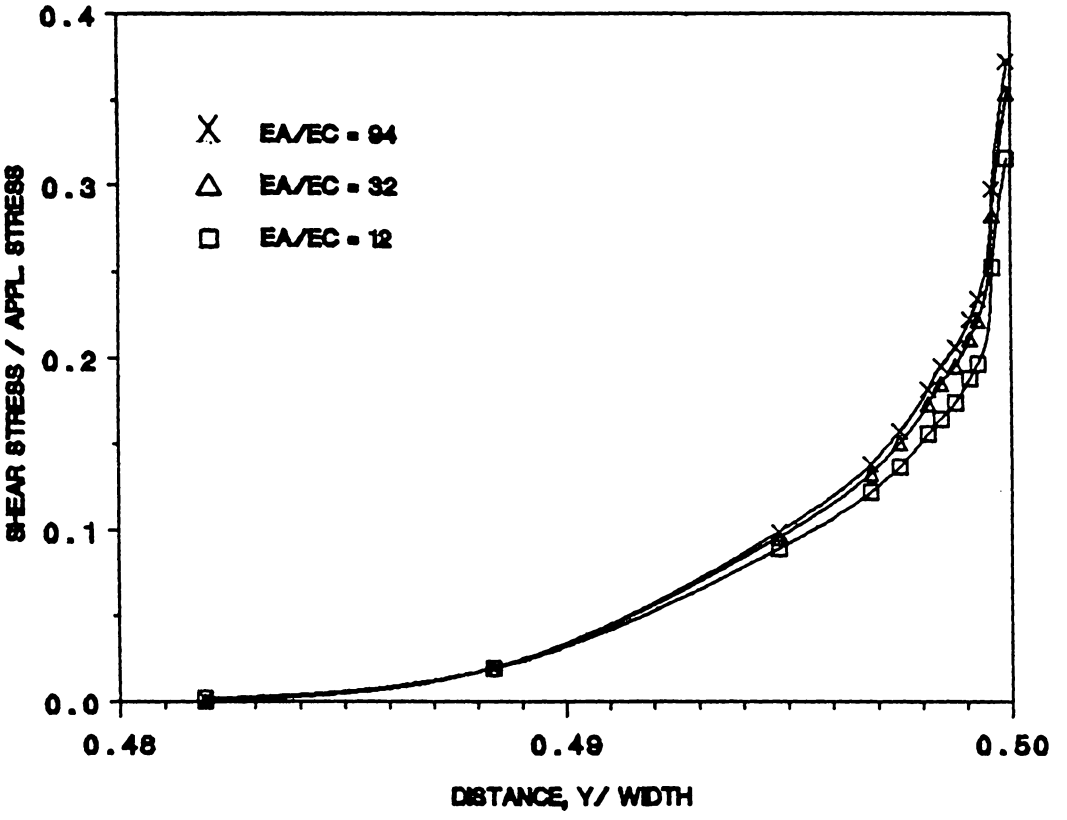

Figure 56. Influence of Modulus Ratio on Adhesive Shear Stress.

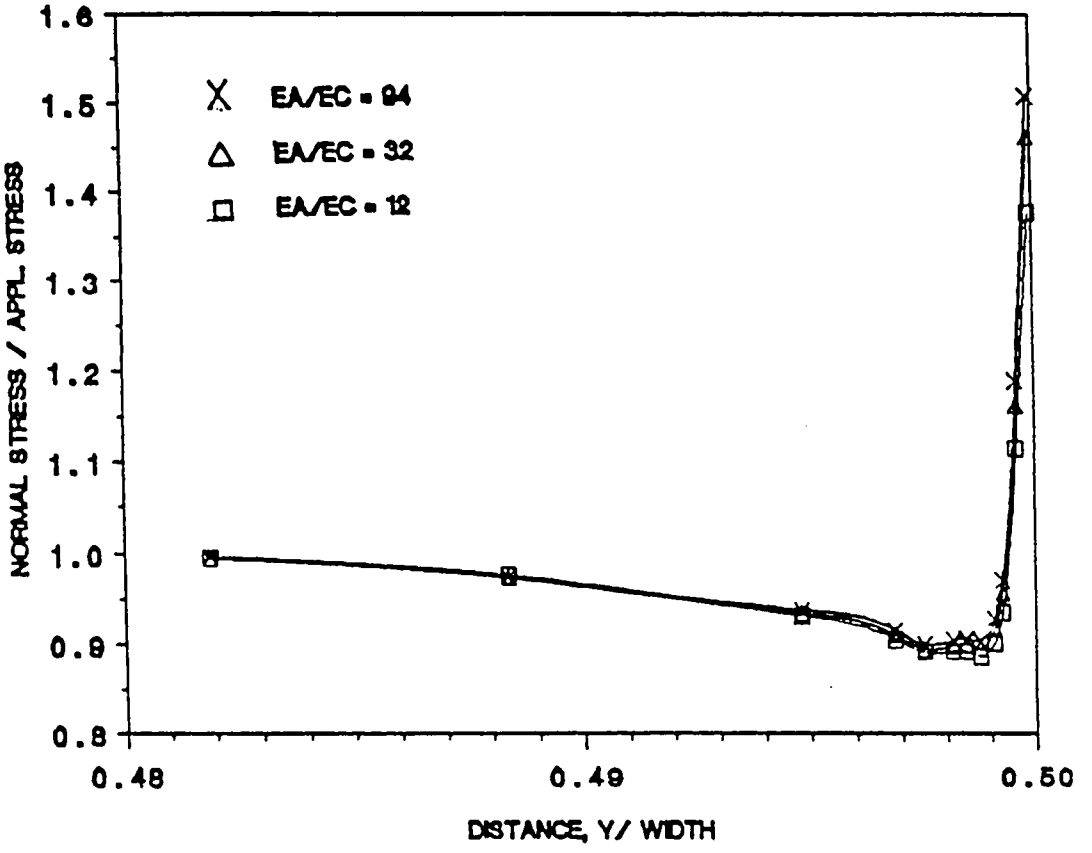

Figure 57. Influence of Modulus Ratio on Adhesive Normal Stress.

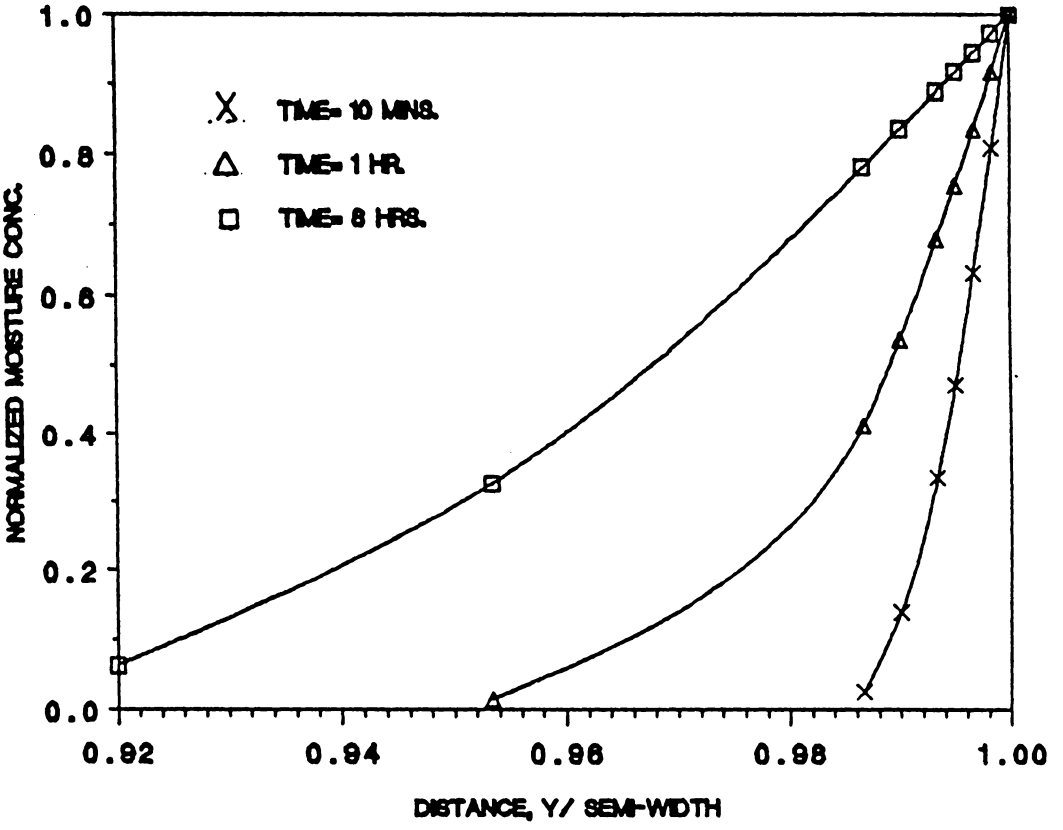

Figure 58. Moisture Profiles Within the Adhesive When There Is No Coupling.

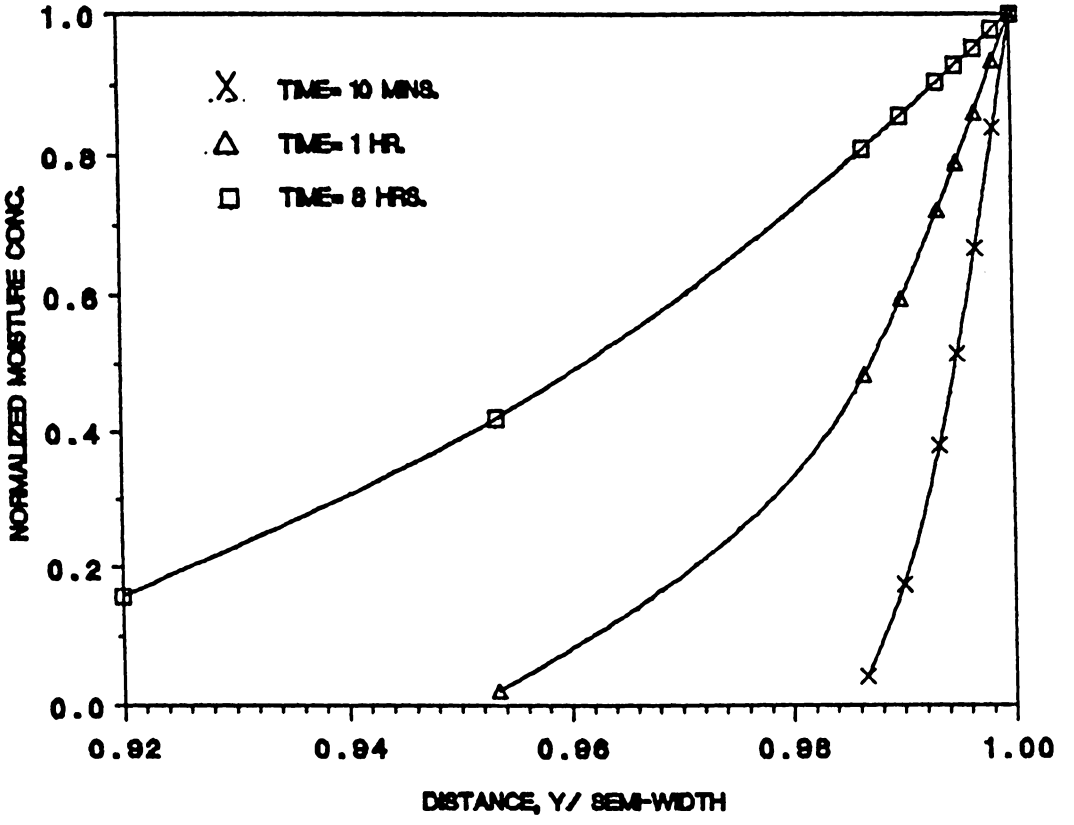

Figure 59. Moisture Profiles Within the Adhesive For Only Viscoelastic Coupling.

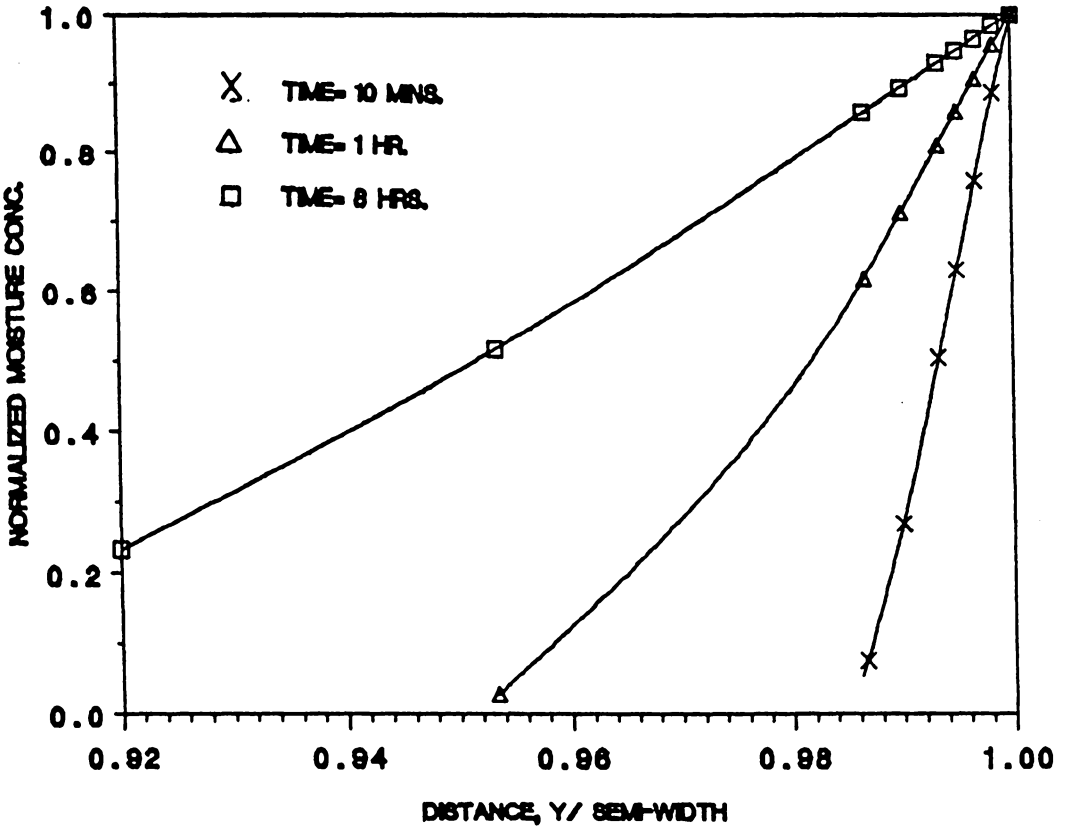

Figure 60. Moisture Profiles Within the Adhesive For Viscoelastic and Moisture Coupling.

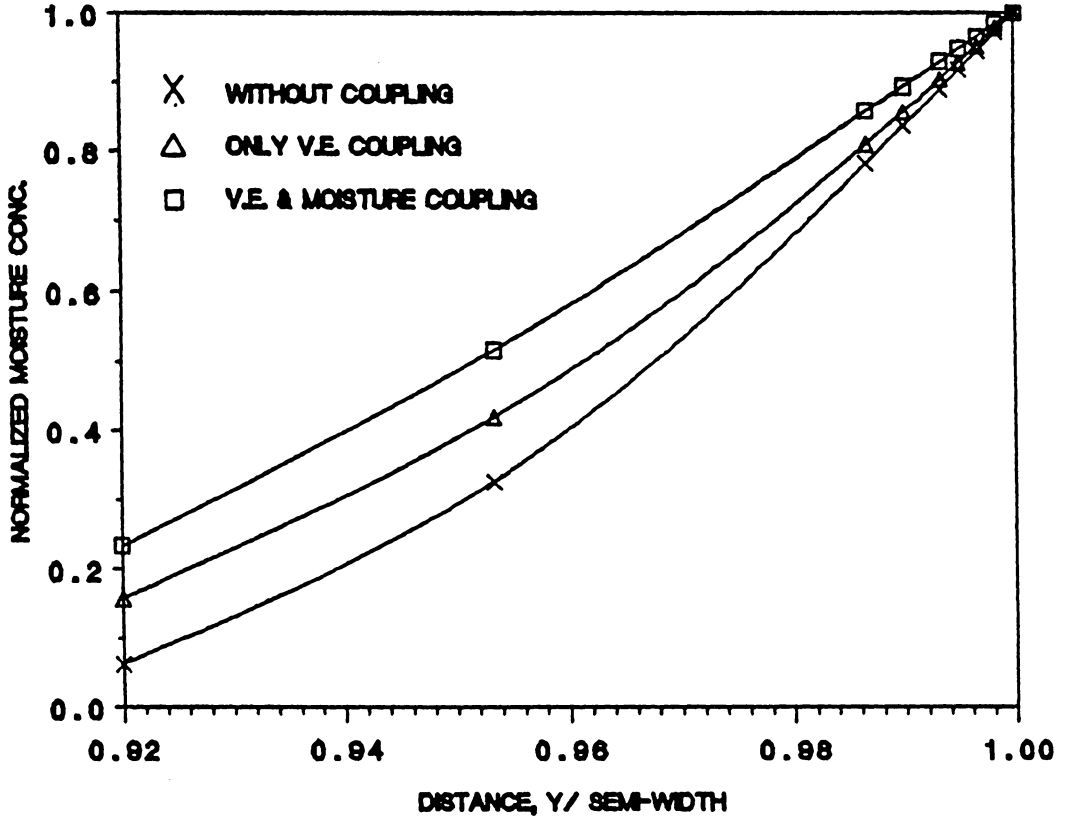

Figure 61. Influence of Coupling on Moisture Profiles at Time = 8 Hours.

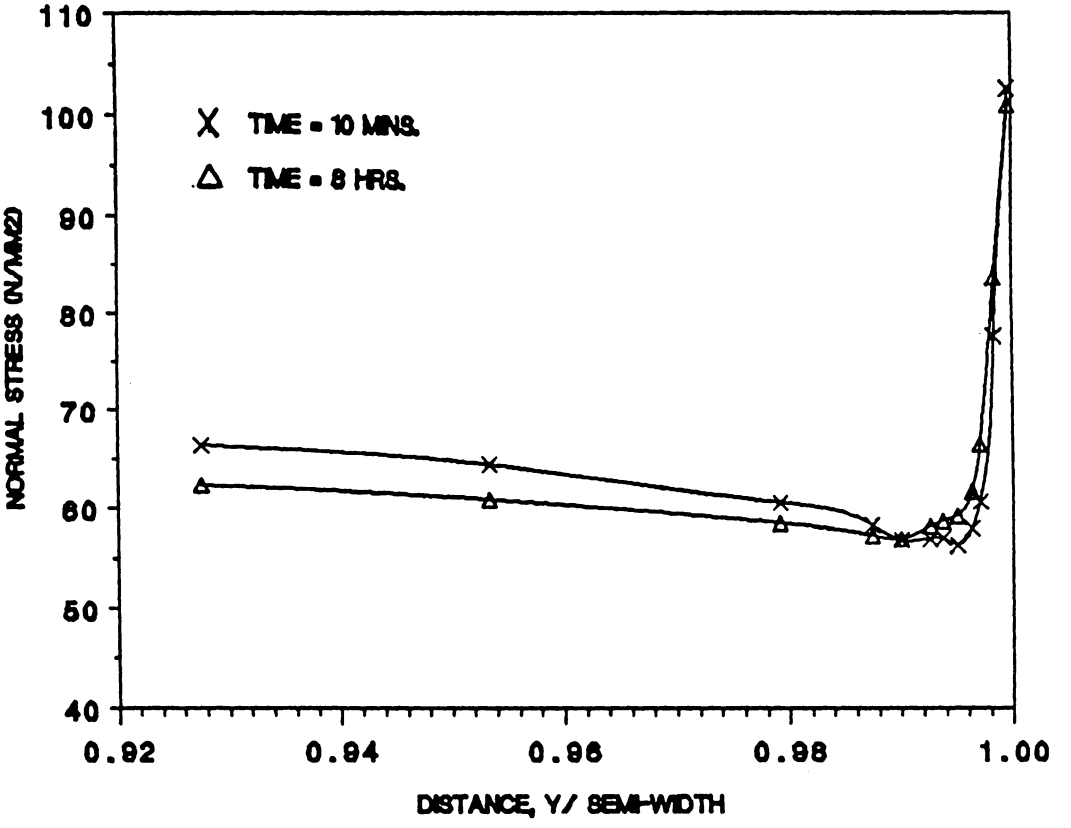

Figure 62. Variation of Normal Stress in the Adhesive With Time For Viscoelastic Coupling.

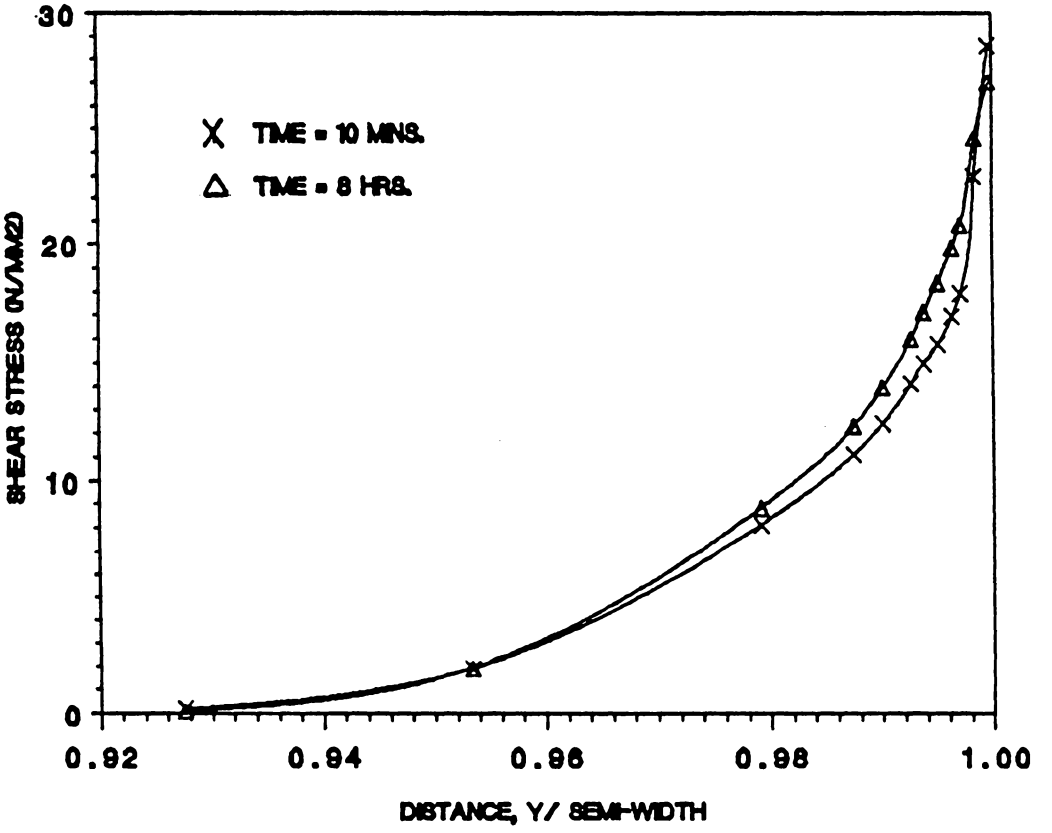

Figure 63. Variation of Shear Stress in the Adhesive With Time For Viscoelastic Coupling.

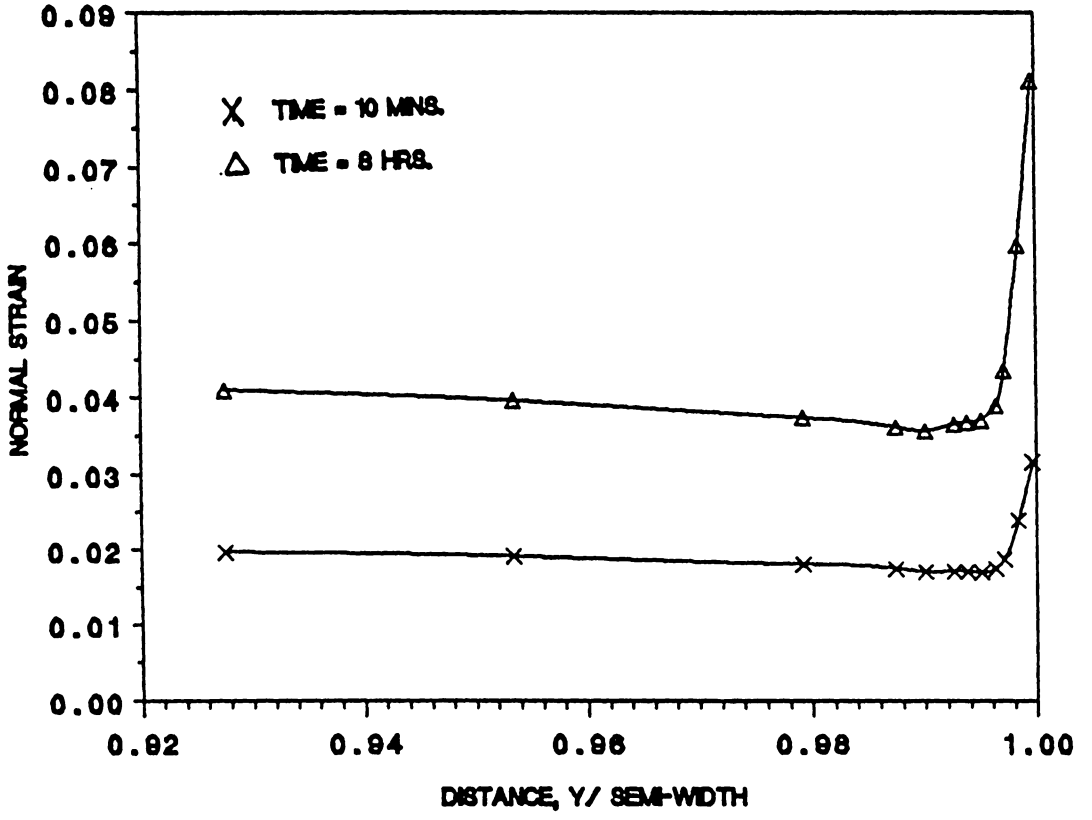

Figure 64. Variation of Normal Strain in the Adhesive With Time For Viscoelastic Coupling.

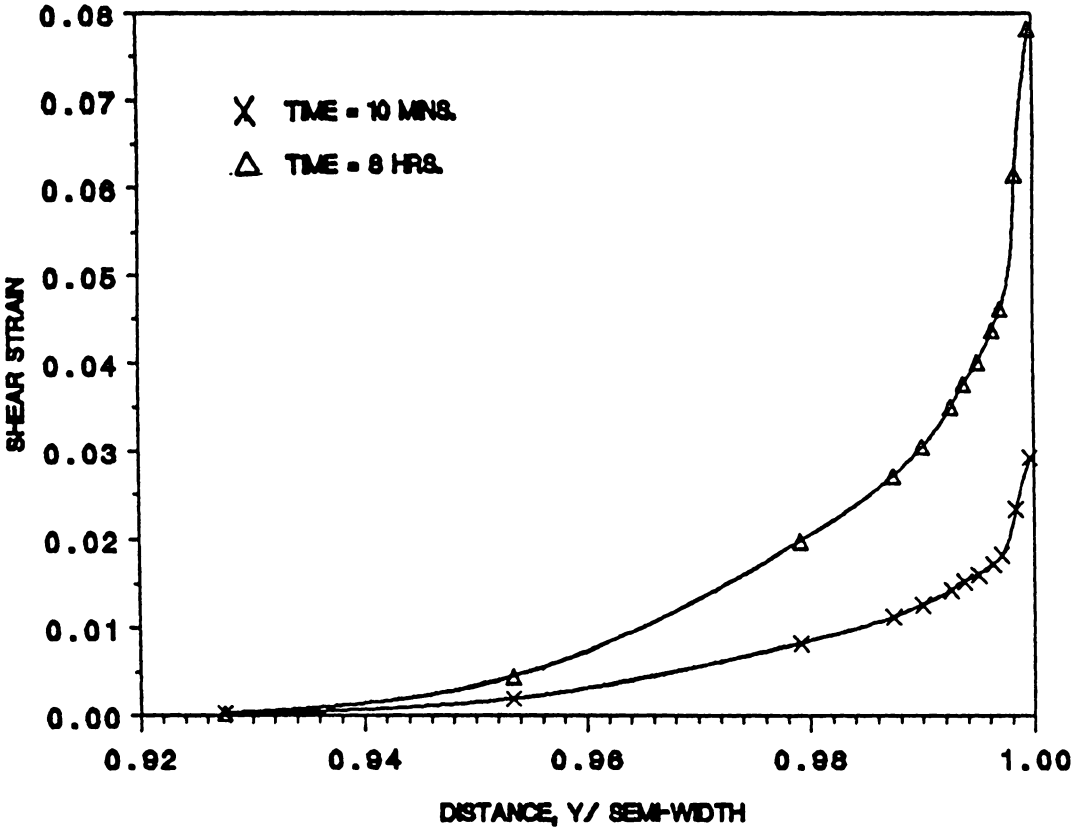

Figure 65. Variation of Shear Strain in the Adhesive With Time For Viscoelastic Coupling.

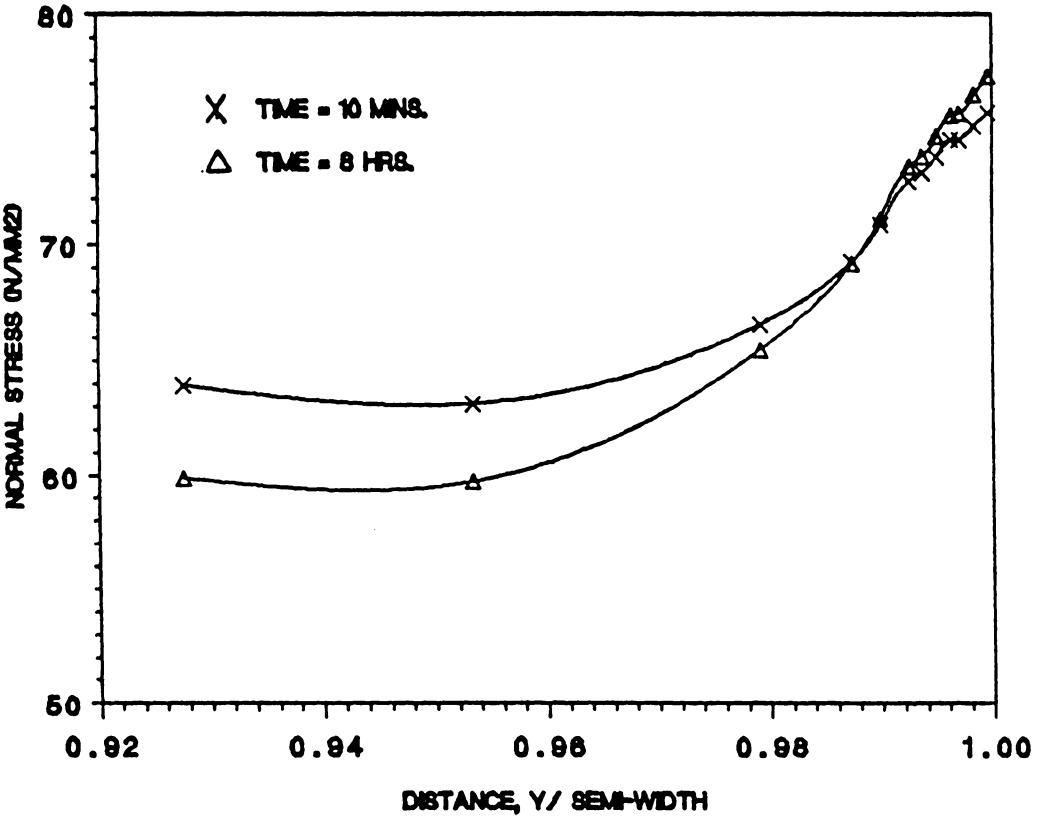

Figure 66. Variation of Normal Stress in the Adherend With Time For Viscoelastic Coupling.

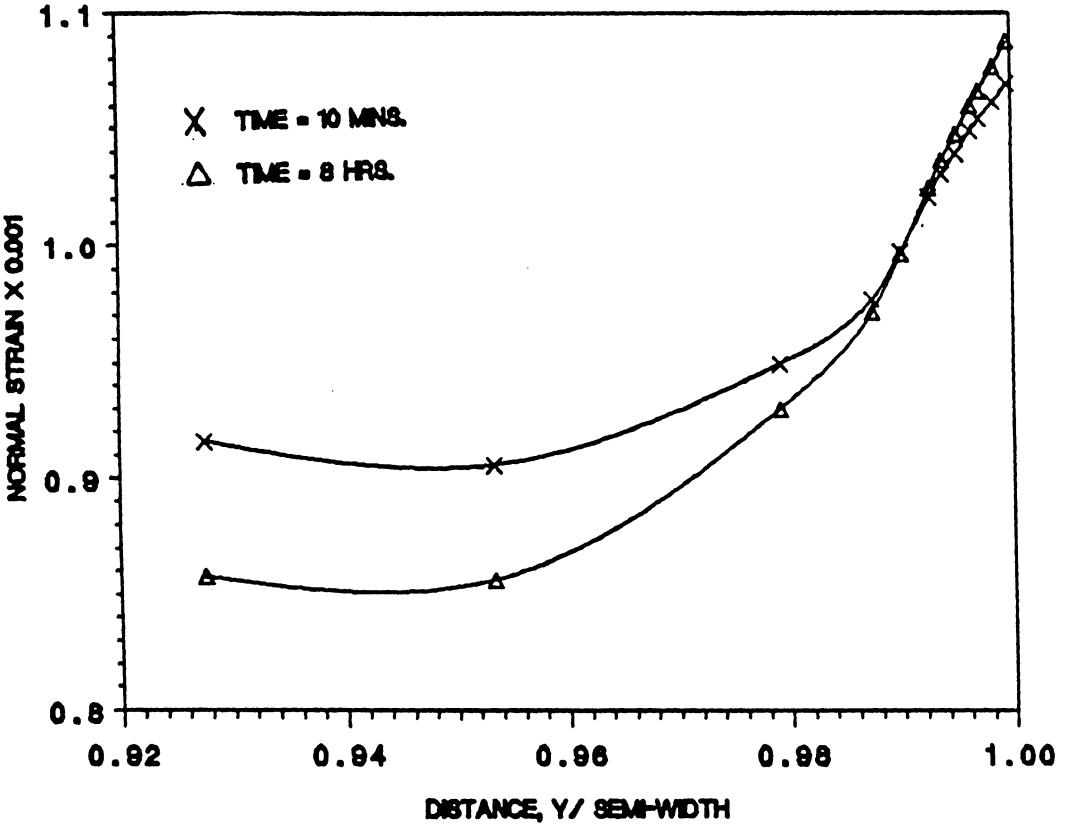

Figure 67. Variation of Normal Strain in the Adherend With Time For Viscoelastic Coupling.

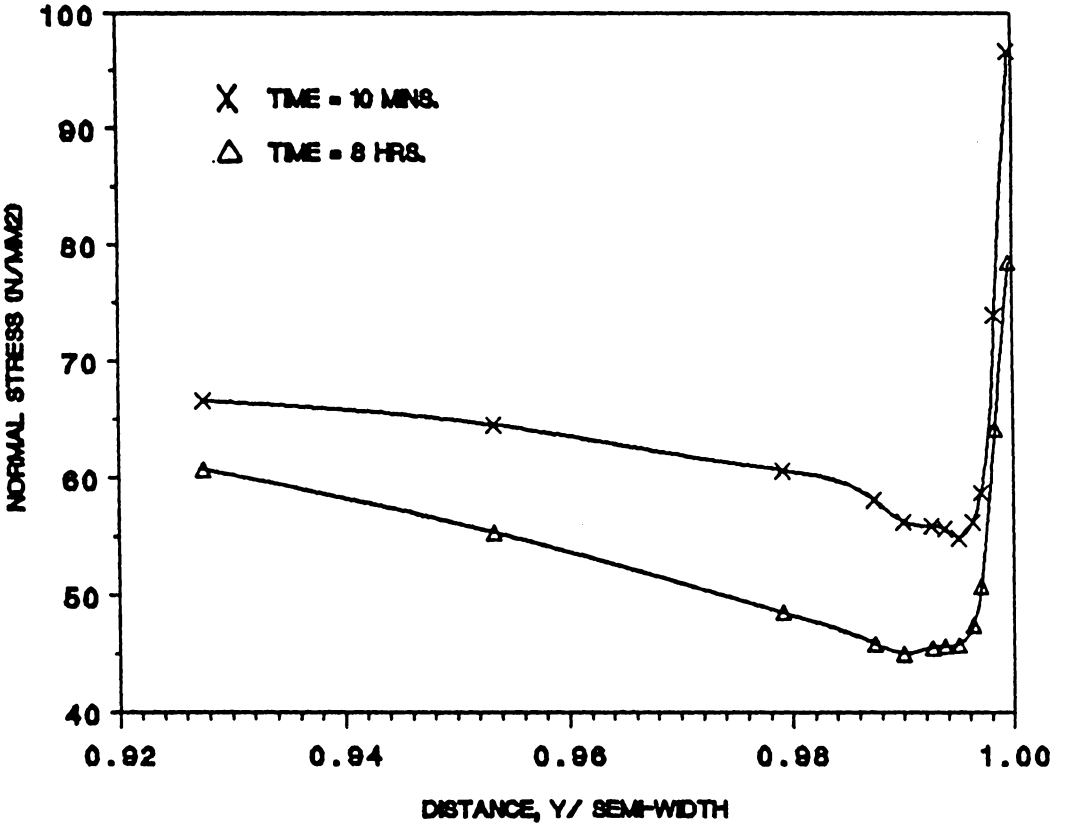

Figure 68. Variation of Normal Stress in the Adhesive With Time For Viscoelastic and Moisture Coupling.

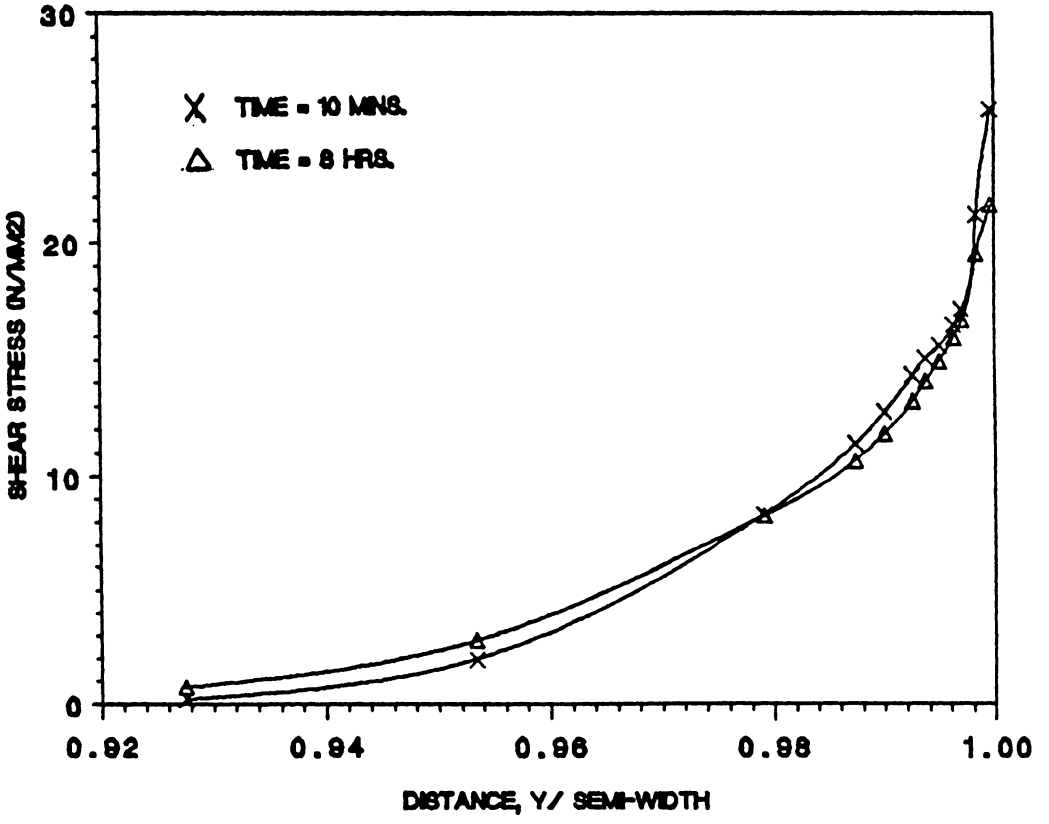

Figure 69. Variation of Shear Stress in the Adhesive With Time For Viscoelastic and Moisture Coupling.

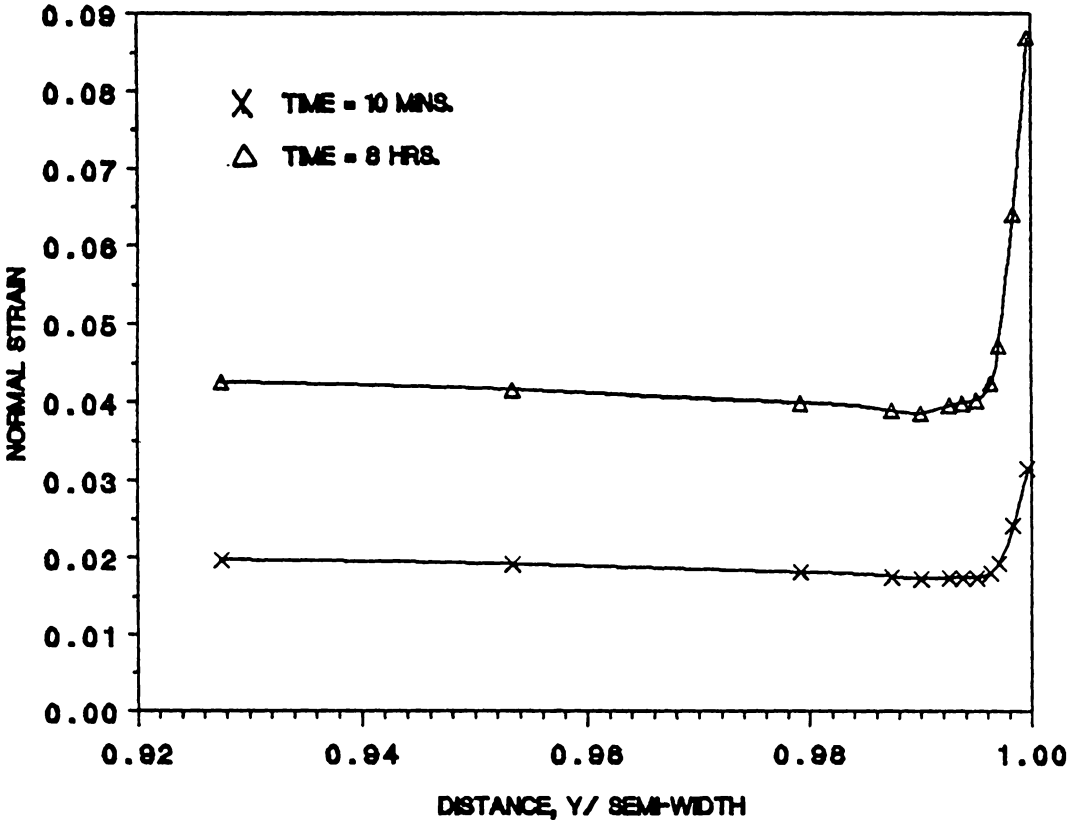

Figure 70. Variation of Normal Strain in the Adhesive With Time For Viscoelastic and Moisture Coupling.

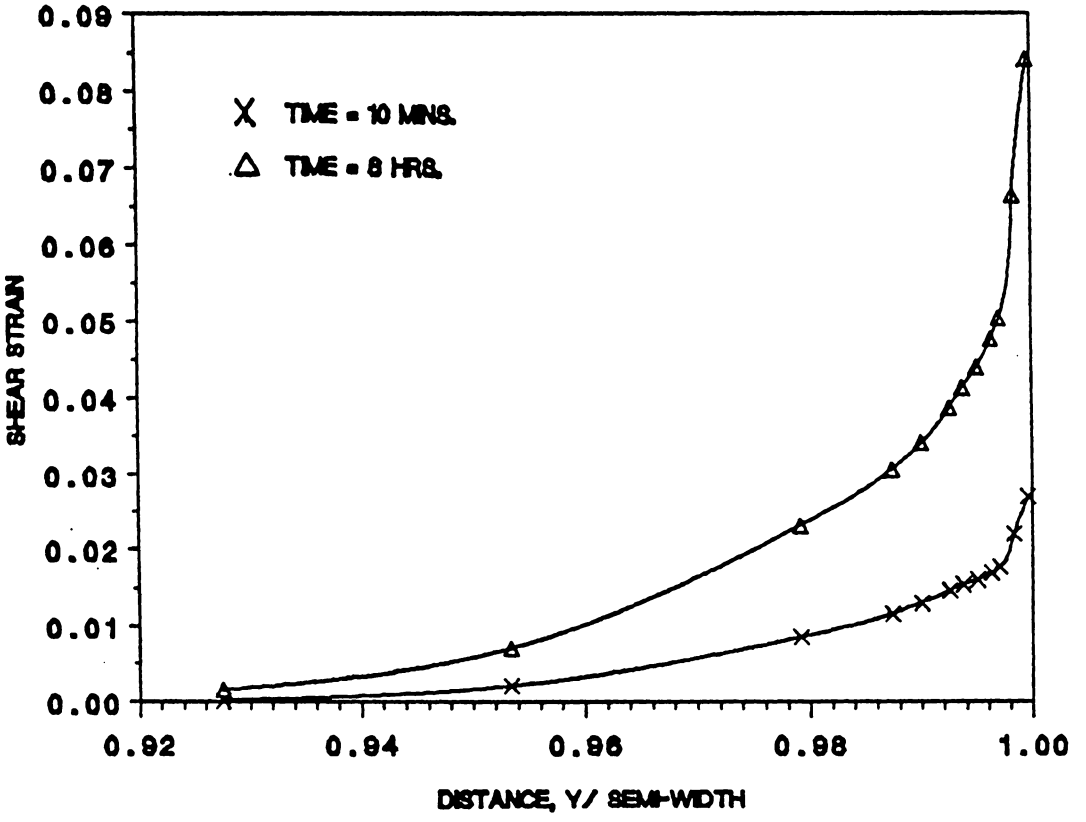

Figure 71. Variation of Shear Strain in the Adhesive With Time For Viscoelastic and Moisture Coupling.

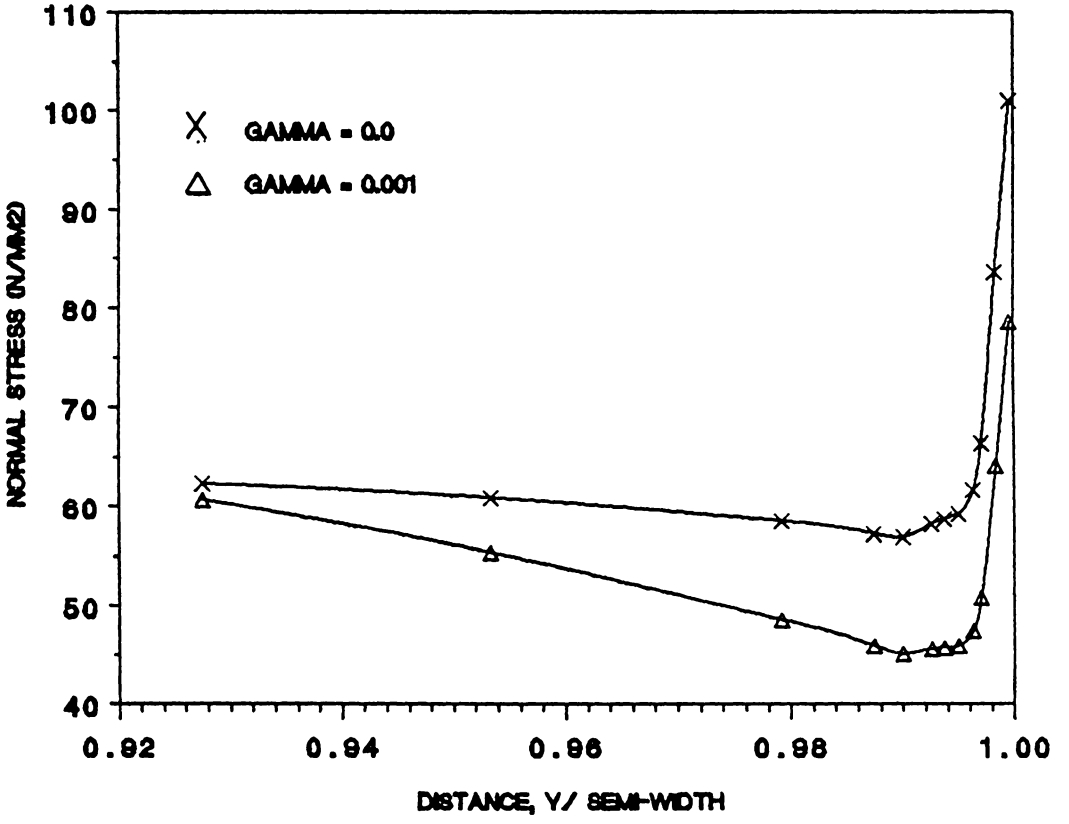

Figure 72. Influence of Moisture Coefficient on Adhesive Normal Stress at Time = 8 Hours.

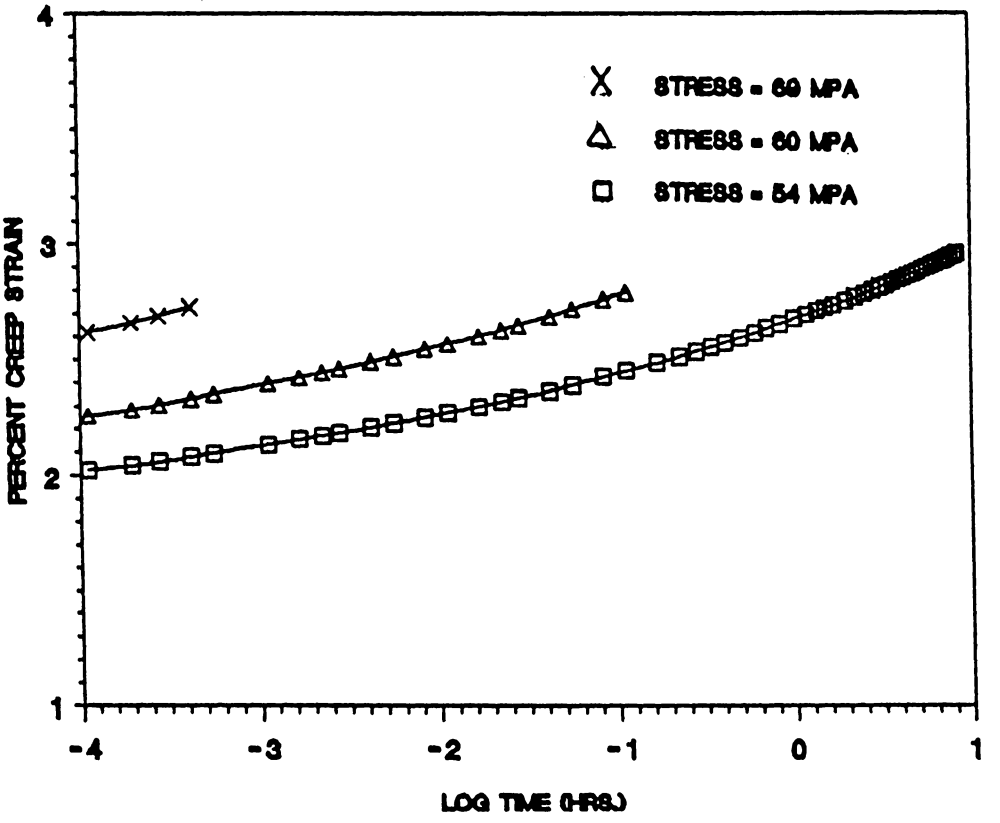

Figure 73. Creep Strain in FM-73 for Different Applied Stress Levels.

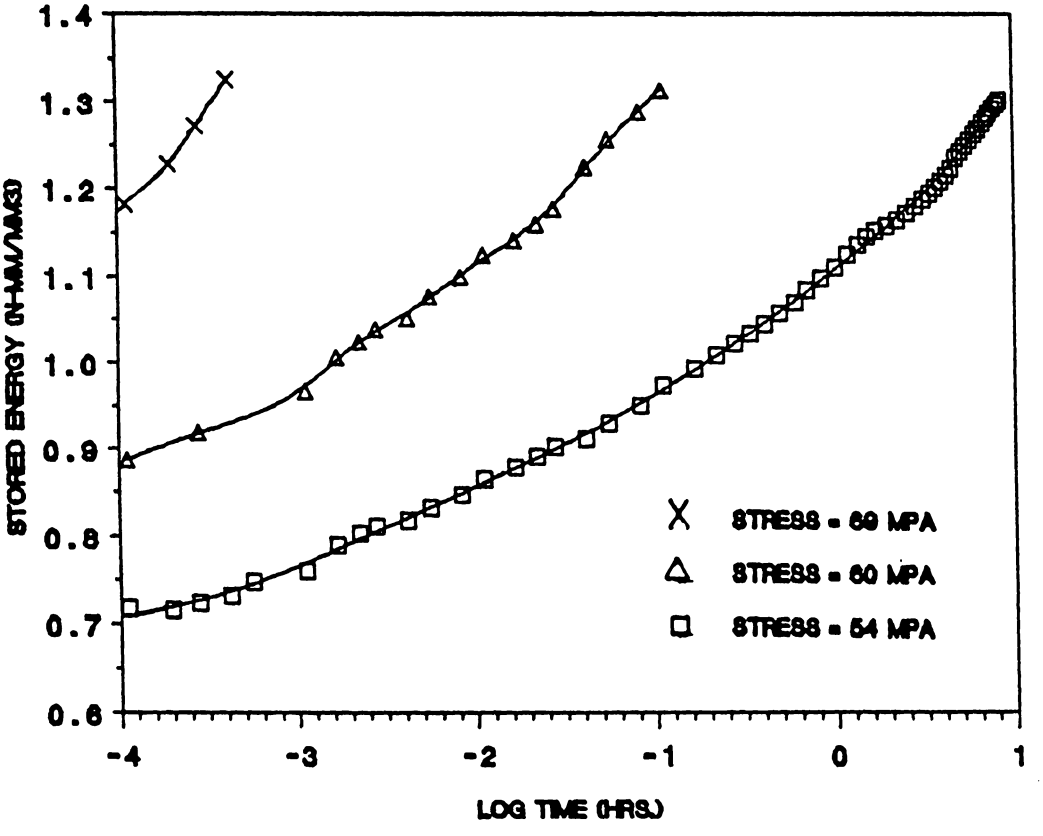

Figure 74. Stored Energy in FM-73 for Different Applied Stress Levels.

REFERENCES

1. J. N. Reddy and S. Roy, Finite Element Analysis of Adhesively Bonded Joints, Report No. VPI-E-85.18, ONR, Department of Engineering Science and Mechanics, VPI&SU, Blacksburg, VA (August 1985).

2. S. Roy and J. N. Reddy, Nonlinear Viscoelastic Analysis of Adhesively Bonded Joints, Report No. VPI-E-86.28, ONR, Department of Engineering Science and Mechanics, Virginia Polytechnic Institute and State University, Blacksburg VA, (November 1986).

3. M. Goland and E. Reissner, The Stresses in Cemented Joints, Applied Mechanics, 1, A17-A27 (1944).

4. F. Erdogan and M. Ratwani, Stress Distributions in Bonded Joints, Composite Materials, 5, 378-393 (1971).

5. G. R. Wooley and D. R. Carver, Stress Concentration Factors for Bonded Lap Joints, J. Aircraft, 8, 817-820 (1971).

6. L. J. Hart-Smith, Adhesive Bonded Single Lap Joints, NASA CR-112236 (January 1973).

7. A. T. Liu, Linear Elastic and Elasto-Plastic Stress Analysis for Adhesive Lap Joints, T.A.M. Report No. 410, University of Illinois at Urbana-Champaign (July 1976).

8. R. D. Adams and N. A. Peppiatt, Stress Analysis of Adhesively Bonded Lap Joints, Strain Analysis, 9, 185-196 (1974).

9. R. D. Adams and N. A. Peppiatt, Stress Analysis of Lap Joints in Fibre Reinforced Composite Materials, Fibre Reinforced Plastics, London, ICE, p. 45 (1977).

10. E. A. Humphreys and C. T. Herakovich, Nonlinear Analysis of Bonded Joints with Thermal Effects, Report VPI-E-77.19, Department of Engineering Science and Mechanics, Virginia Polytechnic Institute and State University, Blacksburg, VA (June 1977).

11. D. J. Allman, A Theory for Elastic Stresses in Adhesive Bonded Lap Joints, Mechanics and Applied Mathematics, 30, 415-436 (1977).

12. L. J. Hart-Smith, Analysis and Design of Advanced Composite Bonded Joints, NASA CR-2218 (April 1974).

13. U. Yuceoglu and D. P. Updike, Stress Analysis of Bonded Plates and Joints, Engineering Mechanics Division, ASCE, 106, 37-56 (1980).

14. F. Delale and F. Erdogan, Viscoelastic Analysis of Adhesively Bonded Joint, J. Appl. Mechanics, 48, 331-338 (1981).

15. F. Delale and F. Erdogan, Time-Temperature Effect in Adhesively Bonded Joints, J. Composite Materials, 5, 561-581 (1981).

16. S. Gali and O. Ishai, Interlaminar Stress Distribution Within an Adhesive Layer in the Non-linear Range, Journal of Adhesion, 9, 253-266 (1978).

17. Y. R. Nagaraja and R. S. Alwar, Nonlinear Stress Analysis of an Adhesive Tubular Lap Joint, Journal of Adhesion, 10, 97-106 (1979).

18. Y. R. Nagaraja and R. S. Alwar, Viscoelastic Analysis of an Adhesive-Bonded Plane Lap Joint, Computers and Structures, 6, 621-627 (1980).

19. E. C. Francis, W. L. Hufferd, D. G. Lemini, R. E. Thompson, W. E. Briggs and R. R. Parmerter, Time Dependent Fracture in Adhesive Bonded Joints, Chemical Systems Division, Sunnyvale, California, Interim Reports CSD 2769-1R-01/02 (May and Nov. 1982).

20. B. Dattaguru, R. A. Everette, Jr., J. D. Whitcomb, and W. S. Johnson, Geometrically Nonlinear Analysis of Adhesively Bonded Joints, J. Engng. Materials and Technology, 106, 59-65 (1984).

21. L. R. Botha, R. M. Jones, and H. F. Brinson, Viscoelastic Analysis of Adhesive Stresses in Bonded Joints, Report VPI-E-83-17, Department of Engineering Science and Mechanics, Virginia Polytechnic Institute, Blacksburg, VA (May 1983).

22. M. Henriksen, Nonlinear Viscoelastic Stress Analysis - A Finite Element Approach, Computers and Structures, 18, 133-139 (1984).

23. E. B. Becker et al., Viscoelastic Stress Analysis Including Moisture Diffusion for Adhesively Bonded Joints, Report AFWAL-TR-84-4057, General Dynamics, Fort-Worth Division, TX (August 1984).

24. S. Yadagiri and C. Papi Reddy, Viscoelastic Analysis of Nearly Incompressible Solids, Computers and Structures, 20, 817-825 (1985).

25. R. A. Schapery, Further Development of a Thermodynamic Constitutive Theory: Stress Formulation, A&S Report No. 69-2, Purdue University, W. Lafayette (Feb. 1969).

26. D. Peretz and Y. Weitsman, The Non-Linear Thermo-Viscoelastic Characterizations of FM-73 Adhesives, J. Rheology, 26, 245-261 (1983).

27. W. G. Knauss and I. J. Emri, Nonlinear Viscoelasticity Based on Free Volume Considerations, Computers and Structures, 13, 123-128 (1981).

28. A. K. Prickett and L. Hollaway, The Analysis of Elastic-Plastic Adhesive Stress in Bonded Lap Joints in FRP Structures, Composite Structures, 4, 135-160 (1985).

29. R. A. Schapery, A Method of Viscoelastic Stress Analysis Using Elastic Solutions, Journal of the Franklin Institute, 279, 268-289 (1965).

30. Y. Weitsman, An Investigation of Non-Linear Viscoelastic Effects on Load Transfer in a Symmetric Double Lap Joint, J. Adhesion, 11, 279-289 (1981).

31. S. Aivazzadeh and G. Verchery, "Stress Analysis at the Interface in Adhesive Joints by Special Finite Elements," Int. J. Adhesion and Adhesives, Vol. 6, No. 4, October 1986, p. 185.

32. F. L. Matthews, P. F. Kilty, and E. W. Godwin, "A Review of the Strength of Joints in Fibre-Reinforced Plastics, Part Two: Adhesively Bonded Joints," Composites 13, January 1982, p. 29.

33. M. N. Reddy and P. K. Sinha, "Stresses in Adhesive-Bonded Joints for Composites," Fibre Sci. and Tech. 8, 1975, p. 33.

34. W. J. Renton and J. R. Vinson, "Analysis of Adhesively Bonded Joints Between Panels of Composite Materials," J. Appl. Mech., March 1977, p. 101.

35. R. M. Barker and F. Hatt, "Analysis of Bonded Joints in Vehicular Structures," AIAA Journal, Vol. 11, No. 12, Dec. 1973, p. 1650.

36. R. D. Adams, N. A. Peppiatt and J. Coppendale, "Prediction of Strength of Joints Between Composite Materials," Symposium on Jointing in Fibre Reinforced Plastics, Imperial College, London, 1978.

37. W. J. Renton and J. R. Vinson, "On the Behavior of Bonded Joints in Composite Material Structures," Engineering Fracture Mech. 7, 1975, p. 41.

38. B. G. Schaffer and D. F. Adams, Non-Linear Viscoelastic Analysis of a Unidirectional Composite Material, J. Appl. Mech., 48, 859-865 (1981).

39. H. Ghoneim and Y. Chen, A Viscoelastic-Viscoplastic Constitutive Equation and its Finite Element Implementation, Computers and Structures, 17, 499-509 (1983).

40. R. A. Schapery, Correspondence Principles and a Generalized J Integral for Large Deformation and Fracture Analysis of Viscoelastic Media, International Journal of Fracture, 25, 195-223 (1984).

41. P. Czarnocki and K. Piekarski, Nonlinear Numerical Stress Analysis of a Symmetric Adhesively Bonded Lap Joint, International Journal of Adhesion and Adhesives, 6, 157-160 (1986).

42. P. M. Nagdhi and S. A. Murch,"On the Mechanical Behavior of Viscoelastic-Plastic Solids," Journal of Applied Mechanics, 30, 327, (1963).

43. M. J. Crochet, "Symmetric Deformations of Viscoelastic Plastic Cylinders," Journal of Applied Mechanics, 33, 327-334 (1966).

44. M. Reiner and K. Weisenberg, "A Thermodynamic Theory of the Strength of Materials," Rheology Leaflet No. 10, 12-20, 1939.

45. O. S. Brüller, "On the Damage Energy of Polymers in Creep," Polymer Engineering and Science, 18, (1) (1978).

46. Clement Hiel, A. H. Cardon, and H. F. Brinson, "The Nonlinear Viscoelastic Response of Resin Matrix Composite Laminates," Report No. VPI-E-83-6, Department of Engineering Science and Mechanics, VPI&SU, Blacksburg, VA, (March 1983).

47. Y. Weitsman, "Stresses in Adhesive Joints Due to Moisture and Temperature," J. Composite Materials, 11, 368 (Oct. 1977).

48. Y. Weitsman, "Interfacial Stresses in Viscoelastic Adhesive-Layers Due to Moisture Sorption," Int. J. Solids Structures, 15, 701-713, (1979).

49. F. E. L. Tobing, M. S. Shephard and S. S. Sternstein, "Finite Element Analysis of Moisture Effects in Graphite-Epoxy Composites," Computers & Structures, 16, (1-4), 457-469 (1983).

50. G. Yaniv and O. Ishai, "Hygrothermal Effects on Stresses and Deformations in a Bonded Fiber-Reinforced Plastic/Aluminum System," Composites Technology Review, 6, (2), 63-73 (1984).

51. D. R. Lefebvre, T. C. Ward, D. A. Dillard, H. F. Brinson, "A Nonlinear Constitutive Behavior for Diffusion in Polymers," Report No. VPI-E-87-2, CAS/ESM-87-1, Virginia Polytechnic Institute and State University, Blacksburg, VA, February 1987.

52. G. P. Anderson and K. L. DeVries, Stress State in Lap Shear Specimens, The Adhesion Society News Letter, 6 (1983).

53. J. N. Reddy, Energy and Variational Methods in Applied Mechanics, Wiley, New York (1984).

54. J. N. Reddy, An Introduction to the Finite Element Method, McGraw-Hill, New York (1984).

55. C. Hiel, A. H. Cardon, and H. F. Brinson, The Nonlinear Viscoelastic Response of Resin Matrix Composite Laminates, Department of Engineering Science and Mechanics, Virginia Polytechnic Institute and State University, Blacksburg, VA (March 1983).

56. R. A. Schapery, On the Characterization of Nonlinear Viscoelastic Materials, Polymer Engineering and Science, July, 1969, Vol. 9, No. 4, p. 295.

57. Quarterly Progress Report No. 6 (1 Dec. 1980 to 23 Feb. 1981), Integrated Methodology for Adhesive Bonded Joint Life Predictions, General Dynamics, Fort Worth Division, Technical Report FZM-6961 (March 1981).

58. E. Sancaktar and H. F. Brinson, The Viscoelastic Shear Behavior of a Structural Adhesive, in: Adhesion and Adsorption of Polymers (L. H. Lee, ed.), Plenum Press, 279-299 (1980).

59. J. Romanko and W. G. Knauss, On the Time Dependence of the Poisson's Ratio of a Commercial Adhesive Material, J. Adhesion, 10, 269-272 (1980).

60. L. J. Hart-Smith, Difference Between Adhesive Behavior in Test Coupons and Structural Joints, ASTM Adhesive Committee D-14 Meeting, Paper 7066, Phoenix, Arizona (March 1981).

61. M. A. Rochefort and H. F. Brinson, Nonlinear Viscoelastic Characterization of Structural Adhesives, Report VPI-E-83.26, NASA Contractor Report 172279, Department of Engineering Science and Mechanics, Virginia Polytechnic Institute and State University, Blacksburg, Virginia (July 1983).

62. E. Sancaktar, S. C. Schenck and S. Padgilwar, Material Characterization of Structural Adhesives in the Lap Shear Mode. 1. The Effects of Rate, 2. Temperature-Dependent Delayed Failure, Ind. Eng. Chem. Proc. Res. Div., 23, 426-434 (1984) and 24, 257-63 (1985).

63. C. Hiel, A. H. Cardon and H. F. Brinson, Viscoelastic Modelling of Epoxy-Resins for Adhesive and Composite Applications, Proc. 5th Int. Congress on Experimental Mechanics, June 10-15, Montreal, Society for Experimental Stress Analysis, 263-266 (1984).

64. B. M. Barthelemy, M. P. Kamat and H. F. Brinson, "Finite Element Analysis of Bonded Joints," Report No. VPI-E-84.15, Department of Engineering Science and Mechanics, Virginia Polytechnic Institute and State University, Blacksburg, VA, April 1984.

65. J. A. Harris and R. D. Adams, Strength Prediction of Bonded Single Lap Joints by Non-Linear Finite Element Methods, International Journal of Adhesion and Adhesives, Vol. 4, No. 2, pg. 65 (1984).

66. J. Crank, The Mathematics of Diffusion, Second Edition, Clarendon Press, Oxford, 1975.

67. Giovanni Levita and Thor L. Smith, Effect of Tensile Strain, Time, and Temperature on Gas Transport in Biaxially Oriented Polystyrene, Polymer Engineering and Science, Vol. 21, No. 14, p. 536 (1981).

68. J. D. Ferry, Viscoelastic Properties of Polymers, 3rd Edition, Wiley, New York, (1980).

69. L. C. E. Struik, Physical Aging in Amorphous Polymers and Other Materials, Elsevier, (1978).

70. G. Dolev and O. Ishai, Mechanical Characterization of Adhesive Layer In-Situ and as Bulk Material, J. Adhesion, Vol. 12, pp. 283-294, (1981).

The vita has been removed from the scanned document